

การสังเคราะห์อนุพันธ์พาราควิลฟีนอกซี-1,8-แนฟทาลิไมด์เพื่อเป็นสารเพิ่มความสว่าง

นายเจียรชัย ชูปวา

วิทยานิพนธ์นี้เป็นส่วนหนึ่งของการศึกษาตามหลักสูตรปริญญาวิทยาศาสตรมหาบัณฑิต

สาขาวิชาเคมี ภาควิชาเคมี

คณะวิทยาศาสตร์ จุฬาลงกรณ์มหาวิทยาลัย

ปีการศึกษา 2555

ลิขสิทธิ์ของจุฬาลงกรณ์มหาวิทยาลัย

บทคัดย่อและแฟ้มข้อมูลฉบับเต็มของวิทยานิพนธ์ตั้งแต่ปีการศึกษา 2554 ที่ให้บริการในคลังปัญญาจุฬาฯ (CUIR)
เป็นแฟ้มข้อมูลของนิสิตเจ้าของวิทยานิพนธ์ที่ส่งผ่านทางบัณฑิตวิทยาลัย

The abstract and full text of theses from the academic year 2011 in Chulalongkorn University Intellectual Repository (CUIR)
are the thesis authors' files submitted through the Graduate School.

SYNTHESIS OF *p*-CUMYLPHENOXY-1,8-NAPHTHALIMIDE DERIVATIVES
AS BRIGHTENERS

Mr. Tianchai Chooppawa

A Thesis Submitted in Partial Fulfillment of the Requirements
for the Degree of Master of Science Program in Chemistry

Department of Chemistry

Faculty of Science

Chulalongkorn University

Academic Year 2012

Copyright of Chulalongkorn University

Thesis Title SYNTHESIS OF *p*-CUMYLPHENOXY-1,8-
NAPHTHALIMIDE DERIVATIVES AS
BRIGHTENERS
By Mr. Tianchai Chooppawa
Field of Study Chemistry
Thesis Advisor Assistant Professor Paitoon Rashatasakhon, Ph.D.
Thesis Co-advisor Associate Professor Mongkol Sukwattanasinitt, Ph.D.

Accepted by the Faculty of Science, Chulalongkorn University in Partial
Fulfillment of the Requirements for the Master's Degree

.....Dean of the Faculty of Science
(Professor Supot Hannongbua, Dr.rer.nat)

THESIS COMMITTEE

.....Chairman
(Assistant Professor Warinthorn Chavasiri, Ph.D.)

.....Thesis Advisor
(Assistant Professor Paitoon Rashatasakhon, Ph.D.)

.....Thesis Co-advisor
(Associate Professor Mongkol Sukwattanasinitt, Ph.D.)

.....Examiner
(Anawat Ajavakom, Ph.D.)

.....External Examiner
(Jutatip Boonsombat, Ph.D.)

ธีรชัย ชูปวา: การสังเคราะห์อนุพันธ์พาราควิลฟีนอกซี-1,8-แนฟทาลิไมด์เพื่อเป็นสารเพิ่มความสว่าง (SYNTHESIS OF *p*-CUMYLPHENOXY-1,8-NAPHTHALIMIDE DERIVATIVES AS BRIGHTENERS) อ. ที่ปรึกษาวิทยานิพนธ์หลัก: ผศ.ดร. ไพฑูรย์ รัชตะสาคร อ. ที่ปรึกษาวิทยานิพนธ์ร่วม: รศ.ดร. มงคล สุขวัฒนาสินธิ์, 102 หน้า.

อนุพันธ์ 4-แอลคอกซี หรือ 4-เอริลลอกซี-1,8-แนฟทาลิไมด์จำนวนหนึ่งได้สังเคราะห์และนำไปศึกษาสมบัติทางกายภาพเชิงแสง ความเสถียรต่อความร้อนและความเสถียรต่อแสง วิธีสังเคราะห์ได้เริ่มจากปฏิกิริยาเอมิเตชันของ 4-โบรโม-1,8-แนฟทาลิไมด์ที่มีจำหน่ายเชิงพาณิชย์ กับอนุพันธ์ต่างๆของแอนิลีน การแทนที่ของหมู่โบรโมด้วยฟีนอลหรือแอลิเฟติกแอลกอฮอล์นำไปสู่สารเป้าหมายในปริมาณผลผลิตที่ดี สารทุกตัวมีสัญญาณการดูดกลืนแสงในช่วงความยาวคลื่น 364-368 นาโนเมตร และคายพลังงานแสงในช่วงความยาวคลื่น 425-436 นาโนเมตร ซึ่งเป็นสมบัติที่พึงประสงค์ของสารที่จะใช้เป็นสารเพิ่มความสว่าง โดยพบว่าเสถียรภาพเชิงแสงของสารที่สังเคราะห์ได้มีความใกล้เคียงกับสารเพิ่มความสว่างที่มีจำหน่ายในท้องตลาด เช่นทีโนพล แต่เสถียรภาพทางความร้อนของสารที่สังเคราะห์ได้ดีกว่าและสามารถปรับให้ดีขึ้นได้อีกด้วยการแทนที่ด้วยหมู่ควิควิมฟีนอกซีที่ตำแหน่ง 4 อย่างไรก็ตาม งานวิจัยนี้พบว่าประสิทธิภาพทางแสงของสารในกลุ่มนี้ขึ้นอยู่กับหมู่แทนที่ที่ตำแหน่ง 4 เป็นหลัก โดยสารที่มีหมู่แอลคอกซีและหมู่ฟีนอกซีมีประสิทธิภาพทางแสงที่สูง แต่สารที่มีหมู่เอริลลอกซีแบบมีหมู่แทนที่มีประสิทธิภาพทางแสงที่ต่ำกว่า โดยสันนิษฐานว่าผลทางอิเล็กทรอนิกส์จากหมู่แทนที่ในหมู่เอริลลอกซีที่ตำแหน่งที่ 4 ส่งผลไปยังกระบวนการส่งผ่านอิเล็กตรอนที่เหนี่ยวนำโดยแสง ซึ่งนำไปสู่การเปลี่ยนแปลงสัญญาณฟลูออเรสเซนซ์

สาขาวิชา.....เคมี.....

ลายมือชื่อนิสิต.....

สาขาวิชา.....เคมี.....

ลายมือชื่อ อ. ที่ปรึกษาวิทยานิพนธ์หลัก.....

ปีการศึกษา.....2555.....

ลายมือชื่อ อ. ที่ปรึกษาวิทยานิพนธ์ร่วม.....

##5372264923: MAJOR ORGANIC CHEMISTRY SCIENCE

KEYWORDS: FLUORESCENCE / OPTICAL BRIGHTENER / THERMAL STABILITY / 1,8-NAPHTHALIMIDE / QUANTUM YIELD / PHOTO-INDUCED ELECTRON TRANSFER

TIANCHAI CHOOPAWA: SYNTHESIS OF *p*-CUMYLPHENOXY-1,8-NAPHTHALIMIDE DERIVATIVES AS BRIGHTENERS

ADVISOR: ASST. PROF. PAITON RASHATASAKHON, Ph.D.

CO-ADVISOR: ASSOC. PROF. MONGKOL SUKWATTANASINITT, Ph.D., 102 pp.

A series of 4-alkoxy or 4-aryloxy-*N*-aryl-1,8-naphthalimides were synthesized and evaluated for their optical properties as well as thermal and photo stabilities. The synthesis began with the imidation of the commercially available 4-bromo-1,8-naphthalic anhydride with various aniline derivatives. Substitution of the bromine with phenol or aliphatic alcohol provided the target molecules in good yields. All compounds had absorption wavelengths around 364-368 nm and emission wavelengths of 425-436 nm, which were desirable properties for optical brightening agents (OBA). In comparison with the commercially available OBA - Tinopal - their photostability were closely similar but their thermal stabilities are more superior and could significantly be improved by substitution at the 4-position with a cumylphenoxy group. In this research, it was found that their quantum efficiencies were exclusively dependent on the substituents at the 4-position. Compounds with alkoxy and phenoxy groups exhibited high quantum efficiencies whereas those compounds with substituted aryloxy groups showed lower quantum efficiencies. It is postulated that the electronic effect of the substituents on the 4-aryloxy groups influences the photo-induced electron transfer (PET) process, which causes variations in fluorescence signal.

Department: Chemistry

Student Signature.....

Field of study: Chemistry

Advisor Signature.....

Academic Year: 2012

Co-advisor Signature.....

ACKNOWLEDGEMENTS

First of all, I would like to thank you Assistant Professor Paitoon Rashataskhon, Ph.D. my advisor, Associate Professor Mongkol Sukwattanasintt, Ph.D., my co-advisor, and the team members from Material Advancement via Proficient Synthesis (MAPS) for supporting my thesis regarding fluorescent compounds and their properties. Not only giving me an opportunity to study and achieve this research, Assistant Professor Paitoon also provides me Teacher Assistant Scholarship (TA), from Center of Excellence on Petrochemical and Materials Technology (ADB), and PTT phenol.

Furthermore, this thesis would not have been accomplished without many precious and valuable advice and comments from all my thesis committee, Assistant Professor Warinthorn Chavasiri, Ph.D., Dr. Anawat Ajavakorn, and Dr. Jutathip Boonsombat.

Ultimately, I am most grateful to my mother, my aunt, Ms. Sophin, and all family members for their personal supports at all times.

CONTENTS

	Page
ABSTRACT (THAI).....	iv
ABSTRACT (ENGLISH)	v
ACKNOWLEDGEMENTS.....	vi
CONTENTS.....	vii
LIST OF TABLES.....	x
LIST OF FIGURES.....	xi
LIST OF SCHEMES.....	xix
LIST OF ABBREVIATIONS.....	xx
CHAPTER	
I INTRODUCTION.....	1
1.1. Overview.....	1
1.2. Fluorescent Brightening Agents (FBAs)	1
1.3. Basic fluorescence principle.....	5
1.4. Internal Charge Transfer process (ICT process)	6
1.5. Photo-induced Electron Transfer (PET).....	7
1.6. Fluorescent compounds from naphthalimides and their derivatives.....	11
1.7. Thermal stability.....	18
II EXPERIMENTAL.....	19
2.1. Materials and chemicals.....	19
2.2. Synthesis.....	19
2.2.1. 4-Bromo- <i>N</i> -phenyl-1,8-naphthalimide (2a).....	20
2.2.2. 4-Bromo- <i>N</i> -(2-methoxycarbonyl-phenyl)-1,8- naphthalimide (2b).....	20
2.2.3. 4-Bromo- <i>N</i> -(4-methoxy-phenyl)-1,8-naphthalimide (2c)..	21
2.2.4. 4-Bromo- <i>N</i> -(2,6-diisopropyl-phenyl)-1,8- naphthalimide (2d).....	22
2.2.5. 4-Phenoxy- <i>N</i> -phenyl-1,8-naphthalimide (3a)	22

CHAPTER	Page
2.2.6. 4-Cumylphenoxy- <i>N</i> -(phenyl)-1,8-naphthalimide (3b) Method A.....	23
2.2.7. 4-Cumylphenoxy- <i>N</i> -(phenyl)-1,8-naphthalimide (3b) Method B (General procedure).....	24
2.2.8. 4-Cumylphenoxy- <i>N</i> -(2-methoxycarbonyl-phenyl)-1,8- naphthalimide (3c)	24
2.2.9. 4-Cumylphenoxy- <i>N</i> -(4-methoxy-phenyl)-1,8- naphthalimide (3d)	25
2.2.10. 4-Cumylphenoxy- <i>N</i> -(2,6-diisopropyl-phenyl)- 1,8-naphthalimide (3e)	25
2.2.11. 4-Phenoxy- <i>N</i> -(2,6-diisopropyl-phenyl)-1,8- naphthalimide (3f)	26
2.2.12. 4-(4- <i>tert</i> -Butyl-phenoxy)- <i>N</i> -(2,6-diisopropyl-phenyl) -1,8-naphthalimide (3g)	27
2.2.13. 4-(4-Methoxy-phenoxy)- <i>N</i> -(2,6-diisopropyl-phenyl) -1,8-naphthalimide (3h)	27
2.2.14. 4-(4-Chloro-phenoxy)- <i>N</i> -(2,6-diisopropyl-phenyl) -1,8-naphthalimide (3i)	28
2.2.15. Methyl 4-hydroxybenzoate (4)	28
2.2.16. 4-(4-Methoxycarbonyl-phenoxy)- <i>N</i> - (2,6-diisopropyl-phenyl)-1,8-naphthalimide (3j).....	29
2.2.17. 4-(4-Nitro-phenoxy)- <i>N</i> -(2,6-diisopropyl-phenyl) -1,8-naphthalimide (3k)	29
2.2.18. 4-Butoxy- <i>N</i> -(2,6-diisopropyl-phenyl)-1,8- naphthalimide (3l)	30
2.2.19. 5,6-Dibromoacenaphthene (5)	31
2.2.20. 4,5-Dibromo-1,8-naphthalic anhydride (6)	31
2.2.21. 4,5-Dibromo- <i>N</i> -(2,6-diisopropyl-phenyl)-1,8- naphthalimide (2e)	32

CHAPTER	Page
2.2.22. 4,5-Dicumylphenoxy- <i>N</i> -(2,6-diisopropyl-phenyl) -1,8-naphthalimide (3m)	32
2.3. Photophysical test.....	33
2.3.1. Absorption.....	33
2.3.2. Emission or fluorescence.....	33
2.3.3. Quantum yield.....	33
2.4. Photostability test.....	34
2.5. Thermal stability test.....	34
2.6. Electronic test	34
III RESULTS AND DISCUSSION.....	36
3.1. Synthesis and characterization.....	36
3.2. Photophysical study.....	39
3.3. Photostability test.....	45
3.4. Thermal stability test.....	46
3.5. Electronic test.....	47
IV CONCLUSION.....	49
4.1. Conclusion.....	49
4.2. Suggestion for future works.....	50
REFERENCES.....	51
APPENDIX.....	58
VITAE.....	102

LIST OF TABLES

Table	Page
3.1. Structure of target naphthalimides	39
3.2. The photophysical properties of 3a-3h	41
3.3. Thermal stabilities.....	46

LIST OF FIGURES

Figure	Page
1.1 Principles of whiteness improvement [2].....	2
1.2 Commercial FBAs in [1].....	3
1.3 CI86 structure and example of synthesized compound [4].....	3
1.4 Example FBAs organic compounds BRI [6] Bri [7] hybrid material and their percent UV transmission 4a and 4b [8] Tinopal OB.....	4
1.5 Jablonski energy diagram [10].....	5
1.6 ICT process mechanism via Frank condon principle.....	6
1.7 Example of electron delocalization [14].....	7
1.8 1,8-naphthalimide sensor via ICT process [15].....	7
1.9 De-excitation route by PET mechanism [16].....	8
1.10 The description of PET process by energy diagram in case (a) free (b) coupled with analyte [16].....	8
1.11. The relative energy diagram of compounds [16].....	9
1.12. Structures of tmeda-PPETE and dea-PPETE [18].....	9
1.13. Synthesized sensor structures and interference study, M(II): Pb ²⁺ , Hg ²⁺ , Co ²⁺ , Fe ²⁺ , Cd ²⁺ , Mg ²⁺ , Ba ²⁺ at excitation 339 nm.....	10
1.14. 1,8-naphthalimide structure.....	11
1.15. Poly(acrylonitrile)- <i>co</i> -1,8-naphthalimide dyes [23].....	11
1.16. anti-tumor 1,8-naphthalimide drugs [28].....	12
1.17. 1,8-naphthalimide drugs, such as NNM-25 [25], ANISpm [26] and triazole derivatives [28].....	12
1.18. Acid generation of 1,8-naphthalimide derivatives [29].....	13
1.19. Expected mechanism (left) quenching mechanism (right) [30].....	13
1.20. Proposed mechanism in the presence of F ⁻ [31].....	14
1.21. The color response of sensor [32].....	14
1.22. Anion sensor from 1,8-naphthalimides and response phenomenon [34]..	15
1.23. Hg ²⁺ naphthalimide sensor [35] and H ⁺ [36].....	15
1.24. The color change into B when the acid was added [37].....	16

Figure	Page
1.25. Compound 3, 5 and 6 [38], their photophysical properties and proposed PET pathway [38].....	16
1.26. Structures of 1,8-naphthalimides prepared by Y. Wang <i>et al.</i> [40].....	17
1.27. Synthesis of substituted 1,8-naphthalimide [42].....	17
1.28. Blue emissive polymer [43].....	18
1.29. Structures of various FBAs reported by Liu and coworkers [44].....	18
3.1. ¹ H NMR spectra of 4-bromo-1,8-naphthalic anhydride or 1 (top), 2,6-diisopropylaniline (middle) and 4-bromo- <i>N</i> -(2,6-diisopropyl-phenyl)- 1,8-naphthalimide (2d) in CDCl ₃	37
3.2. ¹ H NMR spectrum of 4-(4- <i>tert</i> -butylphenoxy)- <i>N</i> -(2,6-diisopropyl-phenyl)- 1,8-naphthalimide (3g) in CDCl ₃	38
3.3. Proposed side product structures.....	43
3.4. Proposed electron donating mechanism in 3d and 3h for synergistic ICT process.....	44
3.5. Proposed electron withdrawing mechanism in 3k for synergistic ICT Process.....	45
3.6. The remaining percentage of each compounds upon exposure to UVA....	45
3.7. HOMO (down) and LUMO (up) energy level of synthesized 1,8-naphthalimides.....	47
4.1. 3a-3l fluorescence under black light.....	49
A.1 ¹ H NMR of 4-bromo- <i>N</i> -(phenyl)-1,8-naphthalimide (2a) in CDCl ₃	59
A.2 ¹ H NMR of 4-bromo- <i>N</i> -(2-acethoxy-phenyl)-1,8-naphthalimide (2b) in CDCl ₃	59
A.3 ¹ H NMR of 4-bromo- <i>N</i> -(4-meyhoxy-phenyl)-1,8-naphthalimide (2c) in CDCl ₃60
A.4 ¹ H NMR of 4-bromo- <i>N</i> -(2,6-diisopropyl-phenyl)-1,8-naphthalimide (2d) in CDCl ₃	60
A.5 ¹ H NMR of 4-phenoxy- <i>N</i> -(phenyl)-1,8-naphthalimide (3a) in CDCl ₃	61
A.6 ¹³ C NMR of 4-phenoxy- <i>N</i> -(phenyl)-1,8-naphthalimide (3a) in CDCl ₃	61

Figure	Page
A.7 ^1H NMR of 4-cumylphenoxy- <i>N</i> -(phenyl)-1,8-naphthalimide (3b) by KOH in CDCl_3	62
A.8 ^{13}C NMR of 4-cumylphenoxy- <i>N</i> -(phenyl)-1,8-naphthalimide (3b) by KOH in CDCl_3	62
A.9 ^1H NMR of 4-cumylphenoxy- <i>N</i> -(phenyl)-1,8-naphthalimide (3b) by K_2CO_3 in CDCl_3	63
A.10 ^1H NMR of 4-cumylphenoxy- <i>N</i> -(2-acethoxy-phenyl)-1,8-naphthalimide (3c) in CDCl_3	63
A.11 ^{13}C NMR of 4-cumylphenoxy- <i>N</i> -(2-acethoxy-phenyl)-1,8-naphthalimide (3c) in CDCl_3	64
A.12 ^1H NMR of 4-cumylphenoxy- <i>N</i> -(4-methoxy-phenyl)-1,8-naphthalimide (3d) in CDCl_3	64
A.13 ^{13}C NMR of 4-cumylphenoxy- <i>N</i> -(4-methoxy-phenyl)-1,8-naphthalimide (3d) in CDCl_3	65
A.14 ^1H NMR of 4-cumylphenoxy- <i>N</i> -(2,6-diisopropyl-phenyl)-1,8-naphthalimide (3e) in CDCl_3	65
A.15 ^{13}C NMR of 4-cumylphenoxy- <i>N</i> -(2,6-diisopropyl-phenyl)-1,8-naphthalimide (3e) in CDCl_3	66
A.16 ^1H NMR of 4-phenoxy- <i>N</i> -(2,6-diisopropyl-phenyl)-1,8-naphthalimide (3f) in CDCl_3	66
A.17 ^{13}C NMR of 4-phenoxy- <i>N</i> -(2,6-diisopropyl-phenyl)-1,8-naphthalimide (3f) in CDCl_3	67
A.18 ^1H NMR of 4-(4- <i>tert</i> -butyl-phenoxy)- <i>N</i> -(2,6-diisopropyl-phenyl)-1,8-naphthalimide (3g) in CDCl_3	67
A.19 ^{13}C NMR of 4-(4- <i>tert</i> -butyl-phenoxy)- <i>N</i> -(2,6-diisopropyl-phenyl)-1,8-naphthalimide (3g) in CDCl_3	68
A.20 ^1H NMR of 4-(4-methoxy-phenoxy)- <i>N</i> -(2,6-diisopropyl-phenyl)-1,8-naphthalimide (3h) in CDCl_3	68
A.21 ^{13}C NMR of 4-(4-methoxy-phenoxy)- <i>N</i> -(2,6-diisopropyl-phenyl)-1,8-naphthalimide (3h) in CDCl_3	69

Figure	Page
A.22 ¹ H NMR of 4-(4-chloro-phenoxy)- <i>N</i> -(2,6-diisopropyl-phenyl)-1,8-naphthalimide (3i) in CDCl ₃	69
A.23 ¹³ C NMR of 4-(4-chloro-phenoxy)- <i>N</i> -(2,6-diisopropyl-phenyl)-1,8-naphthalimide (3i) in CDCl ₃	70
A.24 ¹ H NMR of methyl 4-hydroxybenzoate (4) in CDCl ₃	70
A.25 ¹ H NMR of 4-(4-acethoxy-phenoxy)- <i>N</i> -(2,6-diisopropyl-phenyl)-1,8-naphthalimide (3j) in CDCl ₃	71
A.26 ¹³ C NMR of 4-(4-acethoxy-phenoxy)- <i>N</i> -(2,6-diisopropyl-phenyl)-1,8-naphthalimide (3j) in CDCl ₃	71
A.27 ¹ H NMR of 4-(4-nitro-phenoxy)- <i>N</i> -(2,6-diisopropyl-phenyl)-1,8-naphthalimide (3k) in CDCl ₃	72
A.28 ¹³ C NMR of 4-(4-nitro-phenoxy)- <i>N</i> -(2,6-diisopropyl-phenyl)-1,8-naphthalimide (3k) in CDCl ₃	72
A.29 ¹ H NMR of 4-butoxy- <i>N</i> -(2,6-diisopropyl-phenyl)-1,8-naphthalimide (3l) in CDCl ₃	73
A.30 ¹³ C NMR of 4-butoxy- <i>N</i> -(2,6-diisopropyl-phenyl)-1,8-naphthalimide (3l) in CDCl ₃	73
A.31 ¹ H NMR of 5,6-dibromoacenaphthene (5) in CDCl ₃	74
A.32 FT-IR spectrum of 4,5-dibromo-1,8-naphthalic anhydride (6).....	74
A.33 ¹ H NMR of 4,5-dibromo- <i>N</i> -(2,6-diisopropyl-phenyl)-1,8-naphthalimide (2e) in CDCl ₃	75
A.34 ¹ H NMR of 4,5-dicumylphenoxy- <i>N</i> -(2,6-diisopropyl-phenyl)-1,8-naphthalimide (3m) in CDCl ₃	75
A.35 Mass spectrum of 4,5-dicumylphenoxy- <i>N</i> -(2,6-diisopropyl-phenyl)-1,8-naphthalimide (3m) in EtOAc.....	76
A.36 Molar absorption coefficient plot of 4-phenoxy- <i>N</i> -(phenyl)-1,8-naphthalimide (3a) in CH ₂ Cl ₂	76
A.37 Molar absorption coefficient plot of 4-cumylphenoxy- <i>N</i> -(phenyl)-1,8-naphthalimide (3b) in CH ₂ Cl ₂	77
A.38 Molar absorption coefficient plot of 4-cumylphenoxy- <i>N</i> -	

Figure	Page
(2-acethoxy-phenyl)-1,8-naphthalimide (3c) in CH ₂ Cl ₂	77
A.39 Molar absorption coefficient plot of 4-cumylphenoxy- <i>N</i> - (4-methoxy-phenyl)-1,8-naphthalimide (3d) in CH ₂ Cl ₂	78
A.40 Molar absorption coefficient plot of 4-cumylphenoxy- <i>N</i> - (2,6-diisopropyl-phenyl)-1,8-naphthalimide (3e) in CH ₂ Cl ₂	78
A.41 Molar absorption coefficient plot of 4-phenoxy- <i>N</i> - (2,6-diisopropyl-phenyl)-1,8-naphthalimide (3f) in CH ₂ Cl ₂	79
A.42 Molar absorption coefficient plot of 4-(4- <i>tert</i> -butyl-phenoxy)- <i>N</i> - (2,6-diisopropyl-phenyl)-1,8-naphthalimide (3g) in CH ₂ Cl ₂	79
A.43 Molar absorption coefficient plot of 4-(4-methoxy-phenoxy)- <i>N</i> - (2,6-diisopropyl-phenyl)-1,8-naphthalimide (3h) in CH ₂ Cl ₂	80
A.44 Molar absorption coefficient plot of 4-(4-chloro-phenoxy)- <i>N</i> - (2,6-diisopropyl-phenyl)-1,8-naphthalimide (3i) in CH ₂ Cl ₂	80
A.45 Molar absorption coefficient plot of 4-(4-acethoxy-phenoxy)- <i>N</i> - (2,6-diisopropyl-phenyl)-1,8-naphthalimide (3j) in CH ₂ Cl ₂	81
A.46 Molar absorption coefficient plot of 4-(4-nitro-phenoxy)- <i>N</i> - (2,6-diisopropyl-phenyl)-1,8-naphthalimide (3k) in CH ₂ Cl ₂	81
A.47 Molar absorption coefficient plot of 4-butoxy- <i>N</i> -(2,6-diisopropyl-phenyl)- 1,8-naphthalimide (3l) in CH ₂ Cl ₂	82
A.48 Molar absorption coefficient plot of 4,5-dicumylphenoxy- <i>N</i> - (2,6-diisopropyl-phenyl)-1,8-naphthalimide (3m) in CH ₂ Cl ₂	82
A.49 Molar absorption coefficient plot of Tinopal OB (7) in CH ₂ Cl ₂	83
A.50 Quantum yield plot of 4-phenoxy- <i>N</i> -(phenyl)-1,8-naphthalimide (3a) in CH ₂ Cl ₂ at PMT 540.....	83
A.51 Quantum yield plot of 4-cumylphenoxy- <i>N</i> -(phenyl)-1,8-naphthalimide (3b) in CH ₂ Cl ₂ at PMT 595.....	84
A.52 Quantum yield plot of 4-cumylphenoxy- <i>N</i> -(2-acethoxy-phenyl)-1,8- naphthalimide (3c) in CH ₂ Cl ₂ at PMT 595.....	84
A.53 Quantum yield plot of 4-cumylphenoxy- <i>N</i> -(4-methoxy-phenyl)-1,8- naphthalimide (3d) in CH ₂ Cl ₂ at PMT 595.....	85

Figure	Page
A.54 Quantum yield plot of 4-cumylphenoxy- <i>N</i> -(2,6-diisopropyl-phenyl)-1,8-naphthalimide (3e) in CH ₂ Cl ₂ at PMT 595.....	85
A.55 Quantum yield plot of 4-phenoxy- <i>N</i> -(2,6-diisopropyl-phenyl)-1,8-naphthalimide (3f) in CH ₂ Cl ₂ at PMT 540.....	86
A.56 Quantum yield plot of 4-(4- <i>tert</i> -butyl-phenoxy)- <i>N</i> -(2,6-diisopropyl-phenyl)-1,8-naphthalimide (3g) in CH ₂ Cl ₂ at PMT 595.....	86
A.57 Quantum yield plot of 4-(4-methoxy-phenoxy)- <i>N</i> -(2,6-diisopropyl-phenyl)-1,8-naphthalimide (3h) in CH ₂ Cl ₂ at PMT 595.....	87
A.58 Quantum yield plot of 4-(4-chloro-phenoxy)- <i>N</i> -(2,6-diisopropyl-phenyl)-1,8-naphthalimide (3i) in CH ₂ Cl ₂ at PMT 540.....	87
A.59 Quantum yield plot of 4-(4-acethoxy-phenoxy)- <i>N</i> -(2,6-diisopropyl-phenyl)-1,8-naphthalimide (3j) in CH ₂ Cl ₂ at PMT 540.....	88
A.60 Quantum yield plot of 4-(4-nitro-phenoxy)- <i>N</i> -(2,6-diisopropyl-phenyl)-1,8-naphthalimide (3k) in CH ₂ Cl ₂ at PMT 595.....	88
A.61 Quantum yield plot of 4-butoxy- <i>N</i> -(2,6-diisopropyl-phenyl)-1,8-naphthalimide (3l) in CH ₂ Cl ₂ at PMT 540.....	89
A.62 Quantum yield plot of 4,5-dicumylphenoxy- <i>N</i> -(2,6-diisopropyl-phenyl)-1,8-naphthalimide (3m) in CH ₂ Cl ₂ at PMT 595.....	89
A.63 Quantum yield plot of Tinopal OB (7) in CH ₂ Cl ₂ at PMT 540.....	90
A.64 Quantum yield plot of Quinine sulfate in 0.1 M H ₂ SO ₄ at PMT 540.....	90
A.65 Quantum yield plot of Quinine sulfate in 0.1 M H ₂ SO ₄ at PMT 595.....	90
A.66 DSC measurement of 4-cumylphenoxy- <i>N</i> -(phenyl)-1,8-naphthalimide (3b) on the first heating cycle with a heating rate of 10 °C per minute under N ₂	91
A.67 DSC measurement of 4-cumylphenoxy- <i>N</i> -(phenyl)-1,8-naphthalimide (3b) on the second heating cycle with a heating rate of 10 °C per minute under N ₂	91
A.68 DSC measurement of 4-cumylphenoxy- <i>N</i> -(4-methoxy-phenyl)-1,8-naphthalimide (3d) on the first heating cycle with a heating rate of 10 °C per minute under N ₂	92

Figure	Page
A.69 DSC measurement of 4-cumylphenoxy- <i>N</i> -(4-methoxy-phenyl)-1,8-naphthalimide (3d) on the second heating cycle with a heating rate of 10 °C per minute under N ₂	92
A.70 DSC measurement of 4-cumylphenoxy- <i>N</i> -(2,6-diisopropyl-phenyl)-1,8-naphthalimide (3e) on the first heating cycle with a heating rate of 10 °C per minute under N ₂	93
A.71 DSC measurement of 4-cumylphenoxy- <i>N</i> -(2,6-diisopropyl-phenyl)-1,8-naphthalimide (3e) on the second heating cycle with a heating rate of 10 °C per minute under N ₂	93
A.72 DSC measurement of 4-phenoxy- <i>N</i> -(2,6-diisopropyl-phenyl)-1,8-naphthalimide (3f) on the first heating cycle with a heating rate of 10 °C per minute under N ₂	94
A.73 DSC measurement of 4-phenoxy- <i>N</i> -(2,6-diisopropyl-phenyl)-1,8-naphthalimide (3f) on the second heating cycle with a heating rate of 10 °C per minute under N ₂	94
A.74 DSC measurement of 4-butoxy- <i>N</i> -(2,6-diisopropyl--phenyl)-1,8-naphthalimide (3l) on the first heating cycle with a heating rate of 10 °C per minute under N ₂	95
A.75 DSC measurement of 4-butoxy- <i>N</i> -(2,6-diisopropyl--phenyl)-1,8-naphthalimide (3l) on the second heating cycle with a heating rate of 10 °C per minute under N ₂	95
A.76 DSC measurement of 4,5-dicumylphenoxy- <i>N</i> -(2,6-diisopropyl-phenyl)-1,8-naphthalimide (3m) on the first heating cycle with a heating rate of 10 °C per minute under N ₂	96
A.77 DSC measurement of 4,5-dicumylphenoxy- <i>N</i> -(2,6-diisopropyl-phenyl)-1,8-naphthalimide (3m) on the second heating cycle with a heating rate of 10 °C per minute under N ₂	96
A.78 TGA measurement of 4-cumylphenoxy- <i>N</i> -(phenyl)-1,8-naphthalimide (3b) with a heating rate of 10 °C per minute under N ₂	97

Figure	Page
A.79 TGA measurement of 4-cumylphenoxy- <i>N</i> -(4-methoxy-phenyl)-1,8-naphthalimide (3d) with a heating rate of 10 °C per minute under N ₂	97
A.80 TGA measurement of 4-cumylphenoxy- <i>N</i> -(2,6-diisopropyl-phenyl)-1,8-naphthalimide (3e) with a heating rate of 10 °C per minute under N ₂	97
A.81 TGA measurement of 4-phenoxy- <i>N</i> -(2,6-diisopropyl-phenyl)-1,8-naphthalimide (3f) with a heating rate of 10 °C per minute under N ₂	98
A.82 TGA measurement of 4-butoxy- <i>N</i> -(2,6-diisopropyl--phenyl)-1,8-naphthalimide (3l) with a heating rate of 10 °C per minute under N ₂	98
A.83 TGA measurement of 4,5-dicumylphenoxy- <i>N</i> -(2,6-diisopropyl-phenyl)-1,8-naphthalimide (3m) with a heating rate of 10 °C per minute under N ₂	98
A.84 TGA measurement of Tinopal OB (7) with a heating rate of 10 °C per minute under N ₂	99

LIST OF SCHEMES

Scheme	Page
1.1	Concept of nitric oxide sensor and proposed enhancing mechanism [21].. 10
2.1.	Synthesis methods: (a) appropriate aniline, glacial acetic acid, reflux; (b) appropriate phenol or alcohol, KOH, 18-crown-6, DMF, 70 °C; (c) appropriate phenol or alcohol, K ₂ CO ₃ , DMF, 110 °C..... 21
3.1.	Synthesis methods: (a) appropriate aniline, glacial acetic acid, reflux; (b) appropriate phenol or alcohol, KOH, 18-crown-6, DMF, 70 °C; (c) appropriate phenol or alcohol, K ₂ CO ₃ , DMF, 110 °C..... 36
3.2.	The relative energy level of 1,8-naphthalimide with various substituents at the 4-position-aryloxy-1,8-naphthalimide..... 42

LIST OF ABBREVIATIONS

A	acceptor
Ar	aryl
br	broad (NMR)
calcd	calculated
^{13}C NMR	carbon-13 nuclear magnetic resonance
CDCl_3	deuterated chloroform
D	donor
d	doublet (NMR)
dd	doublet of doublet (NMR)
DMF	<i>N,N</i> -dimethyl formamide
DMSO	dimethylsulfoxide
DSC	differential scanning calorimetry
ESIMS	electrospray ionization mass spectrometry
FBA	fluorescent brightener agent (s)
FRET	forster resonance energy transfer
equiv	equivalent (s)
FT-IR	fourier transform infrared spectroscopy
g	gram (s)
HALS	hindered amine light stabilizer
^1H NMR	proton nuclear magnetic resonance
Hz	hertz
HOMO	highest occupied molecular orbital
HRMS	high resolution mass spectrometry
h	hour (s)
ICT	internal charge transfer
IR	infrared
<i>J</i>	coupling constant
LUMO	lowest unoccupied molecular orbital
mg	milligram (s)

mL	milliliter (s)
mmol	millimole (s)
m/z	mass per charge
m	multiplet (NMR)
min	minute (s)
mp	melting point
MW	molecular weight
M	molar
MHz	megahertz
nm	nanometer (s)
OBA	optical brightener agent (s)
PET	photo-induced electron transfer
PMT	photomultiplier tube
q	quartet (NMR)
rt	room temperature
s	singlet (NMR)
TGA	thermogravimetric analysis
THF	tetrahydrofuran
T_c	crystal temperature
T_d	decomposition temperature
T_g	glass transition temperature
T_m	melting temperature
UV	ultraviolet
δ	chemical shift
$^{\circ}\text{C}$	celsius degree
μL	microliter (s)
μM	micromolar (s)
Φ	quantum yield
% yield	percentage yield
	wavelength
	molar absorption coefficient

CHAPTER I

INTRODUCTION

1.1 Overview

Optical brighteners (OBs) or fluorescent brightening agents (FBAs) are additives that can improve visual properties of materials by absorbing ultraviolet light and re-emitting most of the absorbed energy as blue fluorescent light between 400 and 500 nm. Materials that evenly reflect most of the light at all wavelengths striking their surface appear white to the human eyes [1-2]. For applications in thermoplastic, the brightener should not only have long-lasting stability under UV light (high photo stability), but it also possess high thermal stability in order to retain the desired properties upon high temperature processing. According to a patented information [3], the thermal stabilities of 1,8-naphthalimide fluorescent brighteners can be tuned by incorporating various phenoxy and alkoxy groups into the structure. Most importantly, the brighteners which are derivatives of cumyl phenol usually exhibit a high glass transition temperature (T_g).

This project focused on the design and synthesis of fluorescent brighteners based on phenol substituted 1,8-naphthalimides. For the collaborative research with the PTT Phenol Public Company Limited, this study aims to incorporate cumyl phenol on to the 1,8-naphthalimides in order to enhance their thermal properties. On the other hands, the critical part involves an investigation of the substitution effect on quantum efficiencies of 1,8-naphthalimides.

1.2. Fluorescent Brightening Agents (FBAs)

Fluorescent brightening agents (FBAs) are colorless to weakly colored organic compounds that, in solution or applied to a substrate, absorb ultraviolet light, and re-emit most of the absorbed energy as blue fluorescent light between 400 and 500 nm. The blue fluorescent light at any surface appears white to the human eye. Natural

fibers, for example, generally absorb more light in the blue region of the visible spectrum ('blue defect') than in others because of impurities (natural pigments) they contain. As a result, natural fibers take on an unwanted yellowish cast (**Figure 1.1 a**). Some synthetic fibers also have this yellowish cast, although not as pronounced. In principle, whiteness in substrates can be improved by increasing of reflection (reflectance) and compensating of the blue defect. Before the advent of FBAs, common practice was to apply small amounts of blue or violet dyes (called 'bluing') to boost the visual impression of whiteness. These dyes absorb light in the green-yellow region of the spectrum, thereby reducing lightness. However, since they shift simultaneously the shade of the yellowish material towards blue, the human eye perceives an increase of whiteness (**Figure 1.1 b**). Unlike dyes, FBAs offset the yellowish cast and at the same time improve lightness because their bluing effect is not based on subtracting yellow-green light, but rather on adding blue light (**Figure 1.1 c**). FBAs are virtually colorless compounds which, when present on a substrate, absorb primarily invisible ultraviolet light in the 300-400 nanometer (nm) range and re-emit in the visible violet-to-blue fluorescent light. This ability of FBAs to absorb invisible short wavelength radiation and re-emit in the visible blue light, which imparts a brilliant whiteness to the light reflected by a substrate, is the key to FBAs effectiveness.

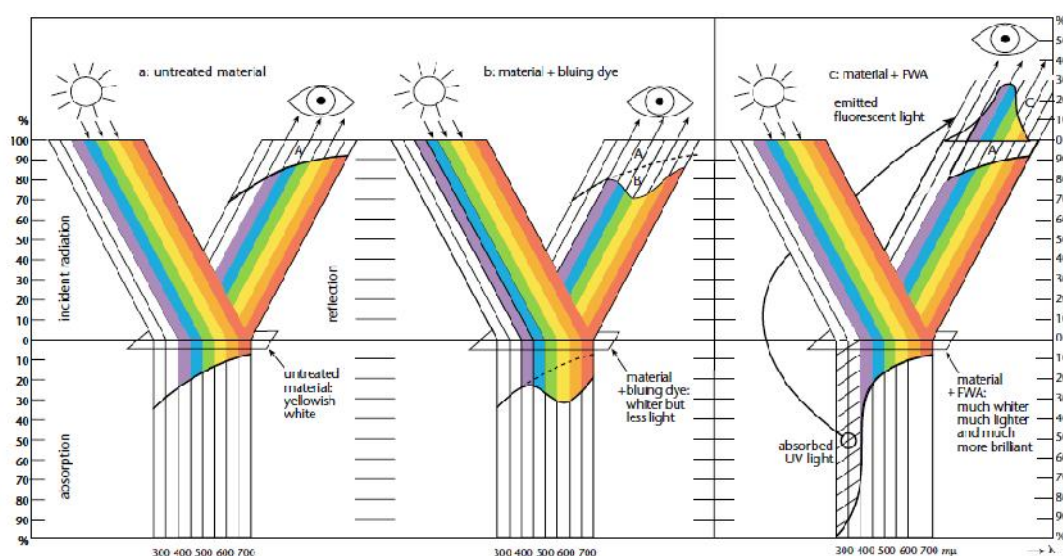


Figure 1.1 Principles of whiteness improvement [2]

Based on their chemical structures, there are several classes of FBAs available commercially. A review of related literatures are summarized below.

In 2003, Daniel A. Jervis [1] reported the use of a bis-benzoxazolyl-stilbene and a bis-benzoxazolyl-thiophene (**Figure 1.2**) as optical brighteners for thermoplastics due to their good stabilities at high-temperature of polymer processing. Moreover, this report suggested that the bis-benzoxazolyl-thiophene with flexible chain showed a better compatibility with polymer and dissolved more easily in common solvents than the bis-benzoxazolyl-stilbene.

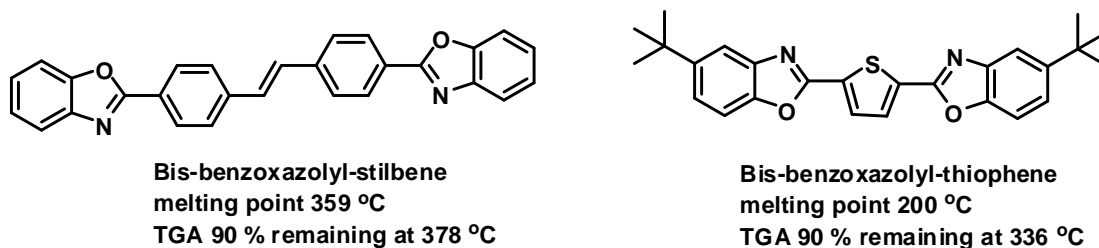


Figure 1.2 Commercial FBAs [1]

In 2005, Joon-Kyun Lee and co-workers [4] prepared 4,4'-bis(1,3,5-triazin-6-yl)diaminostilbene-2,2'-disulfonic acid derivatives, via a 7-step asymmetric synthesis in 75-89% yield from CI86. All products were used as water-soluble fluorescent brighteners and could performed better than CI86 itself.

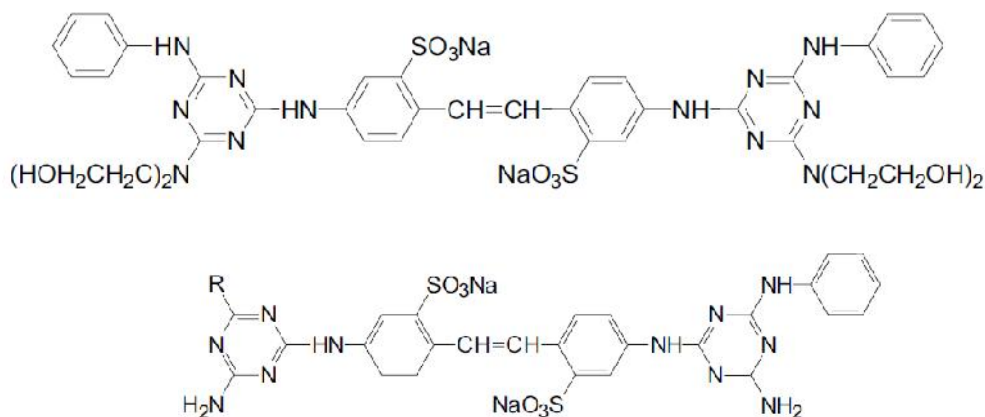


Figure 1.3 CI86 structure (top) and example of synthesized compound R = 4-OMe-phenyl-NH- (bottom) [4]

Titanium dioxide (TiO_2) and zinc oxide (ZnO) can also be used as brighteners but the mechanism is different from FBAs because TiO_2 and ZnO only reflect the light. Therefore, they are often used together with FBAs to enhance whitening efficiency [5]. Organic brighteners generally contain several aromatic rings or double bond conjugation (**Figure 1.4**), for example Tinopal CBS [6], benzenesulfonic acid derivatives [7] and stilbene derivatives [8]. Recently, stilbene derivatives [8] were coupled with 3-aminopropyltrimethoxy silane which can be applied easily as coating material. They compounds could convert harmful UV light into harmless visible light.

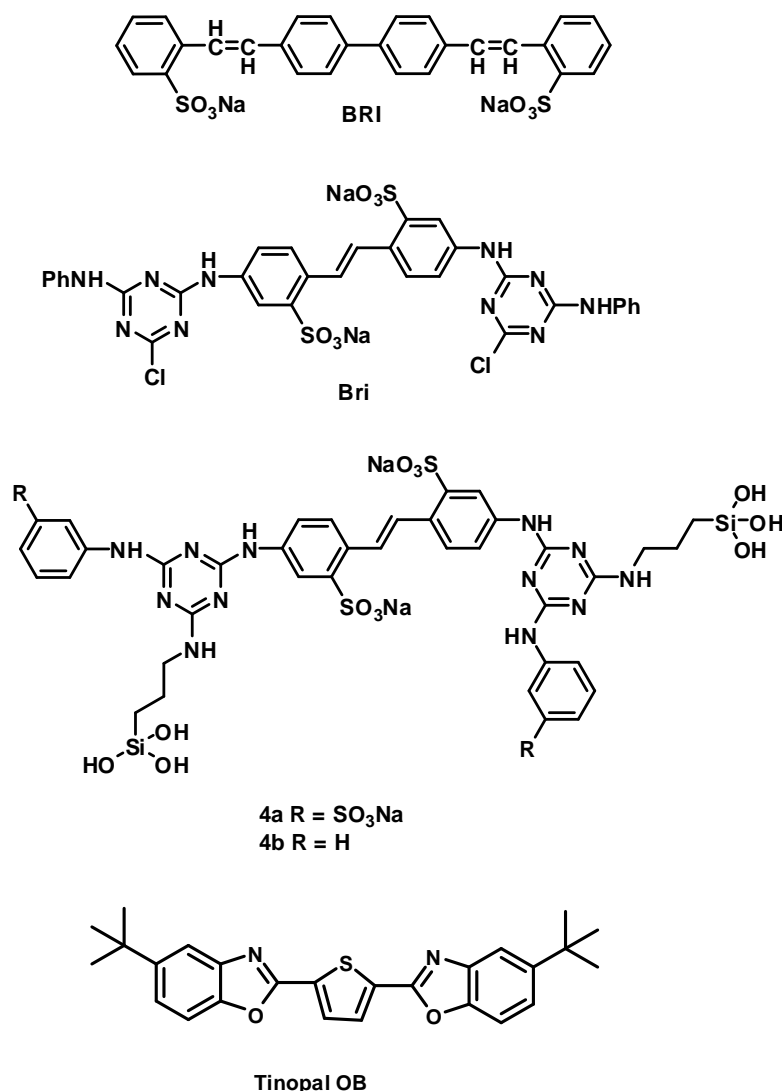


Figure 1.4 Example FBAs organic compounds BRI [6] Bri [7] hybrid material [8] Tinopal OB

1.3 Basic fluorescence principle

To elaborate how FBAs work, Jablonski's diagram is used to demonstrate how the fluorescence process occurs (**Figure 1.5**). First of all, the high-energy photon from ultraviolet radiation is absorbed by fluorophore, for instance FBAs and other conjugated molecules. Subsequently, the electron of fluorophore is excited to a higher electronic state as governed by the selection rule. The excitons or the exciting electrons thus relax to the first excitation state (S_1) by internal conversion and vibrational relaxation. If the excitons relax from S_1 to ground state (S_0) and emit the light or photon energy, this process is called “fluorescence” and it usually occurs in a short period of time (around $10^{-9} - 10^{-7}$ s). However, several non-radiative processes can occur which called “quenching” due to the intensity of emitted light are usually lowered. On the other hand, the excitons at the S_1 state might flip their spins to reside in the excited triplet state (T_1) by a phenomena called “intersystem crossing”. When the triplet excitons relax their energy to ground state, this process is called “phosphorescence”, which has an emissive life-time longer than fluorescence process. For both fluorescence and phosphorescence, the emissive intensity is inversely proportional to the degree of vibrational and rotational relaxation. Therefore, compounds with higher molecular rigidity usually exhibit greater emissive efficiency [9-10].

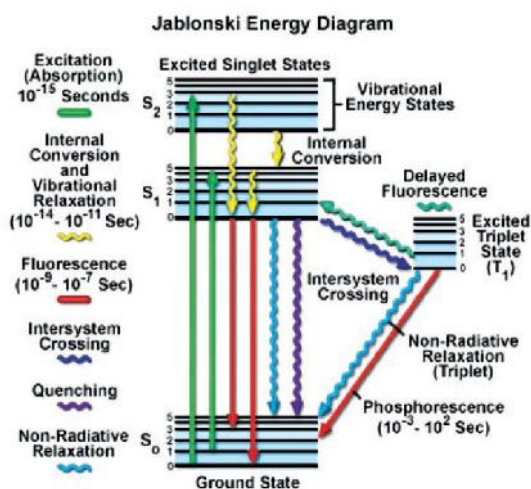


Figure 1.5 Jablonski energy diagram [10]

Nevertheless, the emissive efficiency can be altered by other factors such as electron donor and acceptor that leads to internal charge transfer (ICT) or photo-induced electron transfer (PET). Both processes are described below.

1.4. Internal Charge Transfer (ICT)

ICT process can subsequently occur in the fluorescence process as described by the Jablonski diagram in **Figure 1.6**. In this ICT process, the excited fluorophore changes from its first geometry (S_1) or locally excited state (LE) to ICT state by means of thermodynamic preference. After that, ICT excited state relaxes to the ICT ground state, then transform to the ground state (S_0). Since there are several steps occurring in the ICT process, the emissive photon or brightening efficiency will be reduced. In addition, the emissive wavelength after ICT process is usually longer or red shifted compared to the fluorescence emission because the ICT relaxation gap is narrower than that of fluorescence [11-12].

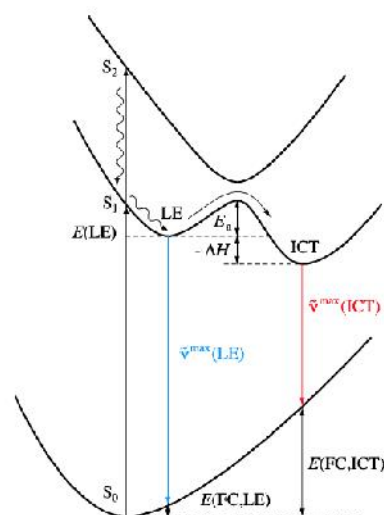


Figure 1.6 ICT process mechanism via Frank condon principle

Typically, the ICT process occurs in molecules with prominent electron delocalization from electron-donor to electron-acceptor moiety via conjugated π -system. In accordance with literature [13], this process is customarily used in fluorescent sensor application in which the fluorophore is adapted as auxochrome.

Besides, the review mentioned that the ICT process is boosted in polar solvent since the molecule can be converted into di-polar molecule which prefers the polar stabilization from solvent (**Figure 1.7**) [13-14]. As for application, Zhaochao Xu [15] synthesized compound **1** that can be moved its emissive radiation from green to red by Cu(II) ions (**Figure 1.8**). They proposed that **1** might be deprotonated by Cu(II) which the 4-N atom is converted to N⁻, promoted its electron donating ability. Thus, the stabilization is increased; the emission shifts to red region by increasing ICT.

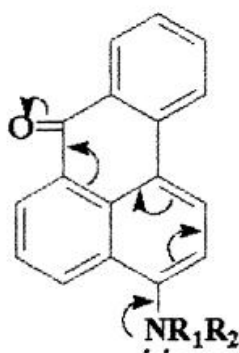


Figure 1.7 Example of electron delocalization [14]



Figure 1.8 1,8-Naphthalimide sensor via ICT process [15]

1.5. Photo-induced Electron Transfer (PET)

The PET process usually befalls in the molecule that contains electron-rich receptor, such as N lone pair (**Figure 1.9**). The electron-poor moiety (usually the excited fluorophore) can be granted the electron through space. As a result, the fluorescence

quantum efficiency is decreased because the relaxation of the PET exciton to the ground state is a more dominant process [16-17].

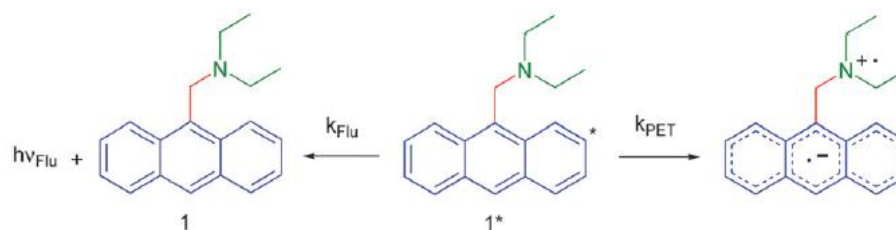


Figure 1.9 De-excitation route by PET mechanism [16]

To explain the PET process by molecular orbital energy diagram, the electron rich receptor provides HOMO (Highest Occupied Molecular Orbital) of the receptor is higher energy than HOMO of fluorophore; as a result, the PET process can occur due to its smaller gap compared with HOMO-LUMO gap of fluorophore. As seen in the **Figure 1.10**, the fluorescent emission can be salvaged by decreasing HOMO receptor when the receptor interacts with electron deficient analyte in sensor application.

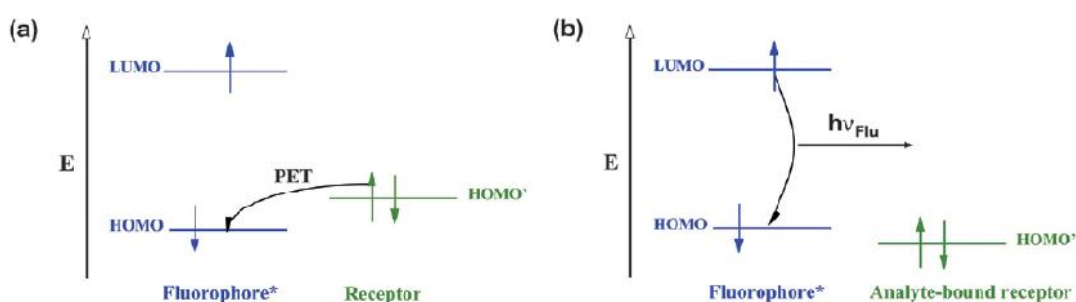


Figure 1.10 The description of PET process by energy diagram in case (a) free (b) coupled with analyte [16]

Regarding to the PET process, it is required that the spacer between receptor and fluorophore should be short so that the electron can migrate easily. To inhibit the

PET process, the electron rich receptor must twist so that the electron could not be granted. Unlike the ICT, PET process does not shift the emissive wavelength due to the absence of geometrical change. Interestingly, the covalent bond between the receptor and fluorophore is not necessary. For instance, fluorophore **2** and receptor **3** were linked together by a supramolecular interaction to obtain PET process as shown in **Figure 1.11**.

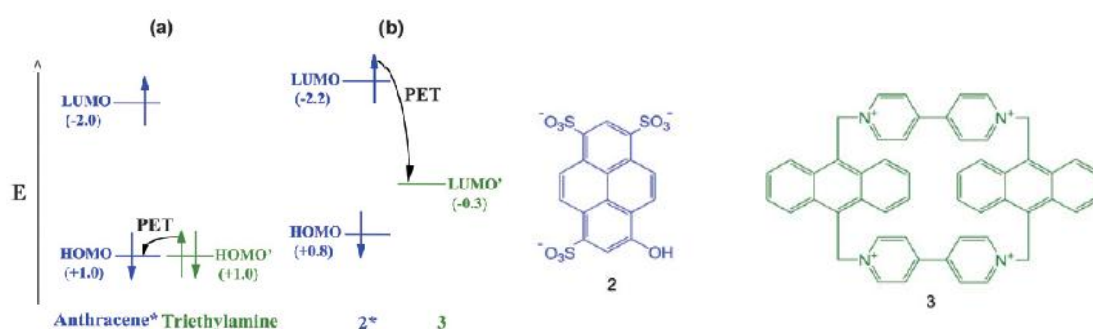


Figure 1.11 The relative energy diagram of compounds **2** and **3** [16]

From the **Figure 1.11**, another mechanism of PET process can be proposed as the exciton migration to the LUMO of the receptor first, then moves to the HOMO of the fluorophore. Thus, the fluorescent pathway is interrupted; and, the quantum efficiency is decreased.

Li-Juan Fan and coworkers [18] found that the quantum yield could be tuned by receptor moiety. *N, N, N'*-trimethylethylenediamino (TMEDA) moiety has a higher energy level than diethylamino moiety (DEA); as a result, DEA polymer quantum efficiency is higher than TMEDA polymer because DEA polymer has larger PET gap than that of TMEDA.

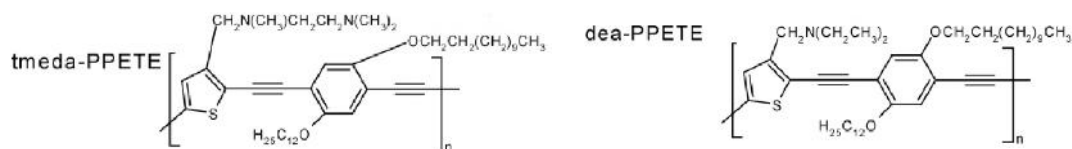


Figure 1.12 Structures of tmeda-PPETE and dea-PPETE [18]

The PET process is a versatile tool for the design and synthesis of new optical-chemosensors [19]. Recently, Balaraman and Danaboyina reported a series of

naphthalimide-based chemosensors [20]. They found that the long spacer provided poor binding constant; fortunately, it could clearly distinguish between Cu(II) and Zn(II) ions.

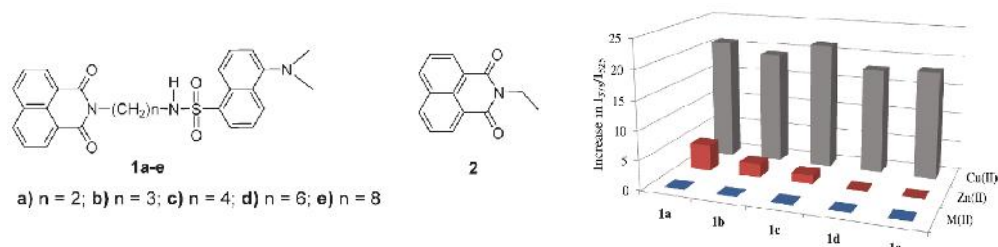
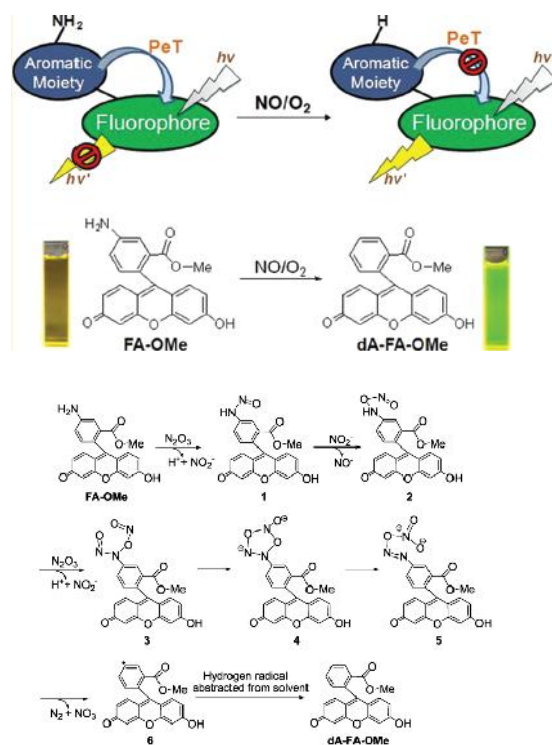


Figure 1.13 Synthesized sensor structures **1** and **2** with of the interference study, M(II): Pb^{2+} , Hg^{2+} , Co^{2+} , Fe^{2+} , Cd^{2+} , Mg^{2+} , Ba^{2+} at excitation 339 nm.

In 2012, Tsun-Wei Shive and co-workers [21] synthesized a nitric oxide sensor (**Scheme 1.1**). When the amino group on the sensor reacted with NO and O_2 to yield the deamination product, the PET process was then inhibited. This mechanism of fluorescent change was also confirmed by Density Functional Theory (DFT) calculation.



Scheme 1.1 Concept of nitric oxide sensor and proposed enhancing mechanism [21]

1.6. Fluorescent compounds from naphthalimides and their derivatives

1,8-Naphthalimide (**Figure 1.14**) can be obtained from the imidation of 1,8-naphthalic anhydride with a primary amine. This type of compound is usually called *N*-imide. In addition, the substituent can be placed using various coupling agents at the 4-position, for example, when an amine is used, 4-amino-1,8-naphthalimide which exhibit an ICT process can be obtained [22].

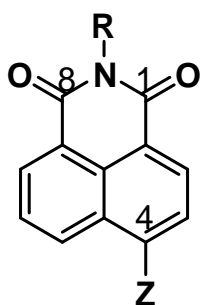


Figure 1.14 1,8-Naphthalimide structure

In past decade, a number of research on 1,8-naphthalimide were published. In 2000, Ivo Grabchev and Vladimir Bojinov [23] prepared a 1,8-naphthalimide fluorescent dye containing an isolated double bond and used it in a co-polymerization with acrylonitrile. The resulted copolymer could emit blue-green light, similar to the original fluorophores. Furthermore, the photo stability of the copolymers was found to be better than that of the blended polyacrylonitrile and 1,8-naphthalimide [23].

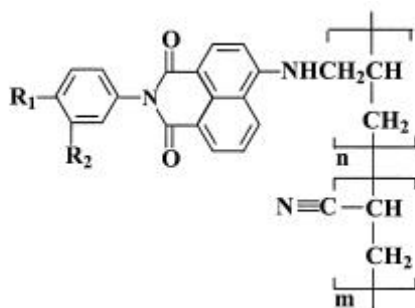


Figure 1.15 Poly(acrylonitrile)-*co*-1,8-naphthalimide dyes [23]

In 2012, Ugir Hossain Sk and co-workers [24] synthesized 1,8-naphthalimide consisting of thiourea, isothiocyanate or 3-nitro moiety that can be used as anti-melanoma tumor creation. Especially 3-nitro moiety and isothiocyanate group increased dramatically anti-tumor effect.

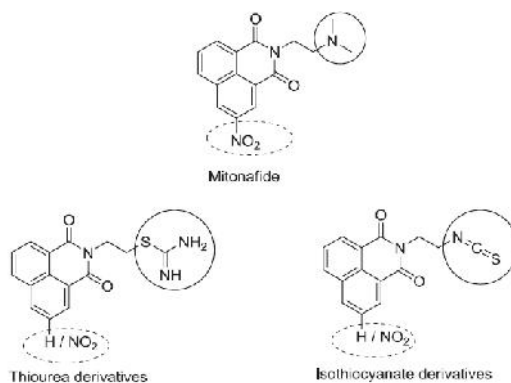


Figure 1.16 Anti-tumor 1,8-naphthalimide drugs [24]

Additionally, 3-nitro naphthalimide derivatives [25] and 4-amino naphthalimide derivative [26] were investigated and used as anti-hepato cellular carcinoma (HCC) agents. Both Shasha Li [27] and Xiaolian Li [28] found that naphthalimides containing triazole moiety can be used as anti-cancer drug.

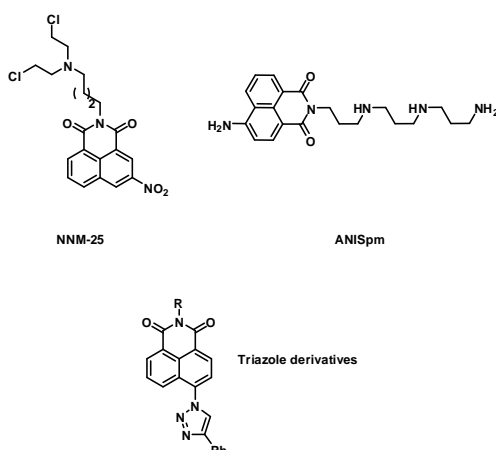


Figure 1.17 1,8-Naphthalimide drugs, such as NNM-25 [25], ANISpm [26] and triazole derivatives [28]

Interestingly, 1,8-naphthalimide derivative could be used as a UV-initiated precursor of sulfonic acid. Jean-Pierre Malval [29] found that fluorinated naphthalimide could generate sulfonic acid via 2 pathways as shown in **Figure 1.18**.

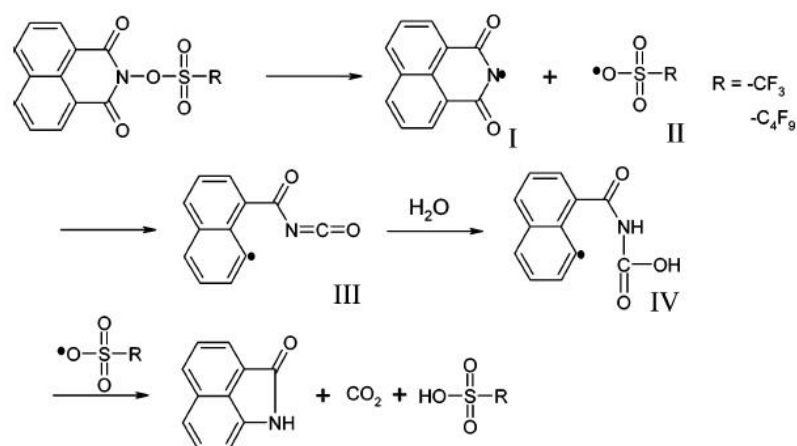


Figure 1.18 Acid generation of 1,8-naphthalimide derivatives [29]

In 2011, Nikolai I. Georgiev *et al.* [30] prepared 1,8-naphthalimide polyamidoamine and used as light harvesting material. They came across the fact that this compound could not show the expected FRET process (Forster Resonance Energy Transfer), in which the photon energy in the blue region is transferred to the 4-amino-1,8-naphthalimide. In fact, a PET process took place and the emission occurred less than expected. However, the photo stability was highly satisfied because of photostabilizing moiety, hindered amine light stabilizer.

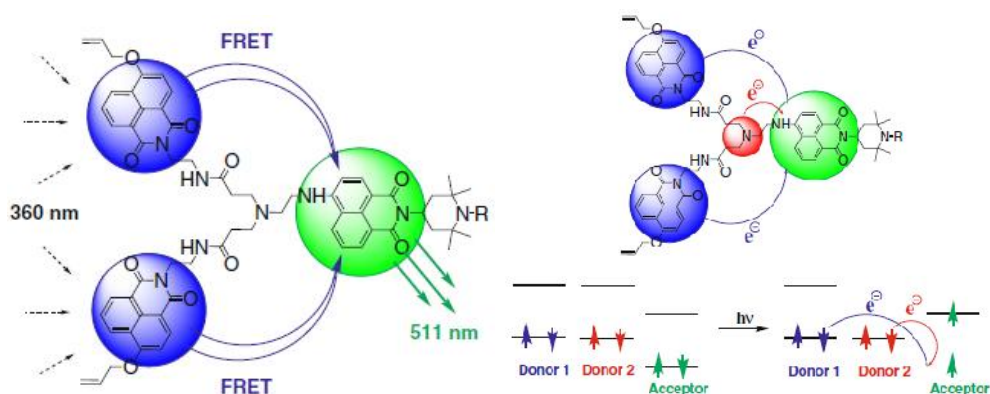


Figure 1.19 Expected mechanism (left) quenching mechanism (right) [30]

In 2009, Rita Ferreira and co-workers [31] synthesized 1,8-naphthalimide logic gate. When the F^- was added, the emission efficiency of 4-amino-1,8-naphthalimide could decrease, and showed NOR logic gate (**Fig 1.20**).

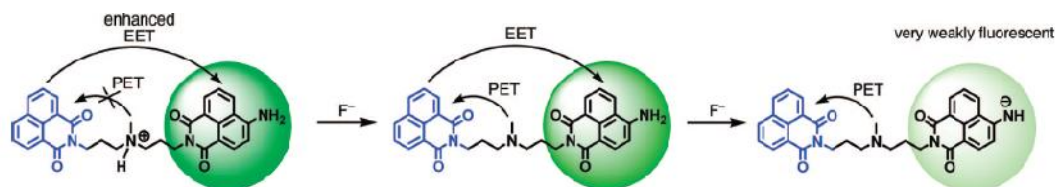


Figure 1.20 Proposed mechanism of in the presence of F^- [31]

1,8-Naphthalimide is also a very attractive building block for chemosensors. For instance, Lihua Jia *et al.* [32] have synthesized 4,5-diamino-1,8-naphthalimide derivatives. From the tested metal ions, the absorption wavelength shifted to red region when $Ag(I)$ ion was added, and the emission efficiency decreased when $Cu(II)$ ion was added.

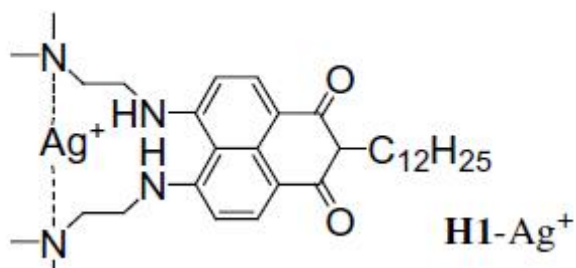


Figure 1.21 The color response of sensor [32]

Chen Hou *et al.* [33] synthesized 1,8-naphthalimide containing an aza-15-crown-5 ether. Its emission signal could be quenched and blue-shifted in the presence of Hg^{2+} . For the anion sensor, Veale and Laugsson [34] reported a thiourea derivative

that showed selective fluorescent quenching by F^- , CH_3COO^- and $H_2PO_4^-$ (**Figure 1.22**).

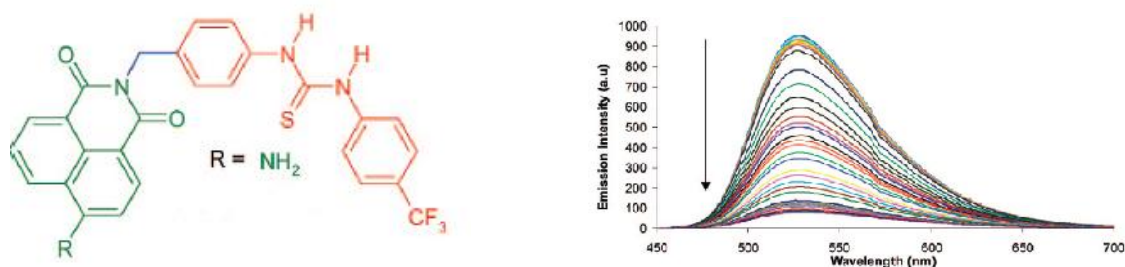


Figure 1.22 Anion sensor (F^-) from 1,8-naphthalimides [34].

Recently, a sensor based on dual process between PET and FRET for detection of Hg^{2+} and H^+ had been reported [35-36]. This concept improved the emission efficiency by compensated energy. (**Figure 1.23**)

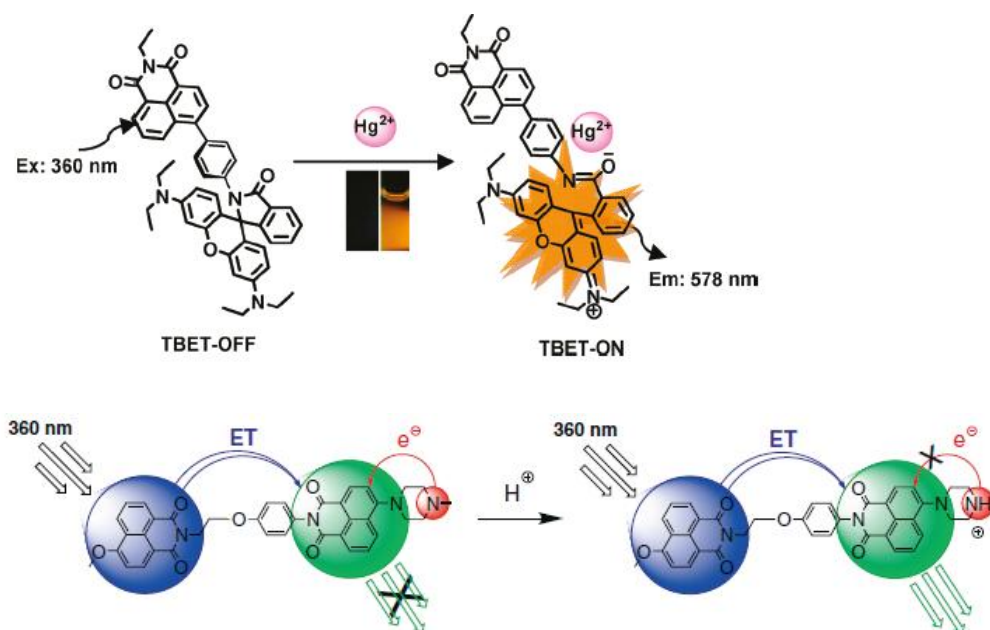


Figure 1.23 Hg^{2+} naphthalimide sensor [35] and H^+ [36]

Not only PET and FRET concept, Nikolai I. Georgiev and co-workers [37] designed a sensor based on a dual process between PET and ICT (**Figure 1.24**). A

devoid PET upon addition of acid caused the enhanced emission signal and the ICT process caused the absorption wavelength shift.

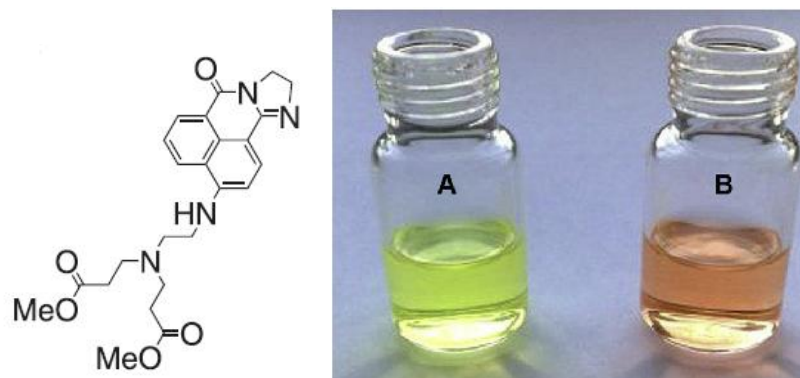


Figure 1.24 The color change from A to B when the acid was added [37].

In 2012, there was an investigation on quantum efficiency as results from PET process (**Figure 1.25**). It was found that **6** has higher quantum efficiency than **5** which indicated PET process is more pronounced in **5**. It was also reported that both **3** and **5** showed selective Cu^{2+} sensing by suppression of PET process [38].

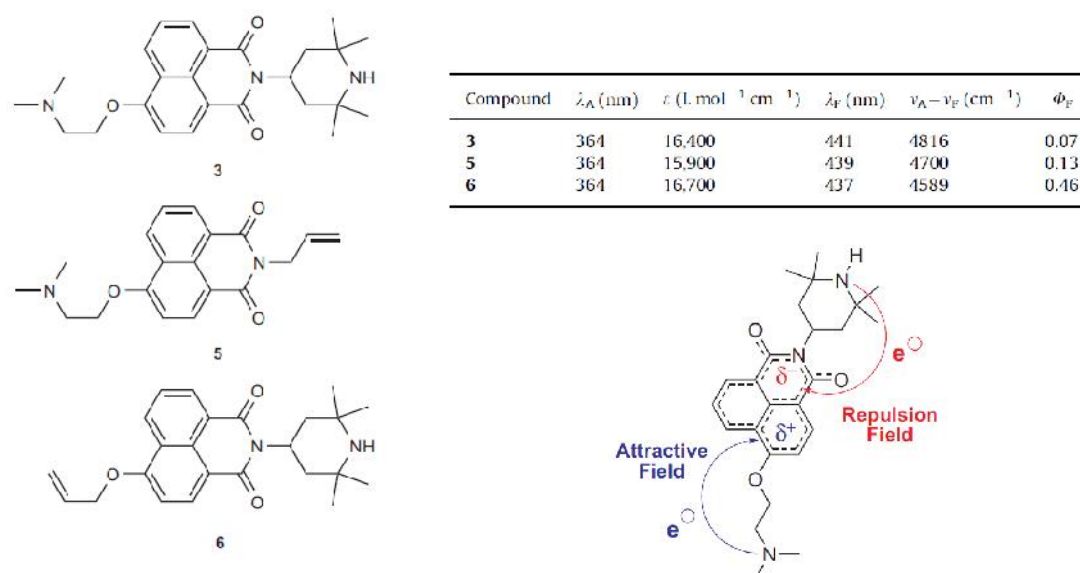


Figure 1.25 Compound **3**, **5** and **6** [38], their photophysical properties and proposed PET pathway [38]

Apart from chemosensor, 1,8-naphthalimide was widely used as LCD (Liquid Crystal Display) [39] and OLED (Organic Light-Emitting Diode) [40-41].

In 2010, Y. Wang and co-workers [40] synthesized 4-phenoxy-1,8-naphthalimide containing various position of *t*-butyl and found that the position of *t*-butyl slightly affect electrochemical property (**Figure 1.26**). However, the amount of *t*-butyl affect on both electrochemical property and quantum efficiency. The result noted that the aggregation occurs in thin film; fortunately, *t*-butyl group can solve this problem.

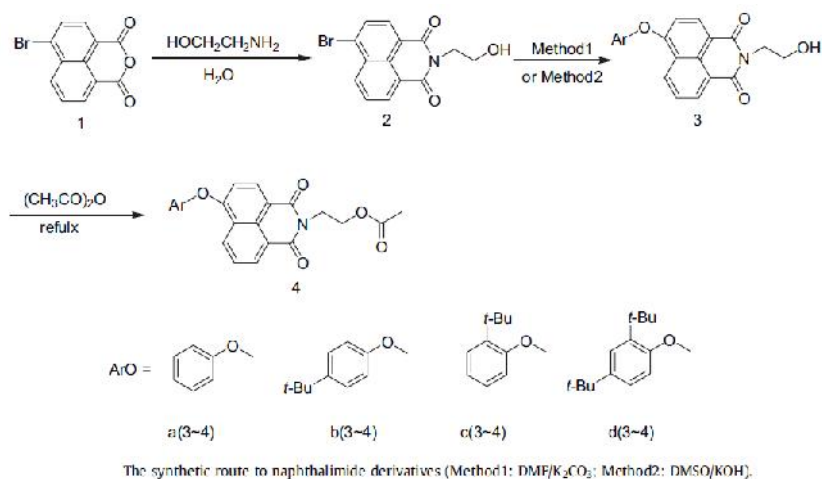


Figure 1.26 Structures of 1,8-naphthalimides prepared by Y. Wang *et al.* [40]

Literature reports on the use of 1,8-naphthalimides as fluorescent brighteners are very few. In 2001, 4-allyloxy-1,8-naphthalimide fluorescent brighteners were prepared with phase transfer catalyst (PTC) [42] (**Figure 1.27**). The suitability of the monomeric fluorescent brighteners for copolymerization with styrene was also demonstrated. The content of the chemically bound fluorescent brightener in the polymer chain was estimated.

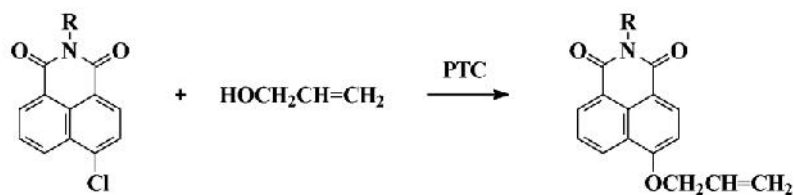


Figure 1.27 Synthesis of substituted 1,8-naphthalimide [42]

Ivo Grabchev *et al.* [43] prepared blue emissive polymer by copolymerization. Both 4-alkoxy and 4-allyloxy-1,8-naphthalimide showed high photo stability because blue emission of FBAs prevented the damage from harmful UV by changing to harmless blue emission.

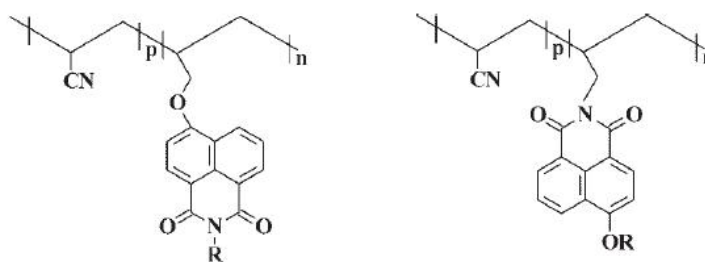


Figure 1.28 Blue emissive polymer [43]

1.7 Thermal stability

For applications with thermoplastic polymer, it is usually required that the FBA possesses high melting point in order to endure their photophysical properties under high temperature process such as molting process. **Figure 1.29** shows some examples of FBAs reported by Liu and co-workers [44]. These compounds absorb light of wavelength around 300-400 nm and emit blue light (400-500 nm.) with high quantum efficiencies. They are thermally stable as their 5% weight loss temperatures are well above 300 °C. These FBAs can be used in thermoplastic processing.

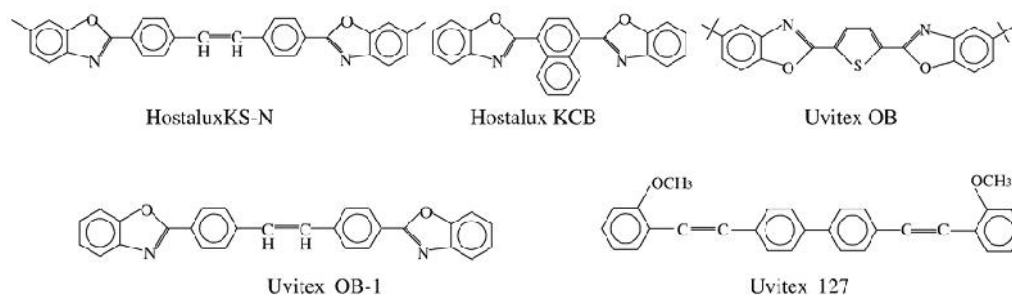


Figure 1.29 Structures of various FBAs reported by Liu and coworkers [44]

CHAPTER II

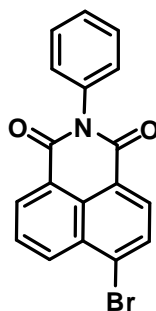
EXPERIMENTAL

2.1. Materials and chemicals

4-Bromo-1,8-naphthalic anhydride, 4-cumylphenol, 4Å molecular sieve, 2,6-diisopropyl aniline, acenaphthene, *N*-bromosuccinamide (NBS), 18-crown-6 were purchased from Sigma-Aldrich (USA) and used without purification. Phenol, 1-butanol, potassium hydroxide, potassium carbonate, and 4-methoxyaniline were purchased from Fluka (Switzerland) and used without purification. Tinopal OB - a standard commercial fluorescent brightener - was supplied by the PTT phenol company. Acetic acid and DMF were reagent grade purchased from Aldrich (USA). They were stored over 4Å molecular sieve with N₂ bubbling for 1 hour prior to use. Aniline was distilled under reduced pressure before use. Commercial *n*-hexane, ethyl acetate and methanol were fractionally distilled before use. The ¹H NMR was determined on Varian Mercury NMR spectrophotometer (Varian, USA) at 400 MHz with chemical shifts reported as ppm in CDCl₃. The ¹³C NMR was measured on Bruker Mercury NMR spectrophotometer (Bruker, Germany, which equipped at 100 MHz with chemical shifts reported as ppm in CDCl₃. To investigate their thermal properties, differential scanning calorimeter (DSC) 204 F1 Phoenix (Netzsch) was used to determine their glass transition temperature (T_g), melting temperature (T_m), and crystal temperature (T_c). UV-2550 UV-visible spectrophotometer (SHIMADZU, Japan) was used for absorption study. The fluorescence or emission spectra were acquired by Carry Eclipse Fluorescence Spectrophotometer (Agilent Technologies). Cyclic voltammograms were conducted on cyclic voltammetry instrument (Autolab). The thermal gravimetric analysis (TGA) experiments were conducted at the PTT Company in Wang-Noi, Ayutthaya.

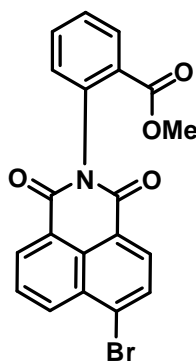
2.2. Synthesis

2.2.1. 4-Bromo-*N*-(phenyl)-1,8-naphthalimide (2a)

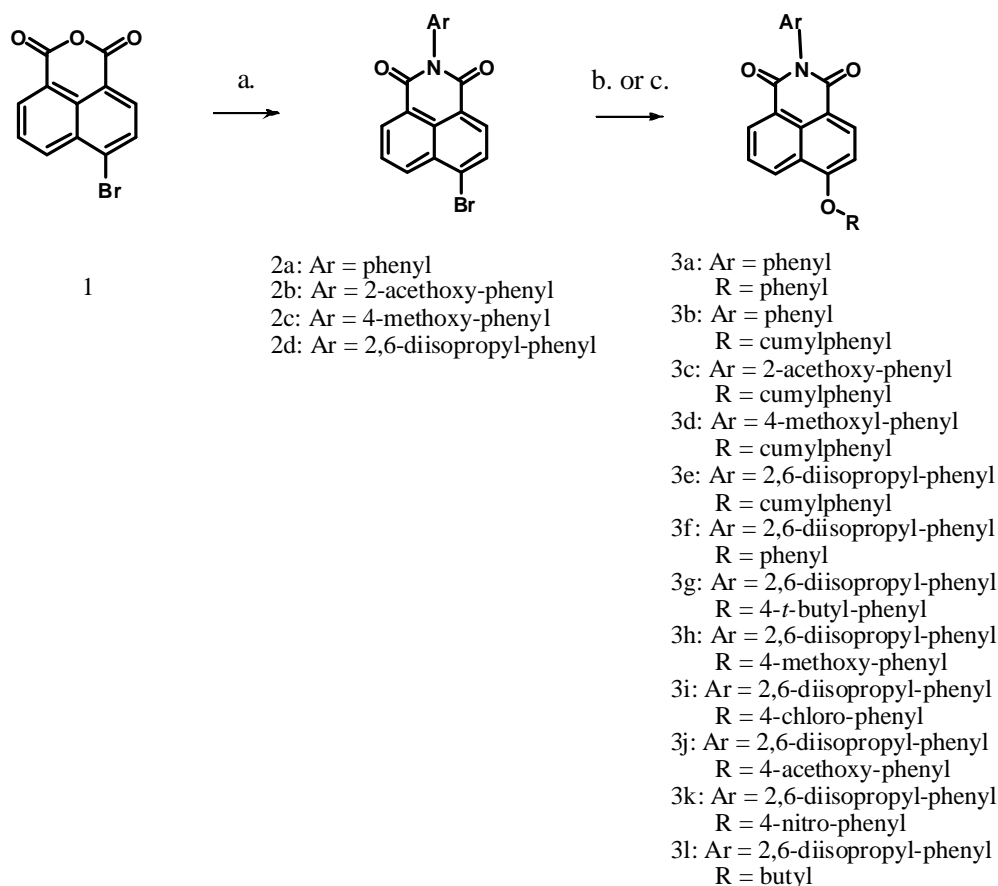


According to literature review [3], 4-bromo-1,8-naphthalic anhydride (**1**) (1.0 g, 1.07 mmol), 6 mL glacial acetic acid, and 4Å Molecular sieve (4Å MS) (10 g) were added into a round bottom flask. Then, aniline (0.16 mL, 0.16 g, 1.76 mmol) was added. The mixture was stirred and heated under refluxing conditions overnight. After the reaction mixture was allowed to cool to room temperature, the mixture was poured into 30 g of ice and the resulting precipitate was filtered, washed with cool water, and dried over a steam bath. The white powder was next purified by column chromatography using hexane/ethyl acetate (10:1) as the eluent to obtain **2a** as white crystalline solid (77%). ¹H NMR (CDCl₃) (ppm) 7.35 (d, *J* = 7.2 Hz, 2H), 7.50-7.64 (m, 3H), 7.90 (t, *J* = 8.0 Hz, 1H), 8.10 (d, *J* = 8.0 Hz, 1H), 8.48 (d, *J* = 8.0 Hz, 1H), 8.66 (d, *J* = 8.0 Hz, 1H), 8.73 (d, *J* = 8.0 Hz, 1H).

2.2.2. 4-Bromo-*N*-(2-acethoxy-phenyl)-1,8-naphthalimide (2b)

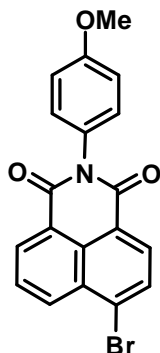


To prepare in a small scale [3], 4-bromo-1,8-naphthalic anhydride (**1**) (0.3 g, 1.20 mmol), 6 mL glacial acetic acid, 4Å Molecular sieve (4Å MS) (1 g) and methyl anthranilate (0.3 mL, 0.35 g, 2.32 mmol) were used. The synthesis of **2b** was conducted using the procedure described for **2a**. After a purification by column chromatography using hexane/ethyl acetate (4:1) as the eluent, **2b** was obtained as an off-white powder (53%). ¹H NMR (CDCl₃) (ppm): 3.70 (s, 3H), 7.40 (d, *J* = 8.0 Hz, 1H), 7.60 (t, *J* = 7.6 Hz, 1H), 7.75 (t, *J* = 7.6 Hz, 1H), 7.85 (t, *J* = 8.4 Hz, 1H), 8.08 (d, *J* = 7.6 Hz, 1H), 8.25 (d, *J* = 7.6 Hz, 1H), 8.45 (d, *J* = 8.0 Hz, 1H), 8.63 (d, *J* = 8.4 Hz, 1H), 8.69 (d, *J* = 8.4 Hz, 1H).



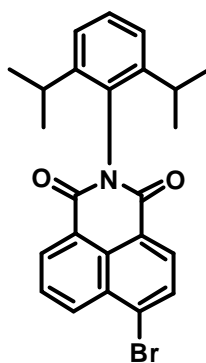
Scheme 2.1 Synthesis methods: (a) appropriate aniline, glacial acetic acid, reflux; (b) appropriate phenol or alcohol, KOH, 18-crown-6, DMF, 70 °C; (c) appropriate phenol or alcohol, K₂CO₃, DMF, 110 °C

2.2.3. 4-Bromo-*N*-(4-methoxy-phenyl)-1,8-naphthalimide (**2c**)



The synthesis of **2c** was conducted using the procedure described for **2b**. After a purification by column chromatography using hexane/ethyl acetate (4:1) as the eluent, **2c** was obtained as an off-white powder (56%). ^1H NMR (CDCl_3) (ppm): 3.80 (s, 3H), 7.00 (d, $J = 8.8$ Hz, 2H), 7.15 (d, $J = 8.8$ Hz, 2H), 7.80 (t, $J = 8.0$ Hz, 1H), 8.01 (d, $J = 8.0$ Hz, 1H), 8.39 (d, $J = 8.0$ Hz, 1H), 8.57 (d, $J = 8.0$ Hz, 1H), 8.64 (d, $J = 8.0$ Hz, 1H).

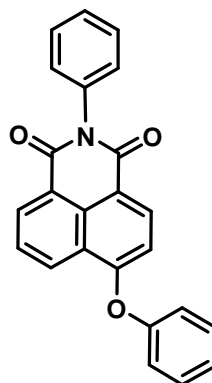
2.2.4. 4-Bromo-*N*-(2,6-diisopropyl-phenyl)-1,8-naphthalimide (**2d**)



The synthesis of **2d** was conducted using the procedure described for **2b**. After a purification by column chromatography using hexane/ethyl acetate (10:1) as the eluent, **2d** was obtained as an off-white powder (81%). ^1H NMR (CDCl_3) (ppm): 1.05 (d, 12H), 2.65 (m, 2H), 7.25 (d, $J = 7.6$ Hz, 2H), 7.42 (t, $J = 7.6$ Hz, 1H), 7.85 (t,

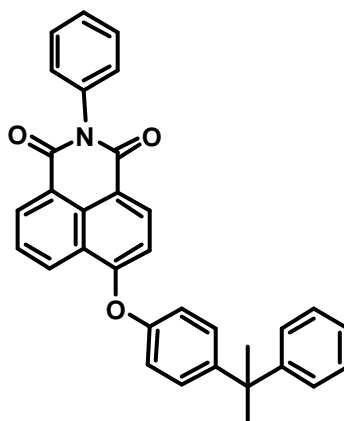
$J = 7.8$ Hz, 1H), 8.05 (d, $J = 8.0$ Hz, 1H), 8.40 (d, $J = 8.0$ Hz, 1H), 8.59 (d, $J = 7.8$ Hz, 1H), 8.66 (d, $J = 7.8$ Hz, 1H).

2.2.5. 4-Phenoxy-*N*-phenyl-1,8-naphthalimide (3a)



A mixture of **2a** (4.6 g, 12.99 mmol), phenol (2.5 g, 26.67 mmol), anhydrous potassium carbonate (5.4 g, 39.32 mmol) in DMF (200 mL) was heated and stirred at 120 °C 8 hours. The mixture was then poured into ice/water and the crude precipitate was collected by vacuum filtration and washed with water. After purification by column chromatography using hexane/ethyl acetate (10:1) as the eluent, **3a** was obtained as a pale powder solid (87%). ¹H NMR (CDCl₃) (ppm): 6.90 (d, $J = 8.4$ Hz, 1H), 7.16 (d, $J = 8.4$ Hz, 2H), 7.23 – 7.29 (m, 3H), 7.40 – 7.52 (m, 5H), 7.75 (t, $J = 8.4$ Hz, 1H), 8.45 (d, $J = 8.4$ Hz, 1H), 8.64 (d, $J = 8.4$ Hz, 1H), 8.72 (d, $J = 8.4$ Hz, 1H). ¹³C NMR (CDCl₃) (ppm): 110.7, 116.7, 120.8, 122.8, 124.1, 125.7, 126.6, 128.6, 128.9, 129.3, 130.4, 132.3, 133.2, 135.6, 154.8, 160.2, 163.9, 164.6

2.2.6. 4-Cumylphenoxy-*N*-(phenyl)-1,8-naphthalimide (3b): Method A

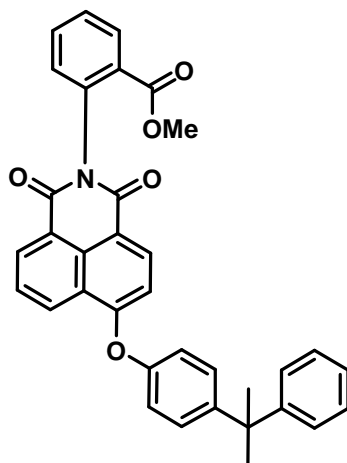


From patent [3], a mixture of **2a** (0.21 g, 0.59 mmol), 4-cumylphenol (0.25 g, 1.19 mmol), potassium hydroxide (0.05 g, 0.91 mmol), and 18-crown-6 (catalytic amount) in DMF (2 mL) was heated and stirred at 70°C overnight. The mixture was then poured into ice/water and the crude precipitate was collected by vacuum filtration and washed with water. After purification by column chromatography using hexane/ethyl acetate (4:1) as the eluent, **3b** was obtained as a pale powder solid (16%). ¹H NMR (CDCl₃) (ppm): 1.67 (s, 6H), 6.89 (dd, *J* = 7.6 Hz and 8.4 Hz, 1H), 7.04 (d, *J* = 8.4 Hz, 2H), 7.12 – 7.34 (m, 9H), 7.39 – 7.48 (m, 3H), 7.74 (t, *J* = 8.0 Hz, 1H), 8.42 (d, *J* = 8.0 Hz, 1H), 8.63(d, *J* = 8.0 Hz, 1H), 8.70 (d, *J* = 8.0 Hz, 1H). ¹³C NMR (CDCl₃) (ppm): 30.7, 42.8, 110.5, 116.5, 120.2, 122.7, 124.1, 125.9, 126.5, 126.8, 128.5, 128.6, 128.7, 129.3, 129.5, 130.0, 130.1, 130.3, 133.3, 148.4, 150.3, 152.4, 160.3, 164.6.

2.2.7. 4-Cumylphenoxy-*N*-(phenyl)-1,8-naphthalimide (**3b**): Method B (General procedure)

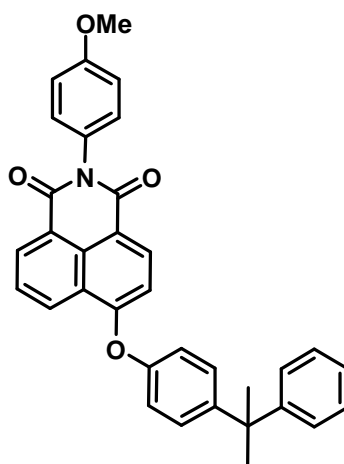
A mixture of **2a** (2.6 g, 7.39 mmol), 4-cumylphenol (3.24 g, 15.26 mmol), anhydrous potassium carbonate (3.03 g, 21.91 mmol) in DMF (120 mL) was heated and stirred at 110 °C overnight. The mixture was then poured into ice/water and the crude precipitate was collected by vacuum filtration and washed with water. After purification by column chromatography using hexane/ethyl acetate (10:1) as the eluent, **3b** was obtained as a pale powder solid (66%).

2.2.8. 4-Cumylphenoxy-*N*-(2-acethoxy-phenyl)-1,8-naphthalimide (**3c**)



2b (0.26 g, 0.64 mmol), 4-cumylphenol (0.37 g, 1.76 mmol), anhydrous potassium carbonate (0.53 g, 3.82 mmol) in DMF (10 mL) was heated and stirred to obtain **3c** was obtained as a pale powder solid (20%). ^1H NMR (CDCl_3) (ppm): 1.75 (s, 6H), 3.70 (s, 3H), 6.95 (d, $J = 8.0$ Hz, 1H), 7.10 (d, $J = 8.0$ Hz, 2H), 7.20 – 7.40 (m, 9H), 7.57 (t, $J = 8.0$ Hz, 1H), 7.73 (t, $J = 8.0$ Hz, 1H), 7.80 (t, $J = 8.0$ Hz, 1H), 8.24 (d, $J = 8.0$ Hz, 1H), 8.49 (d, $J = 8.0$ Hz, 1H), 8.68 (d, $J = 8.0$ Hz, 1H), 8.76 (d, $J = 8.0$ Hz, 1H). ^{13}C NMR (CDCl_3) (ppm): 30.9, 42.8, 52.1, 110.5, 116.6, 120.2, 122.8, 124.2, 125.9, 126.4, 128.2, 128.7, 128.9, 130.3, 130.7, 131.9, 132.1, 133.1, 133.6, 136.7, 148.3, 150.2, 152.5, 160.4, 164.8

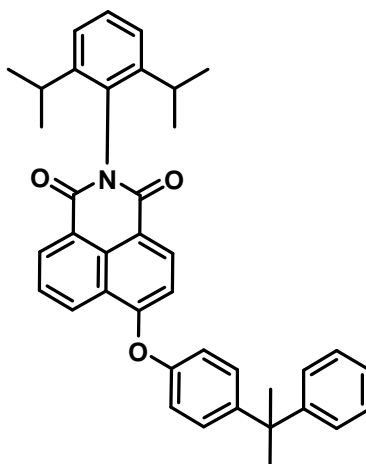
2.2.9. 4-Cumylphenoxy-*N*-(4-methoxy-phenyl)-1,8-naphthalimide (**3d**)



4-bromo-*N*-(4-methoxy-phenyl)-1,8-naphthalimide (**2c**) was used instead of **2b** to obtain **3d** was obtained as a yellow powder solid (91%). ^1H NMR (CDCl_3) (ppm): 1.74 (s, 6H), 3.87 (s, 3H), 6.95 (d, $J = 8.4$ Hz, 1H), 7.06 (d, $J = 8.8$ Hz, 2H), 7.11 (d, $J = 8.8$ Hz, 2H), 7.20 – 7.40 (m, 9H), 7.82 (t, $J = 8.4$ Hz, 1H), 8.50 (d, $J = 8.4$ Hz, 1H), 8.70 (d, $J = 8.4$ Hz, 1H), 8.76 (d, $J = 8.4$ Hz, 1H). ^{13}C NMR (CDCl_3) (ppm): 30.9, 55.5, 110.5, 114.7, 120.2, 125.9, 126.5, 126.7, 128.2, 128.8, 128.9, 129.6, 132.3, 133.2, 148.4, 152.5, 159.5.

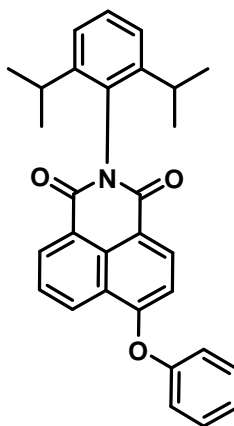
2.2.10. 4-Cumylphenoxy-*N*-(2,6-diisopropyl-phenyl)-1,8-naphthalimide

(**3e**)



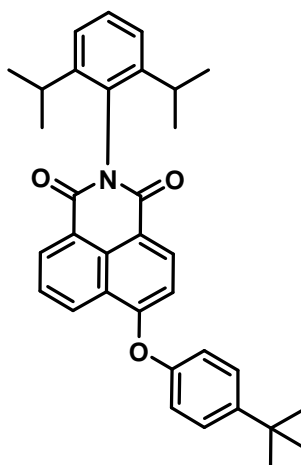
4-bromo-*N*-(2,6-diisopropyl-phenyl)-1,8-naphthalimide (**2d**) was used instead of **2b** to obtain **3e** was obtained as a white powder solid (89%). ^1H NMR (CDCl_3) (ppm): 1.08 (d, 12H), 1.67 (s, 6H), 2.67 (m, 2H), 6.80 - 7.30 (m, 12H), 7.39 (t, $J = 8.4$ Hz, 1H), 7.75 (t, $J = 8.4$ Hz, 1H), 8.45 (d, $J = 8.4$ Hz, 1H), 8.64 (d, $J = 8.4$ Hz, 1H), 8.70 (d, $J = 8.4$ Hz, 1H), ^{13}C NMR (CDCl_3) (ppm): 24.0, 29.2, 30.9, 42.9, 110.7, 114.8, 120.2, 125.9, 126.8, 128.2, 128.9, 129.4, 132.4, 133.4, 145.8, 148.4, 150.3, 152.6, 160.3, 163.8, 164.5.

2.2.11. 4-Phenoxy-*N*-(2,6-diisopropyl-phenyl)-1,8-naphthalimide (**3f**)



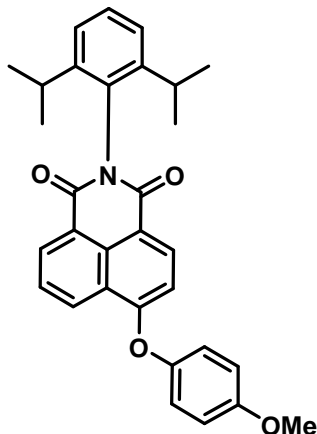
Use phenol instead of 4-cumylphenol. And, 4-bromo-*N*-(2,6-diisopropylphenyl)-1,8-naphthalimide (**2d**) was used instead of **2b** to obtain **3f** was obtained as a white powder solid (79%). ¹H NMR (CDCl₃) (ppm): 1.20 (d, 12H), 2.80 (m, 2H), 7.00 (d, *J* = 8.0 Hz, 1H), 7.25 (d, *J* = 7.6 Hz, 2H), 7.36 (d, *J* = 7.6 Hz, 3H), 7.53 (dd, *J* = 6.4 Hz and 7.6 Hz, 3H), 7.85 (t, *J* = 8.0 Hz, 1H), 8.57 (d, *J* = 8.0 Hz, 1H), 8.77 (d, *J* = 8.0 Hz, 1H), 8.83 (d, *J* = 8.0 Hz, 1H). ¹³C NMR (CDCl₃) (ppm): 14.2, 24.0, 29.3, 110.9, 115.4, 116.7, 120.8, 122.8, 124.3, 125.7, 126.7, 128.9, 129.5, 130.5, 131.1, 132.5, 133.4, 145.8, 155.0, 160.2, 163.8, 164.5.

2.2.12. 4-(4-*tert*-butyl-phenoxy)-*N*-(2,6-diisopropylphenyl)-1,8-naphthalimide (3g)



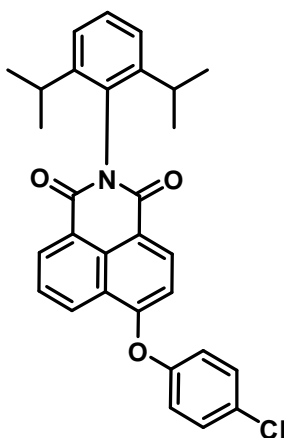
A mixture of **2d** (0.11 g, 0.25 mmol), 4-*tert*-butylphenol (0.09 g, 0.57 mmol), anhydrous potassium carbonate (0.14 g, 0.99 mmol) in DMF (6 mL) was heated and stirred to obtain **3g** was obtained as a pale powder solid (78%). ¹H NMR (CDCl₃) (ppm): 1.16 (d, 12H), 1.39 (s, 9H), 2.75 (m, 2H), 7.00 (d, *J* = 8.4 Hz, 1H), 7.25 (d, *J* = 8.0 Hz, 2H), 7.32 (d, *J* = 8.0 Hz, 2H), 7.45 – 7.55 (m, 3H), 7.85 (t, *J* = 8.4 Hz, 1H), 8.52 (d, *J* = 8.4 Hz, 1H), 8.73 (d, *J* = 8.4 Hz, 1H), 8.80 (d, *J* = 8.4 Hz, 1H). ¹³C NMR (CDCl₃) (ppm): 24.0, 29.1, 31.5, 34.6, 110.5, 116.4, 120.2, 122.7, 124.0, 124.2, 126.5, 127.3, 128.9, 129.4, 130.4, 131.0, 132.4, 133.4, 133.6, 145.7, 148.7, 152.4, 160.4, 163.8, 164.4

2.2.13. **4-(4-methoxy-phenoxy)-*N*-(2,6-diisopropyl-phenyl)-1,8-naphthalimide (3h)**



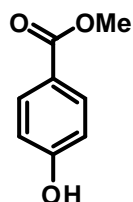
3h was collected as a pale powder (81%). ^1H NMR (CDCl_3) (ppm): 1.15 (m, 12H), 2.74 (m, 2H), 3.88 (s, 3H), 6.90 (d, $J = 8.4$ Hz, 1H), 7.00 (d, $J = 9.2$ Hz, 2H), 7.15 (d, $J = 9.2$ Hz, 2H), 7.32 (d, $J = 7.6$ Hz, 2H), 7.45 (t, $J = 7.6$ Hz, 1H), 7.83 (t, $J = 8.4$ Hz, 1H), 8.50 (d, $J = 8.4$ Hz, 1H), 8.70 (d, $J = 8.4$ Hz, 1H), 8.80 (d, $J = 8.4$ Hz, 1H). ^{13}C NMR (CDCl_3) (ppm): 24.0, 29.1, 55.7, 109.8, 115.5, 116.2, 122.0, 122.7, 123.9, 126.5, 128.9, 129.4, 130.4, 131.1, 132.4, 133.4, 145.7, 147.9, 157.4, 161.0, 163.8, 164.4

2.2.14. **4-(4-chloro-phenoxy)-*N*-(2,6-diisopropyl-phenyl)-1,8-naphthalimide (3i)**



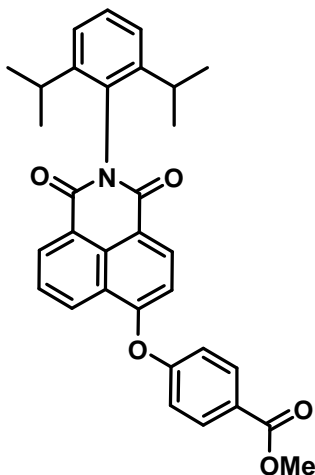
Use 4-chlorophenol instead of 4-*tert*-butyl-phenol to obtain **3i** was obtained as a white powder solid (96%). ^1H NMR (CDCl_3) (ppm): 1.13 (s, 12H), 2.72 (m, 2H), 6.95 (d, $J = 8.0$ Hz, 1H), 7.16 (d, $J = 8.4$ Hz, 2H), 7.32 (d, $J = 8.4$ Hz, 2H), 7.46 (d, $J = 8.4$ Hz, 3H), 7.84 (t, $J = 8.0$ Hz, 1H), 8.50 (d, $J = 8.0$ Hz, 1H), 8.65 – 8.75 (m, 2H). ^{13}C NMR (CDCl_3) (ppm): 24.0, 29.1, 111.0, 117.2, 121.9, 122.8, 124.0, 124.2, 126.8, 128.6, 129.4, 130.4, 130.5, 130.9, 132.5, 133.1, 145.7, 153.6, 159.6, 163.6, 164.3

2.2.15. Methyl 4-hydroxybenzoate (**4**)



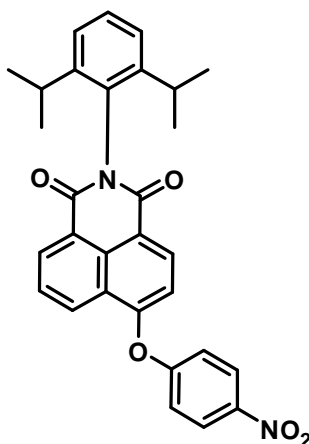
The 4-hydroxybenzoic acid (0.3 g, 2.38 mmol) was dissolved in methanol (13 mL). And then, concentrated sulfuric acid was added as catalyst. Next, the solution mixture was refluxed and mixed for 2 days. After that, the solution was evaporated and dispersed in ethyl acetate. And, saturated sodium carbonate was added into the reaction mixture. The organic solvent was evaporated. **4** was obtained. ^1H NMR (CDCl_3) (ppm): 3.90 (s, 3H), 6.50 (br, 1H), 6.90 (d, 2H), 7.95 (d, 2H).

2.2.16. 4-(4-acethoxy-phenoxy)-*N*-(2,6-diisopropyl-phenyl)-1,8-naphthalimide (**3j**)



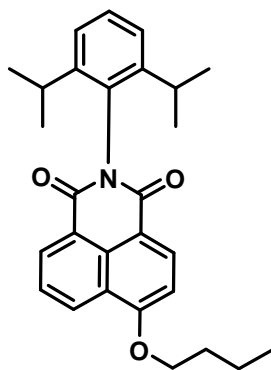
Use methyl 4-hydroxybenzoate instead of 4-*tert*-butyl-phenol to obtain **3j** was obtained as a yellow powder solid (19%). ^1H NMR (CDCl_3) (ppm): 1.15 (d, 12H), 2.74 (m, 2H), 3.95 (s, 3H), 7.10 (d, $J = 8.4$ Hz, 1H), 7.20 (d, $J = 8.8$ Hz, 2H), 7.33 (d, $J = 7.6$ Hz, 2H), 7.48 (t, $J = 7.6$ Hz, 1H), 7.85 (t, $J = 8.4$ Hz, 1H), 8.15 (d, $J = 8.8$ Hz, 2H), 8.57 (d, $J = 8.4$ Hz, 1H), 8.70 (d, $J = 8.4$ Hz, 1H), 8.74 (d, $J = 8.4$ Hz, 1H). ^{13}C NMR (CDCl_3) (ppm): 24.0, 29.1, 52.3, 112.8, 117.9, 119.5, 122.9, 124.0, 124.6, 127.0, 128.6, 129.5, 130.4, 130.8, 132.2, 132.6, 133.0, 145.7, 158.5, 159.5, 163.6, 164.2, 166.2

2.2.17. 4-(4-nitro-phenoxy)-*N*-(2,6-diisopropyl-phenyl)-1,8-naphthalimide (3k)



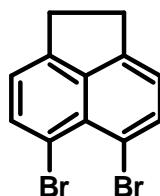
Use methyl 4-nitrophenol instead of 4-*tert*-butyl-phenol to obtain **3k** was obtained as a yellow powder solid (8%). ^1H NMR (CDCl_3) (ppm): 1.10 (d, 12H), 2.68 (m, 2H), 7.10 (d, $J = 8.0$ Hz, 1H), 7.27 (d, $J = 7.6$ Hz, 2H), 7.40 (t, $J = 8.0$ Hz, 1H), 7.80 (t, $J = 7.6$ Hz, 1H), 8.20 – 8.30 (m, 4H), 8.52 (d, $J = 8.0$ Hz, 1H), 8.56 (d, $J = 8.0$ Hz, 1H), 8.68 (d, $J = 8.0$ Hz, 1H). ^{13}C NMR (CDCl_3) (ppm): 24.0, 29.2, 114.4, 119.1, 119.2, 119.3, 123.0, 124.0, 124.8, 126.2, 126.4, 127.4, 128.3, 129.6, 130.5, 130.7, 132.7, 132.8, 145.7, 157.1, 161.3, 163.4, 164.0

2.2.18. 4-Butoxy-*N*-(2,6-diisopropyl-phenyl)-1,8-naphthalimide (3l)



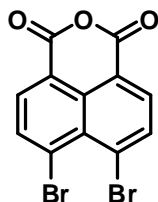
A mixture of **2c** (0.14 g, 0.38 mmol) and K_2CO_3 (0.40 g, 2.92 mmol) was refluxed in n-butanol (7.0 mL, 5.67 g, 76.5 mmol). After the evaporation of solvent and purification by column chromatography, **3e** was obtained as white solid in 76%. 1H NMR ($CDCl_3$) (ppm): 1.07 (t, 3H), 1.15 (d, 12H), 1.65 (m, 2H), 2.00 (m, 2H), 2.75 (m, 2H), 4.43 (m, 2H), 7.08 (d, $J = 8.0$ Hz, 1H), 7.26 – 7.33 (m, 2H), 7.49 (t, $J = 7.4$ Hz, 1H), 7.50 (t, $J = 7.6$ Hz, 1H), 8.61 (d, $J = 8.0$ Hz, 1H), 8.67 (d, $J = 7.6$ Hz, 2H). ^{13}C NMR ($CDCl_3$) (ppm): 13.8, 19.4, 24.0, 29.1, 31.0, 105.9, 114.8, 122.5, 123.9, 125.9, 129.0, 129.3, 130.1, 132.0, 134.1, 145.8, 160.7, 164.0, 164.6

2.2.19. 5,6-dibromoacenaphthene (**5**)



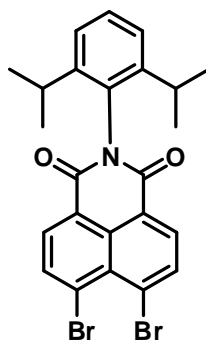
First of all, acenaphthene (4.2 g, 26.94 mmol) was dissolved completely in DMF. Next, *N*-bromosuccinamide (NBS) (16.5 g, 92.87 mmol) was put in small flask and dissolved in DMF. Then, acenaphthene solution and NBS solution was cooled in ice bath that its temperature did not above 5 °C. When the both solutions was cold, NBS solution had been added in acenaphthene solution for 5 hours. After that, the reaction mixture had been stirred at the same temperature for 6 hours. To precipitate crude product, mixture was kept at room temperature. Crude product was filtered and refluxed in ethanol 4 hours. Ethanol suspension was filtered. The solid (**5**) was collected (17%). 1H NMR ($CDCl_3$) (ppm): 3.30 (t, 4H), 7.10 (d, 2H), 7.80 (d, 2H) [45].

2.2.20. 4,5-dibromo-1,8-naphthalic anhydride (**6**)



5,6-dibromoacenaphthene (0.4 g, 1.24 mmol) and potassium dichromate (2.4 g, 7.99 mmol) was added in sealed tube [46]. Acetic acid (15 mL) was poured and refluxed in the tube. To oxidize at the benzylic carbon, the solution color was changed from orange to dark green [47-48]. Then, iced was added and green precipitate was filtered. Because of contaminating chromate salt, precipitate was dispersed in warm 1 M sodium hydroxide (60 mL). To dissolve contaminating salt, dilute hydrochloric acid was added until acidic condition was detected [49-50]. The resulting solid was filtered, dried on steam bath and used without purification. FTIR (cm^{-1}): 1219.8, 1310.4, 1312.3, 1355.7, 1451.2, 1547.6, 1592.9, 1718.3, 1765.9

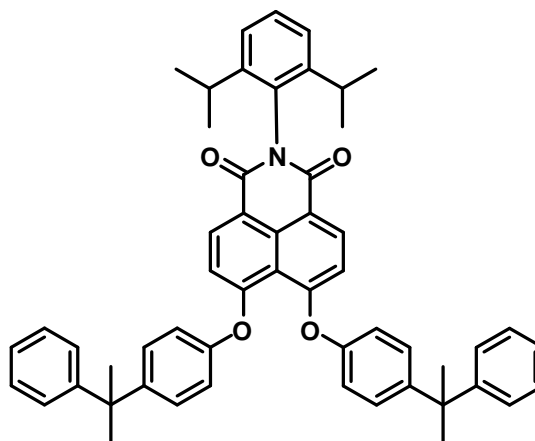
2.2.21. 4,5-dibromo-*N*-(2,6-diisopropyl-phenyl)-1,8-naphthalimide (**2e**)



5,6-Dibromo-1,8-naphthalic anhydride (**6**) (0.4 g, 1.24 mmol), 6 mL glacial acetic acid, and 4Å Molecular sieve (4Å MS) (1 g) were added into a round bottom flask. Then, 2,6-diisopropylaniline (0.35 mL, 0.33 g, 1.85 mmol) was added. The mixture was stirred and heated under refluxing conditions overnight. After the reaction mixture was allowed to cool to room temperature, the mixture was poured into 30 g of ice and the black precipitate was filtered, washed with cool water, and dried over a steam bath. The black powder was next purified by column chromatography that used hexane/dichloromethane (1:1) as the eluent to obtain **2e** as

black crystalline solid (11%). $^1\text{H NMR}$ (CDCl_3) (ppm): 1.14 (d, 12H), 2.65 (m, 2H), 7.30 (d, $J = 8.0$ Hz, 2H), 7.50 (t, $J = 7.6$ Hz, 1H), 8.30 (d, $J = 7.6$ Hz, 2H), 8.48 (d, $J = 8.0$ Hz, 2H).

2.2.22. 4,5-dicumylphenoxy-*N*-(2,6-diisopropyl-phenyl)-1,8-naphthalimide (3m)



2e (0.07 g, 0.14 mmol), cumylphenol (0.25 g, 1.18 mmol), anhydrous potassium carbonate (0.12 g, 0.90 mmol) in DMF (3 mL) was heated and stirred at 110 °C overnight. The ice was then poured into mixture and the crude precipitate was obtained by vacuum filtration and washed with water. After purification by column chromatography using hexane/ethyl acetate (10:1) as the eluent, **3m** was obtained as a yellow solid (52%). $^1\text{H NMR}$ (CDCl_3) (ppm): 1.15 (d, 12H), 1.68 (s, 12H), 2.75 (m, 2H), 6.80 (d, $J = 8.4$ Hz, 4H), 7.10 (d, $J = 8.4$ Hz, 2H), 7.20 - 7.35 (m, 16H), 7.48 (t, $J = 8.4$ Hz, 1H), 8.60 (d, $J = 8.4$ Hz, 2H). $[\text{M}+\text{Na}]$ 800.3678

2.3. Photophysical test

2.3.1. Absorption

The stock solutions of each compound were prepared in CH_2Cl_2 at $10^{-3} - 10^{-5}$ M, then diluted to more than 5 different concentrations. To obtain the accurate result, all absorbance should not exceed 1.0 arbitrary unit (a.u.) because it gives non-linear effect that belong to Beer's law, $A = bc$ which A is absorbance, b is absorption coefficient and c is concentration. The molar absorptivity (ϵ) was obtained from the

slope of the calibration curve between concentration and absorbance. The λ_{max} was chosen from the wavelength that provides the highest absorbance.

2.3.2. Emission or Fluorescence

To collect the complete fluorescent spectra, all compounds were excited at 364 nm and started to collect at each 10 nm interval with a slit width of 5 nm to prevent the residual absorption band. In this work, the PMT was controlled at 595 volts.

2.3.3. Quantum yield

The quantum yield is the ratio of absorbed photons and emissive photons. In the other word, the quantum yield is the value that relates to their emission efficiency. In procedure, the quantum yield was measured between the absorbance of λ_{max} absorption and the sum of all fluorescent intensity at the same absorbance. Then, the gradient or slope from the plot of sum fluorescence intensity and absorbance of all compounds were calculated following the equation below, where Φ_x is quantum yield of the tested compound, Φ_{ST} is quantum yield of standard compound, and n is the refractive index of solvent. Quinine sulfate in 0.1 M H₂SO₄ with a quantum yield of 0.54 was used as the standard [51].

$$\Phi_x = \Phi_{\text{ST}} \left(\frac{\text{Grad}_x}{\text{Grad}_{\text{ST}}} \right) \left(\frac{n_{\text{ST}}^2}{n_x^2} \right)$$

2.4. Photostability test

The photostability of these compounds were tested under irradiation of the DMSO solutions by a UVA sunset (Hostalux, USA, 200 W/m²) for 4, 8, 24, and 48 hr.

2.5. Thermal stability test

The thermal stability was examined by differential scanning calorimeter (DSC) 204 F1 Phoenix (Netzsch) and a thermogravimetric analyzer available at the PTT Company in Wang-Noi, Ayutthaya.

2.6. Electronic test

To obtain cyclic voltammogram, the experiment was set up by utilizing Ag/0.01 M AgNO₃ as reference electrode, glassy carbon as working electrode and Pt wire electrode as counter electrode under nitrogen atmosphere. About sample preparation, all synthesized compounds and ferrocene (external standard) were dissolved in 0.1 M TBAPF₆ in acetonitrile, supporting electrolyte, to get the sample solutions whose concentration were controlled at 1 mM. All determinations of cyclic voltammograms were managed at 50 mV per second scan rate [44].

$$E_{\text{HOMO}} (\text{eV}) = -(E_{\text{onset oxidation at cathode}} - E_{1/2 \text{ ferrocene}} + 4.8)$$

$$E_{\text{HOMO}} (\text{eV}) = -4.8 - E_{\text{onset oxidation at cathode}} + E_{1/2 \text{ ferrocene}}$$

$$E_{\text{LUMO}} = E_{\text{HOMO}} + E_{\text{gap}}$$

$$E_{\text{gap}} = hc/\text{onset wavelength}$$

$$h = \text{plank's constant} = 6.626 \times 10^{-34} \text{ J.s}$$

$$c = 3 \times 10^8 \text{ m/s}$$

onset wavelength is the first longest absorption wavelength which molecule can absorb.

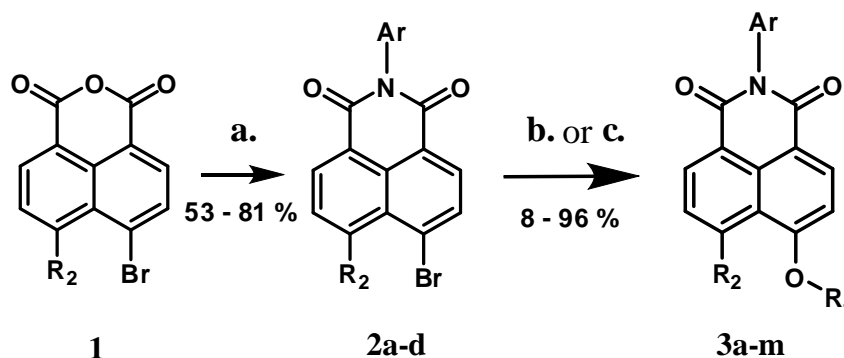
$$1 \text{ eV} = 1.602 \times 10^{-19} \text{ J}$$

CHAPTER III

RESULTS AND DISCUSSION

3.1. Synthesis and characterization

The synthesis of fluorescent brighteners was successfully conducted as shown in **Scheme 3.1**. The commercially available 4-bromo-1,8-naphthalic anhydride (**1**) was first reacted with appropriate anilines in glacial acetic acid to obtain 4-bromo-1,8-naphthalimides **2a-d**, which were then treated with *n*-butyl alcohol or various phenol derivatives in the presence of base and DMF to obtain **3a-3m**.



Scheme 3.1 Synthetic methods: (a) appropriate aniline, glacial acetic acid, reflux; (b) appropriate phenol or alcohol, KOH, 18-crown-6, DMF, 70 °C; (c) appropriate phenol or alcohol, K₂CO₃, DMF, 110 °C

The NMR characterizations of the synthesized compounds in this series are demonstrated using **3g** as the representative example (**Figure 3.1**). Starting from 4-bromo-1,8-naphthalic anhydride, reaction with excess 2,6-diisopropyl aniline gave rise to naphthalimide **2d**, and nucleophilic replacement of bromine afforded **3g** in good yield.

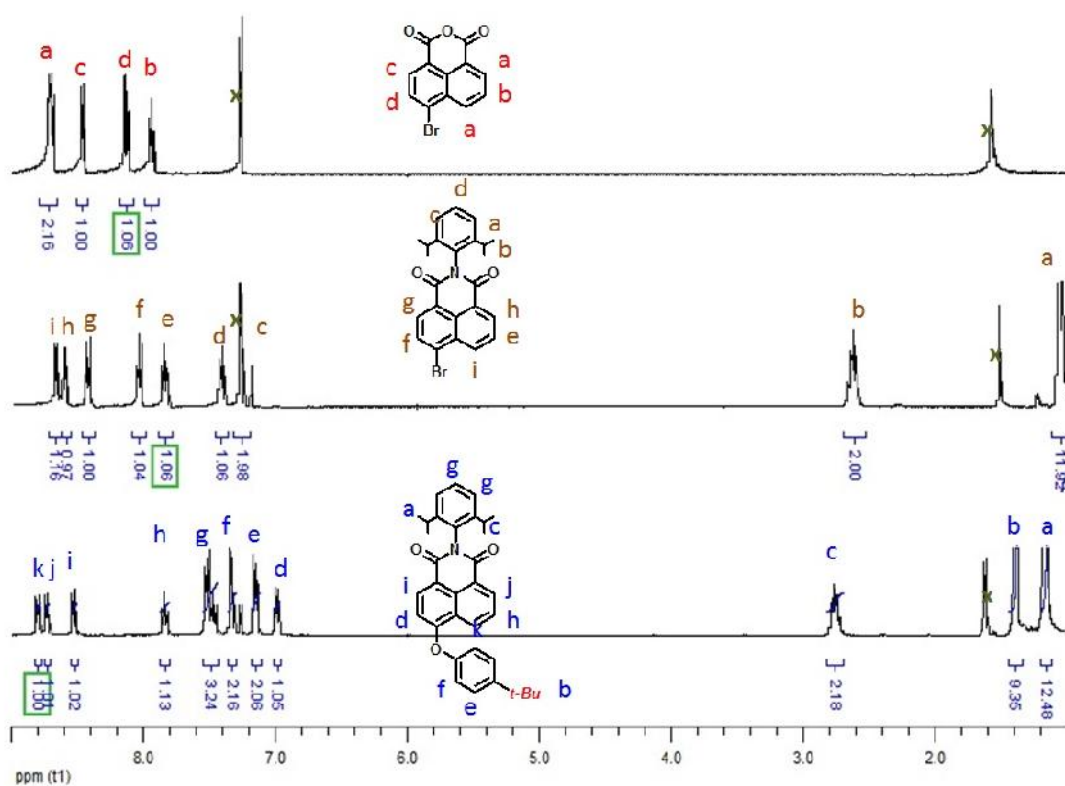


Figure 3.1 ^1H NMR spectra of 4-bromo-1,8-naphthalic anhydride or **1** (top), 4-bromo-*N*-(2,6-diisopropyl-phenyl)-1,8-naphthalimide (**2d**) (middle) 4-(4-*t*-butylphenoxy)-*N*-(2,6-diisopropyl-phenyl)-1,8-naphthalimide (**3g**) (bottom) in CDCl_3

From the ^1H NMR spectra, the reaction between 2,6-diisopropylaniline and 4-bromonaphthalic anhydride was successfully conducted as the signals of the aromatic proton on 2,6-diisopropylaniline moved upfield. Upon a substitution of the bromo group with a 4-*tert*-butylphenoxy group, the signal of the proton at the 3-position of naphthalimide moved from 8.05 (H_f of **2d**) to 7.00 ppm (H_d of **3g**) as a result of dramatic shielding by the aryloxy group.

It is worth noting that the substitution of the bromo group by phenoxy group using the patented condition [3] did not yield appreciable amount of the expected product. In many cases, the hydroxyl substituted was the major product. For examples, the reaction of **2a** and **2c** under the patented condition (Method A in the experimental part) exclusively resulted in the hydroxyl substituted products as shown

in **Figure 3.2**. This transformation had been reported by Parvizi and co-workers in the synthesis of 4-hydroxy-1,8-naphthalimide derivatives using hydroxide as the nucleophile [52-53].

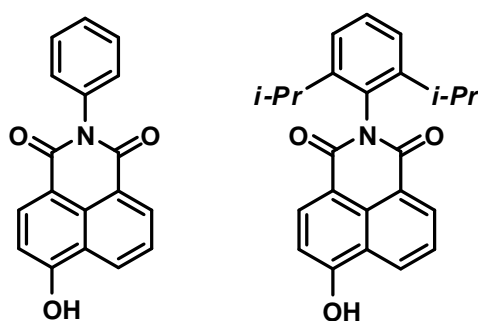
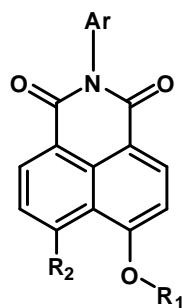


Figure 3.2 Structures of side products

To overcome this undesired result, KOH was replaced by a weaker and non-nucleophilic base – potassium carbonate. The use of weaker non-nucleophilic base required a higher reaction temperature, which resulted in a much greater yield of phenoxy substituted products (**3a-m**). The % yields show in **Table 3.1**.

Table 3.1 Structure of target naphthalimides**3a-m**

Compound	Ar	R ₁	R ₂	% Yield
3a	C ₆ H ₅	C ₆ H ₅	H	91
3b	C ₆ H ₅	4-Me ₂ PhC-C ₆ H ₄	H	66
3c	2-MeOOC-C ₆ H ₄	4-Me ₂ PhC-C ₆ H ₄	H	20
3d	4-MeO-C ₆ H ₄	4-Me ₂ PhC-C ₆ H ₄	H	91
3e	2,6-(<i>i</i> -Pr) ₂ -C ₆ H ₃	4-Me ₂ PhC-C ₆ H ₄	H	69
3f	2,6-(<i>i</i> -Pr) ₂ -C ₆ H ₃	C ₆ H ₅	H	79
3g	2,6-(<i>i</i> -Pr) ₂ -C ₆ H ₃	4-Me ₃ C-C ₆ H ₄	H	78
3h	2,6-(<i>i</i> -Pr) ₂ -C ₆ H ₃	4-MeO-C ₆ H ₄	H	81
3i	2,6-(<i>i</i> -Pr) ₂ -C ₆ H ₃	4-Cl-C ₆ H ₄	H	85
3j	2,6-(<i>i</i> -Pr) ₂ -C ₆ H ₃	4-MeOOC-C ₆ H ₄	H	19
3k	2,6-(<i>i</i> -Pr) ₂ -C ₆ H ₃	4-O ₂ N-C ₆ H ₄	H	8
3l	2,6-(<i>i</i> -Pr) ₂ -C ₆ H ₃	C ₄ H ₉	H	76
3m	2,6-(<i>i</i> -Pr) ₂ -C ₆ H ₃	4-Me ₂ PhC-C ₆ H ₄	<i>O</i> -4-Me ₂ PhC-C ₆ H ₄	52

In the case of reaction with electron withdrawing groups (**3c**, **3j** and **3k**) obtained low % yields because this groups generated poor nucleophile such as poor electron of phenoxide of **3j** and **3k**. So, the substitution of bromine occurred hardly that assumed this substitution reactions are poor.

3.2. Photophysical study

The photophysical properties of all compounds were investigated and described in terms of maxima absorption (λ_{max} absorption) and emission wavelengths (λ_{max} emission), absorption coefficient (ϵ) and fluorescent quantum yield (Φ). It was found that λ_{max} and ϵ of all compounds except **3m** are relatively similar as summarized in **Table 3.2**. Therefore, it could be implied that the Ar, R₁ and R₂ substituents did not significantly affected the π -conjugated system. The λ_{max} of **3m** appeared at a significantly longer wavelength of 380 nm. This may be rationalized by the effect of two electron-donating aryloxy groups present in **3m** which narrows the HOMO-LUMO gap of the compound as evident by the highest onset absorption wavelength at 450 nm.

For the emission properties, all compounds with the exception of **3m** could emit blue light (411-436 nm) upon excitation at their own maximum absorption wavelengths. In the other words, all of the synthesized compounds thus have the right emission wavelength to be used as fluorescent brightener.

To evaluate their emission efficiencies, the quantum yield experiments were conducted using solutions of each compound in CH₂Cl₂ with the absorbance below 0.1 to prevent concentration quenching. The gradients or slopes from the plots between sum of fluorescence intensity and absorbance were calculated by the equation below, where Φ_x is quantum yield of the tested compound, Φ_{ST} is quantum yield of the standard compound, and n is the refractive index of solution. Quinine sulfate in 0.1 M H₂SO₄ with a quantum yield of 0.54 was used as the standard [51].

$$\Phi_x = \Phi_{ST} \left(\frac{Grad_x}{Grad_{ST}} \right) \left(\frac{n_x^2}{n_{ST}^2} \right)$$

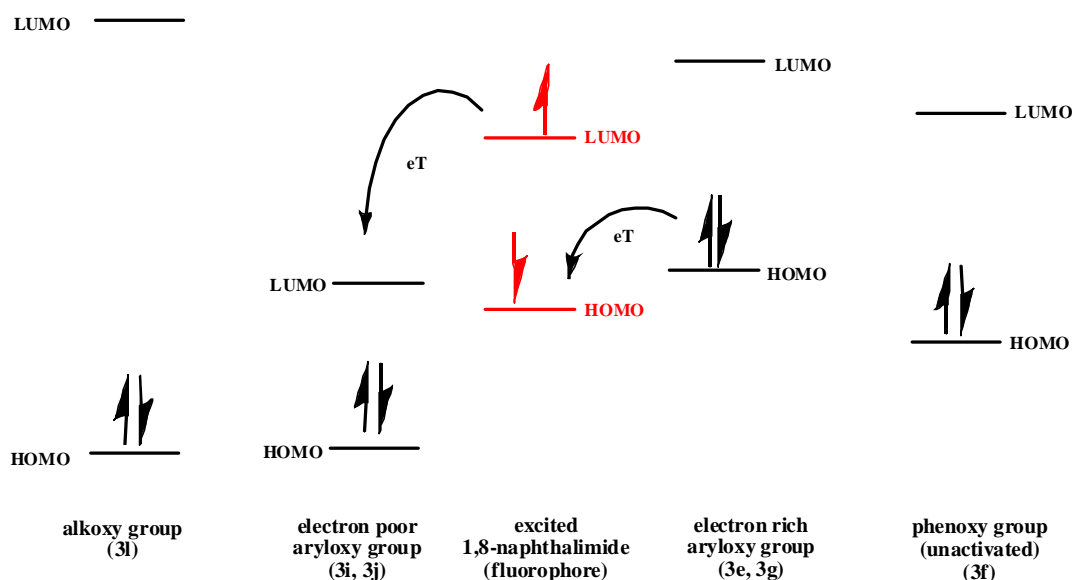
The quantum yields of all synthesized compounds were summarized in **Table 3.2**. Of all compounds synthesized in this study, **3l** exhibits the highest quantum yield of 0.95 indicating that the linear alkoxy group is a good substituent to be used on the naphthalimide fluorophore. Compound **3a** and **3f** displays quantum efficiencies of higher than 0.75 while **3i** and **3j** possess moderate efficiencies of higher 0.50. Interestingly, other compounds generally have poor quantum yields of 0.1 or below. The drastic differences in quantum yields for compounds in this class has been previously reported [40], but detailed explanation or supporting experiments has not yet been published.

Table 3.2 The photophysical properties of **3a-3h**

Compound	Absorption			Emission		Appearance under black light
	max (nm) ^a	onset (nm) ^a	log (M ⁻¹ cm ⁻¹) ^a	max (nm) ^b	^c	
3a	362	411	4.33	426	0.76	
3b	364	411	4.19	433	0.12	
3c	364	411	4.07	432	0.10	
3d	364	415	4.15	436	0.005	
3e	365	410	4.11	435	0.11	
3f	364	404	4.18	425	0.84	
3g	364	410	4.27	434	0.11	
3h	364	414	4.32	435	0.002	
3i	360	405	4.20	423	0.64	
3j	359	401	4.30	421	0.55	
3k	355	396	3.81	411	0.002	
3l	368	415	4.22	431	0.95	
3m	380	450	4.38	445	0.09	NA

[a] measured in diluted CH₂Cl₂ solution.[b] excited at 364 nm.

[c] determined by using quinine sulfate in 0.1 M H₂SO₄ as standard reference.



Scheme 3.2 The relative energy level of 1,8-naphthalimide with various substituents at the 4-position-aryloxy-1,8-naphthalimide

The Photo-induced Electron Transfer (PET) is postulated to be responsible for the variation in quantum efficiencies of this class of compounds. **Scheme 3.2** illustrates the relative energy level of 1,8-naphthalimide with various substituents at the 4-position-aryloxy-1,8-naphthalimide. In case **3i**, the energy gap of fluorophore lies between the large HOMO-LUMO gap of the alkoxy group (- *). So, the PET process should not be possible. This situation should be similar in the case of unactivated aryloxy group (**3f**); although, the HOMO-LUMO gap of the unactivated aryloxy group (- *) is much narrower because of resonance energy in conjugate compound.

In the case of electron rich substituents, the HOMO level of the aryloxy group is in between HOMO and LUMO of the fluorophore. Thus, the electron from HOMO level of the aryloxy group could transfer to HOMO of the fluorophore; and then,

follow by the migration from LUMO of the fluorophore to HOMO. In the other words, PET could occur which resulted in low quantum yield.

In contrast, the HOMO level of electron poor aryloxy group may not be in the HOMO-LUMO gap of the fluorophore, but the LUMO level of the aryloxy group might lie between HOMO-LUMO gap instead. The excited fluorophore can transfer electron to the LUMO of the aryloxy group, then back to the HOMO of the fluorophore. The above energy level diagram shows that the gap between $LUMO_{aryloxy}$ and $HOMO_{fluorophore}$ is larger than $HOMO_{aryloxy}$ and $HOMO_{fluorophore}$. Therefore, PET could occur strongly in the later case because the smaller energy gap could allow the process to take place easier [18].

For **3d**, **3h** and **3k** which exhibit extremely low quantum yields, it might be possible that Internal Charge Transfer (ICT) process also take place. Generally, ICT process can occur in 1,8-naphthalimide derivatives as depicted in **Figure 3.3**. However, the methoxy group could strongly donate electron through bond resulting in mediocre quantum yield [33]. Zhaochao Xu and co-workers [15] proposed that the increasing of donating power could enhance the ICT process. The resonance effect in compounds with a methoxy group (**3d** and **3h**) and a nitro group (**3k**) could promote the ICT process as described in **Figure 3.4**.

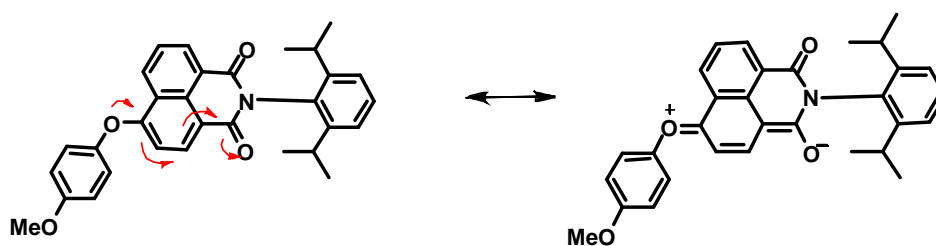


Figure 3.3 General ICT process in 1,8-naphthalimides

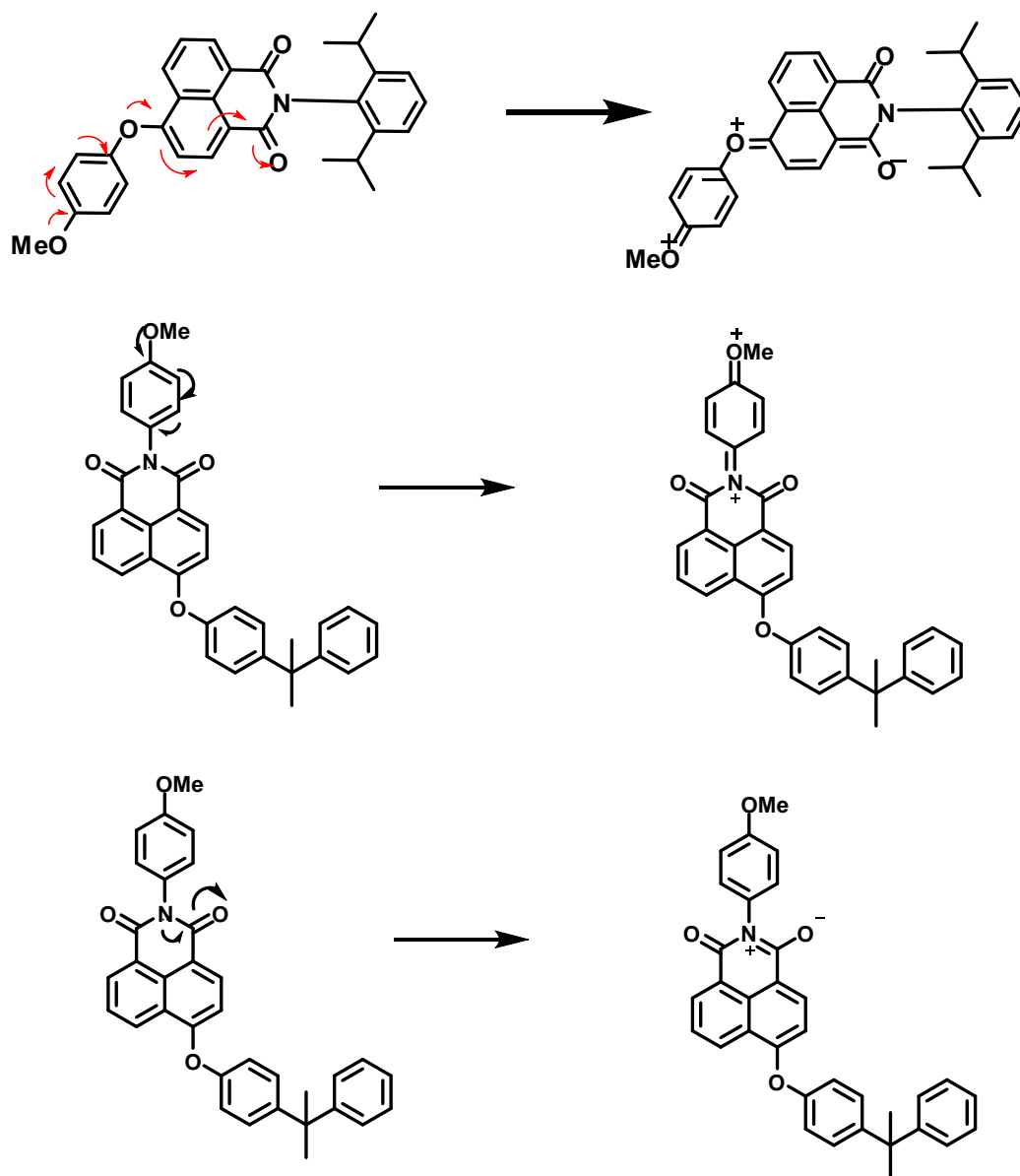


Figure 3.4 Proposed electron donating mechanism in **3d** and **3h** for synergistic ICT process

On the other hand, the ICT mechanism could also take place in **3k** which contains a nitro group at the 4-position. Its electron-withdrawing ability could facilitate the ICT process via mechanism shown in **Figure 3.5**.

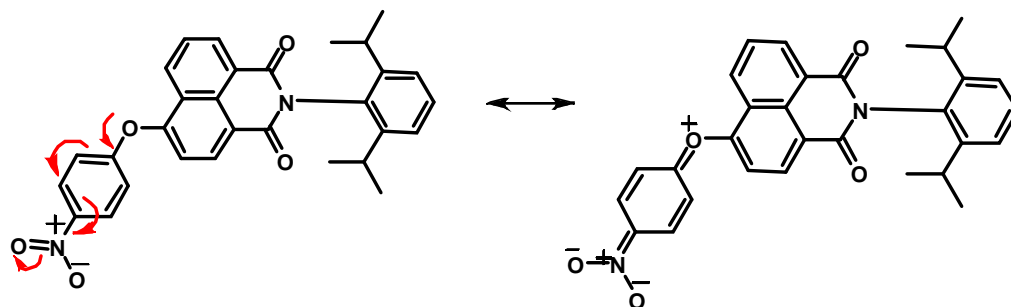


Figure 3.5 Proposed electron withdrawing mechanism in **3k** for synergistic ICT process

3.3. Photostability test

To demonstrate about photo stability (light fastness), the stability of compounds were tested by exposing 200 W/m^2 of UVA; and then, measured their absorbance in DMSO. After measuring, the absorbance of each time interval was divided with the absorbance of non exposing UVA (0 hours) and calculated into percentage to tabulate **Figure 3.6** as shown. The order of photostability or light fastness was **3l** > **3b** > **3e** > **3d** > **3f**. To explain this phenomenon, we have known that the order of quantum yield of sample compounds. The photostability trend is similar trend of quantum yield. Therefore, the bathochromic emission can reduce the harmful UV energy because it was changed into harmless blue region.

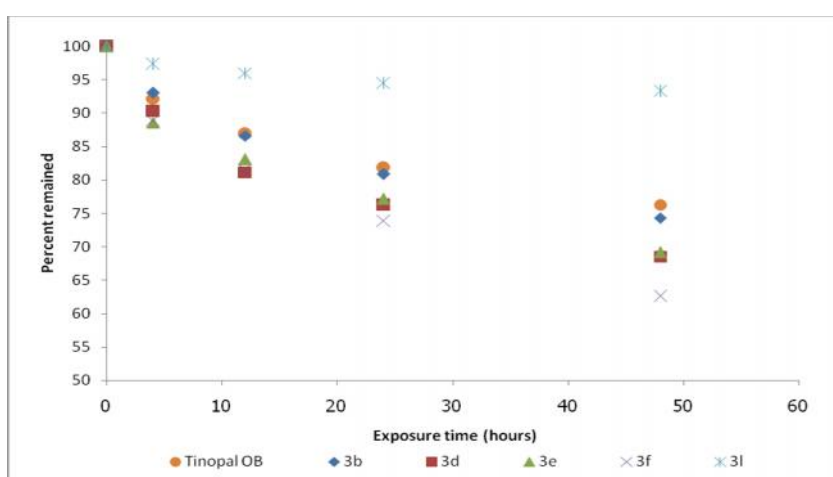


Figure 3.6 The remaining percentage of each compounds upon exposure to UVA

3.4. Thermal stability test

The Differential Scanning Calorimetry (DSC) was equipped for measuring their glass transition temperature (T_g), melting temperature (T_m), and crystal temperature (T_c). T_d of all compounds were obtained by PTT phenol research unit. In this case, our staff used **3b**, **3d**, **3e**, **3f** and **3l** to demonstrate their thermal stabilities. The results show in **Table 3.3** which represents 4-cumylphenoxy derivatives show excellent thermal stability due to their high pi-stack, hydrophobic interaction and aromaticity. So, the less pi-stacking molecules as **3f** and **3l** exhibit moderate and poor thermal stability from DSC measurement, respectively. **3e** is interesting compound because of its thermal stability. Only **3l**'s T_g did not observe due to their excellent decreasing pi-stack. So, **3l** form into glass transition hardly which it has poor dispersibility in plastic and polymer when prepared molten plastic and then the plastic was not good to use. In conclusion of this topic, the phenol moiety assists to enhance the decomposition temperature that the molecule hardly decompose when the compound was used in thermoplastic process [54-64].

Table 3.3 Thermal properties

Compound	T_d (°C) ^c	T_m (°C) ^a	T_g (°C) ^b	T_c (°C) ^a
3b	430	177	72	142
3d	430	242	72	112
3e	430	192	82	-
3f	375	218	83	-
3l	340	212	-	147
3m	425	90	75	-

^[a] and ^[b] obtained from DSC measurements on the first and second heating cycle with a heating rate of 10 °C per minute under N₂.

^[c] 10% decomposition temperature obtained from TGA measurement with a heat rate of 10 °C per minute under N₂.

3.5. Electrochemical analysis

For cyclic voltammogram, an electrochemical cell composed of a Ag/0.01 M AgNO₃ (reference electrode), glassy carbon (working electrode), and Pt wire electrode (counter electrode) was configured under nitrogen atmosphere. The tested compounds or ferrocene (external standard) were dissolved to 1 mM concentration in a solution of TBAPF₆ (0.1 M) in acetonitrile (supporting electrolyte). All determinations of cyclic voltammograms were managed at a scan rate of 50 mV per second [44]. Upon calculation methods described in the experimental part, the resulted energy levels of seven derivatives are shown in **Figure 3.7**.

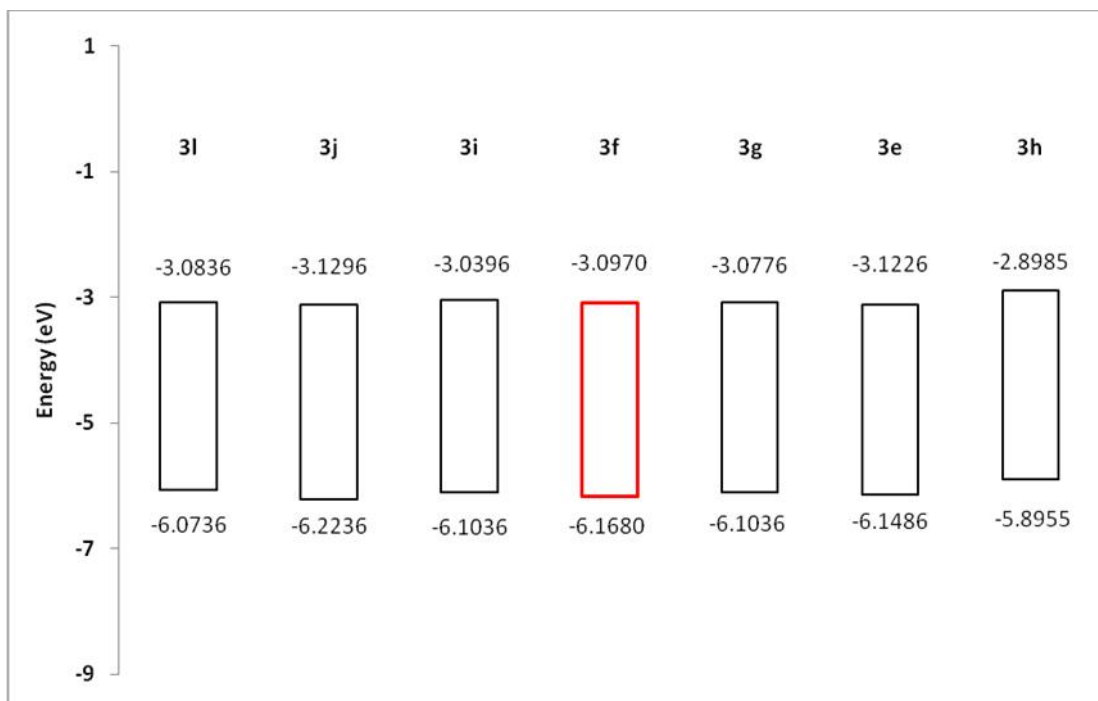


Figure 3.7 HOMO (bottom) and LUMO (top) energy levels of naphthalimides

The data verified that the seven naphthalimide derivatives have similar HOMO-LUMO energy levels, which corresponded to the fact that all of them could emit fluorescent signal in the 425-435 nm ranges. Thus, it could be implied that the substituents at the 4-position could slightly alter this energy level or the emission wavelength. However, they could affect the quantum efficiency by means of PET phenomenon.

CHAPTER IV

CONCLUSIONS

4.1. Conclusion

13 derivatives of *N*-aryl-1,8-naphthalimides were successfully synthesized from the commercially available 4-bromo-1,8-naphthalic anhydride. They were then subjected to a comparative evaluation of the photophysical properties, which revealed that all compounds could function as optical brightening agents since their absorption and emission wavelengths were in the range of 364 nm and 425 nm, respectively. All compounds exhibited good thermal stability as their glass transition temperatures were well above 350 °C, especially for those with the cumylphenoxy groups. For the photostability evaluation, all compounds could tolerate 200 watt per square meter of UVA light, relatively similar to that of commercial OBA Tinopal. Interestingly, the quantum efficiencies of these fluorophores exclusively depended on the substituents at the 4-positions, in which the alkoxy and phenoxy groups caused molecules to have high quantum yields, while the substituted aryloxy groups diminished the fluorescent intensity. Photo-induced electron transfer process

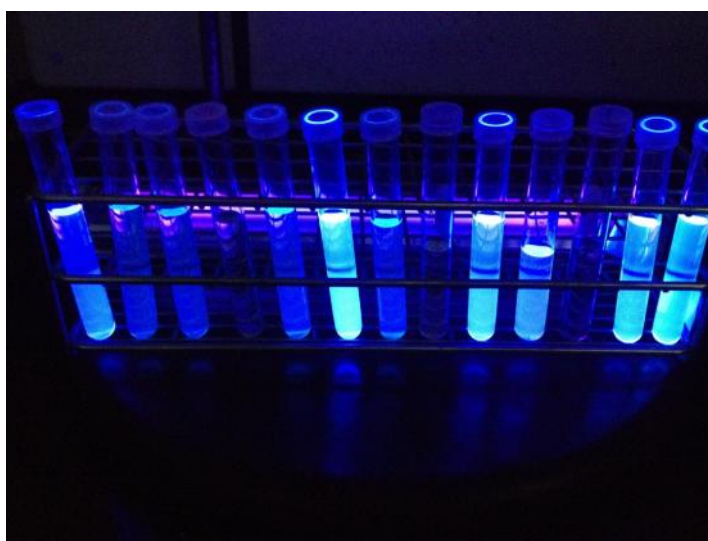


Figure 4.1 Fluorescence of all synthesized compounds under black light (a to l)

4.2 Suggestion for future works

To focus on PET process, we should do experiment about molecular calculation to confirm proposed PET process.

REFERENCES

- [1] Jervis, D. A. "Optical brighteners: improving the colour of plastics" *Plastics Additives & Compounding* November/December 2003, 42- 46, (2003).
- [2] Ciba Specialty Chemecals Inc. *Opticals brighteners* [Online]. 2011. Available from:http://www.mufong.com.tw/Ciba/ciba_guid/optical_brighteners.pdf [2011, September 5]
- [3] Niak, S. N.; Dhalla, A. M.; and Chauhan, Y. B. Fluorescent brighteners, methods of preparation thereof, fluorescent brightener compositions, and methods of preparation and uses thereof. *US patent 20070117887A1*. (2007): 1-14.
- [4] Lee, J. K.; Um, S.; Kang, Y.; and Baek, D. The synthesis and properties of asymmetrically substituted 4,4'-bis(1,3,5-triazin-6-yl)diaminostilbene 2,2'-disulfonic acid derivatives as fluorescent brighteners. *Dyes Pigments* 64 (2005): 25-30.
- [5] Farrar, R. R.; Shapiro, M.; and Javid, I. Photostabilized titanium dioxide and a fluorescent brightener as adjuvants for a nucleopolyhedrovirus. *Biol Control*. 48 (2003): 543-560.
- [6] Shamsipur, M.; Zargoosh, K.; Chaichi, M. J.; Tajbakhsh, M.; and Parach, A. Peroxyoxalate-chemiluminescence of Tinopal CBS as a commercially important optical brightener: mechanistic study and quantification. *J. Lumin.* 130 (2010): 748-755.
- [7] Shamsipur, M.; Faal, A. Y.; Chaichi, M. J.; Tajbakhsh, M.; and Parach, A. A study of chemiluminescence from reaction of bis(2,4,6-trichlorophenyl)oxalate, hydrogen peroxide and an optical brightener 5-(3-anilino-5-chloroanilino)-2-[(E)-2-[4-(3-anilino-5-chloroanilino)-2-sulfonyl]-1-ethenyl]-1-benzenesulfonic acid. *Dyes Pigments* 72 (2007): 113-118.
- [8] Hussain, M.; Shamey, R.; Hinks, D.; Elshafei, A.; and Ali, S. I. Synthesis of novel stilbene-alkoxysilane fluorescent brighteners, and their performance on cotton fiber as fluorescent brightening and ultraviolet absorbing agents. *Dyes Pigments* 92 (2012): 1231-1240.
- [9] Lakowicz, J. R. "Principles of fluorescence spectroscopy", 3rd ed, John Wiley & Sons, Inc, Kluwer, 2006.
- [10] Davidson, M. W. "Luminaries: Alexander Jablonski, Ph. D.: Fluorescence Spectroscopy", *Labmedicine*, pp. 694-695. 2009.

- [11] Galievsky, V. A.; and Zachariassey, K. A. Intramolecular charge transfer with *N,N*-dialkyl-4-(trifluoromethyl) anilines and 4-(dimethylamino) benzonitrile in polar solvents. Investigation of the excitation wavelength dependence of the reaction pathway. *Acta. Phys. Pol.* 112 (2007): 39-56.
- [12] Wikipedia. *Stokes shift* [Online]. 2013. Available from: http://en.wikipedia.org/wiki/Stokes_shift [2013, February 7].
- [13] Rurack, K.; and Genger, U. R. Rigidization, preorientation and electronic decoupling-the 'magic triangle' for the design of highly efficient fluorescent sensors and switches. *Chem. Soc. Rev.* 31 (2002): 116-127.
- [14] Grabchev, I.; Bojinov, V.; and Moneva, I. The synthesis and application of fluorescent dyes based on 3-amino benzanthrone. *Dyes Pigments* 48 (2001): 143-150.
- [15] Xu, Zh.; Qian, X.; and Cui, J. Calorimetric and ratiometric fluorescent chemosensor with a large red-shift in emission: Cu(II)-only sensing by deprotonation of secondary amines as receptor conjugated to naphthalimide fluorophore. *Org. Lett.* 7 (2005): 3029-3032.
- [16] Silva, A. P.; Moody, T. S.; and Wright, G. D. Fluorescent PET (Photoinduced Electron Transfer) sensors as potent analytical tools. *Analyst.* 134 (2009): 2385-2393.
- [17] Silva, A. P.; Fox, D. B.; Huxley, A. J. M.; and Moody, T. S. Combining luminescence, coordination and electron transfer for signaling purposes. *Coordin. Chem. Rev.* 205 (2000): 41-57.
- [18] Fan, L. J.; Zhang, Y.; and Jones, W. E. Design and synthesis of fluorescence "turn- on" chemosensors based on photoinduced electron transfer in conjugated polymer. *Macromolecules* 38 (2005): 2844-2849.
- [19] Silva, A. P.; Mccaughan, B.; Mckinney, B. O. F.; and Querol, M. Newer optical-based molecular devices from older coordination chemistry. *Dalton Trans.* (2003): 1902-1913.
- [20] Shankar, B. H.; and Ramaiah, D. Dansyl-naphthalimide dyads as molecular probes: effect of spacer group on metal ion binding properties. *J. Phys. Chem. B.* 115 (2011): 13292-13299.
- [21] Shiue, T. W.; Chen, Y. H.; Wu, Ch. M.; Singh, G.; Chen, H. Y.; Hung, Ch. H.; Liaw, W. F.; and Wang, Y. M. Nitric oxide turn-on fluorescent probe

- based on deamination of aromatic primary monoamines. *Inorg. Chem.* 51 (2012): 5400-5408.
- [22] Martin, E.; Weigand, R.; and Pardo, A. Solvent dependence of the inhibition of intramolecular charge-transfer in *N*-substituted 1,8-naphthalimide derivatives as dye lasers. *J. Lumin.* 68 (1996): 157-164.
- [23] Grabchev, I.; and Bojinov, V. Synthesis and characterisation of fluorescent polyacrylonitrile copolymers with 1,8-naphthalimide side chains. *Polym. Degrad. Stabil.* 70 (2000): 147-153.
- [24] Sk, U. H.; Gowda, A. S. P.; Crampsie, M. A.; Yun, J. K.; Spratt, T. E.; Amin, S.; and Sharma, A. K. Development of novel naphthalimide derivatives and their evaluation as potential melanoma therapeutics. *Eur. J. Med. Chem.* 46 (2011): 3331-3338.
- [25] Xie, S.; Zhang, Y.; Li, Q.; Xu, F.; Miao, J.; Zhao, J.; and Wang, C. 3-Nitro-naphthalimide and nitrogen mustard conjugate NNM-25 induces hepatocellular carcinoma apoptosis via PARP-1/p 53 pathway. *Apoptosis* 17 (2012): 725-734.
- [26] Li, M.; Li, Q.; Zhang, Y.; Tian, Z.; Ma, H.; Zhao, J.; Xie, S.; and Wang, C. Antitumor effects and preliminary systemic toxicity of ANISpm in vivo and in vitro. *Anti-cancer Drugs* 24 (2013): 32-42.
- [27] Li, S.; Zhong, W.; Li, Z.; and Meng, X. Unprecedented synthesis, in vitro and in vivo anti-cancer evaluation of novel triazol-naphthalimide derivatives. *Eur. J. Med. Chem.* 47 (2012): 546-552.
- [28] Li, X.; Lin, Y.; Wang, Q.; Yuan, Y.; Zhang, H.; and Qian, X. The novel anti-tumor agents of 4-triazol-1,8-naphthalimides: Synthesis, cytotoxicity, DNA intercalation and photocleavage. *Eur. J. Med. Chem.* 46 (2011): 1274-1279.
- [29] Malval, J. P.; Suzuki, S.; Savary, F.; Allonas, X.; Fouassier, J.; Takahara, S.; and Yamaoka, T. Photochemistry of naphthalimide photoacid generators. *J. Phys. Chem. A.* 112 (2008): 3879-3885.
- [30] Georgiev, N. I.; and Bojinov, V. B. Design, synthesis and photostability of novel 1,8-naphthalimide PAMAM light-harvesting dendrons. *J. Fluoresc.* 21 (2011): 51-63.
- [31] Ferreira, R.; Remon, P.; and Pischel, U. Multivalued logic with a tristable fluorescent switch. *J. Phys. Chem. C.* 113 (2009): 5805-5811.

- [32] Jia, L.; Zhang, Y.; Guo, X.; and Qian, X. A novel chromatism switcher with double receptors selectively for Ag^+ in aqueous solution: 4,5-diaminoalkeneamino-*N*-alkyl-1,8-naphthalimides. *Tetrahedron Lett.* 45 (2004): 3969-3973.
- [33] Hou, C.; Urbanec, A. M.; and Cao, H. A rapid Hg^{2+} sensor based on aza-15-crown-5 ether functionalized 1,8-naphthalimide. *Tetrahedron Lett.* 52 (2011): 4903- 4905.
- [34] Veale, E. B.; and Gunnlaugsson, T. Bidirectional photoinduced electron-transfer quenching is observed in 4-amino-1,8-naphthalimide-based fluorescent anion sensors. *J. Org. Chem.* 73 (2008): 8073-8076.
- [35] Kumar, M.; Kumar, N.; Bhalla, V.; Singh, H.; Sharma, P. R.; and Kaur, T. Naphthalimide appended rhodamine derivative: Through bond energy transfer for sensing of Hg^{2+} ions. *Org. Lett.* 13 (2011): 1422-1425.
- [36] Marinova, N. V.; Georgiev, N. I.; and Bojinov, V. B. Design, synthesis and pH sensing properties of novel 1,8-naphthalimide-based bichromophoric system. *J. Photoch. Photobio. A.* 222 (2011): 132-140.
- [37] Georgiev, N. I.; Bojinov, V. B.; and Nikolov, P. S. The design, synthesis and photophysical properties of two novel 1,8-naphthalimide fluorescent pH sensors based on PET and ICT. *Dyes Pigments* 88 (2011): 350-357.
- [38] Georgiev, N. I.; and Bojinov, V. B. Design, synthesis and sensor activity of a highly photostable blue emitting 1,8-naphthalimide. *J. Lumin.* 132 (2012): 2235- 2241.
- [39] Grabchev, I.; Moneva, I.; Bojinov, V.; and Guittonneau, S. Synthesis and properties of fluorescent 1,8-naphthalimide dyes for application in liquid crystal displays. *J. Mater. Chem.* 10 (2000): 1291-1296.
- [40] Wang, Y.; Zhang, X.; Han, B.; Peng, J.; Hou, S.; Huang, Y.; Sun, H.; Xie, M.; and Lu, Z. The synthesis and photoluminescence characteristics of novel blue light-emitting naphthalimide derivatives. *Dyes Pigments.* 86 (2010): 190-196.
- [41] Liu, J.; Li, Y.; Wang, Y.; Sun, H.; Lu, Z.; Wu, H.; Peng, J.; and Huang, Y. Synthesis and luminescent properties of blue sextuple-hydrogen-bond self-assembly molecular duplexes bearing 4-phenoxy-1,8-naphthalimide moieties. *Opt. Mater.* 34 (2012): 1535-1542.

- [42] Bojinov, V.; and Grabchev, I. A new method for synthesis of 4-allyloxy-1,8-naphthalimide derivatives for use as fluorescent brighteners. *Dyes Pigments*. 51 (2001): 57-61.
- [43] Grabchev, I.; Petkov, C.; and Bojinov, V. 1,8-naphthalimides as blue emitting fluorophores for polymer materials. *Macromol. Mater. Eng.* 287 (2002): 904-908.
- [44] Liu, M. O.; Lin, H.; Yang, M.; Lai, M.; Chang, C.; Liu, H.; Shiao, P.; Chen, I.; and Chen, J. Thermal and fluorescent properties of optical brighteners and their whitening effect for pelletization of cycloolefin copolymers. *Mater Lett.* 60 (2006): 2132-2137.
- [45] Neudorff, W. D.; Lentz, D.; Anibarro, M.; and Schluter, A. D. The carbon skeleton of the belt region of fullerene C₈₄ (D₂). *Chem. Eur. J.* 9 (2003): 2745-2757.
- [46] Panah, H. S.; Khosravi, A.; Gharanjig, K.; Khorassani, M.; Zadeh, M. K.; and Taromi, F. A. Synthesis and characterization of new fluorescent polymerizable dyes based on naphthalimide. *Iran. Polym. J.* 19 (2010): 491-500.
- [47] Zhu, W.; Yao, R.; and Tian, H. Synthesis of novel electro-transporting emitting compounds. *Dyes Pigments*. 54 (2002): 147-154.
- [48] Ashry, E. S. H. E.; Hamid, H. A.; Kassem, A. A.; and Shoukry, M. Synthesis and reactions of acenaphthenequinones-part-2. The reactions of acenaphthenequinones. *Molecules*. 7 (2002): 155-188.
- [49] Jones, L. A.; Joyner, C. T.; Kim, H. K.; and Kyff, R. A. Acenaphthene I. the preparation of derivatives of 4,5-diaminonaphthalic anhydride. *Can. J. Chem.* 48 (1970): 3133-3134.
- [50] Bukharkina, T. V.; Grechishkina, O. S.; Digurov, N. G.; and Konkov, I. I. Catalytic oxidation of acenaphthene and its derivatives in acetic acid. *Org. Process. Res. Dev.* 6 (2002): 394-400.
- [51] Melhuish, W. H. Quantum efficiencies of fluorescence of organic substances: effect of solvent and concentration of the fluorescent solute. *J. Phys. Chem.* 65 (1961): 229-235.
- [52] Parvizi, P.; Khosravi, A.; Moradian, S.; and Gharanjig, K. Synthesis and application of some alkali-clearable azo disperse dyes based on naphthalimide derivatives. *J. Chin. Chem. Soc.* 56 (2009): 1035-1042.

- [53] Khalek, A. A. A.; Hassan, E. S.; and Hassan, H. M. Kinetics and mechanism the of hydroxylation of some naphthalene sulphonic acid derivatives by peroxodisulphate. *Indian. J. Chem. Technol.* 14 (2007): 466-472.
- [54] Zhao, C.; Zhang, Y.; Li, R.; Li, X.; and Jiang, J. Di(alkoxy)- and di(alkylthio)-substituted perylene-3,4,9,10-tetracarboxy diimides with tunable electrochemical and photophysical properties. *J. Org. Chem.* 72 (2007): 2402-2410.
- [55] Behniafar, H.; and Khosraviborna, S. Synthesis and characterization of novel aromatics polyamides derived from 2,2'-bis(*p*-phenoxyphenyl)-4,4'-diaminodiphenyl ether. *Polym. Int.*, 58 (2009): 1299-1307.
- [56] Kawaguchi, Y.; Itamura, Y.; Onimura, K.; and Oishi, T. Effects of the chemical structure on the heat resistance of thermoplastic expandable microspheres. *J. Appl. Polym. Sci.* (2004): 1306-1312.
- [57] Kong, G.; Hong, B.; Kim, M.; Han, Y.; and Chun, H. Transparency and high heat resistance of cardo based poly(arylene ether)s. *Macromol. Res.* 19 (2011): 608-612.
- [58] Wang, X.; Qi, G.C.; Zhang, X.; Gao, J.; Li, B.; Song, Z.; and Qiao, J. The abnormal behavior of polymers glass transition temperature increase and its mechanism. *Sci. China. Chem.* 55 (2012): 713-717.
- [59] Chung, Y. S.; Yoo, S. H.; and Kim, C. K. Enhancement of meltdown temperature of the polyethylene lithium-ion battery separator via surface coating with polymer having high thermal resistance. *Ind. Eng. Chem. Res.* 48 (2009): 4346-4351.
- [60] Maehara, T.; Takenaka, J.; Tanaka, K.; Yamaguchi, M.; and Yamamoto, H. Synthesis and polymerization of novel epoxy compounds having an adamantane ring and evaluation of their heat resistance and optical fiber transparency. (2009): 496-504.
- [61] Wenyan, H.; Huili, P.; Bibiao, J.; Qiang, R.; Guangqun, Z.; Lizhi, K.; Dongliang, Z.; and Jianhai, C. Preparation of heat-resistant branched poly(styrene-*alt*-NPMI) by ATRP with divinylbenzene as the branching agent. (2010): 977-982.
- [62] Nakao, R.; Kondo, A.; and Koike, Y. Fabrication of high glass transition temperature graded-index plastic optical fiber: Part 2- fiber fabrication and characterizations. 30 (2012): 969-973.

- [63] Song, L.; Yang, Y; Zhang, Q.; Tian, H.; and Zhu, W. Synthesis and photochromism of naphthopyrans bearing naphthalimide chromophore: Predominant thermal reversibility in color-fading and fluorescence switch. 115 (2011): 14648-14658.
- [64] Refat, M. S.; Killa, H. M. A.; and Fetooh, H. Spectroscopic and thermal characterization of Cu(II), Co(II), Ni(II) and Mn(II) complexes of fluorescent dye 4-N,N-dimethyl-ethanolamine-N-allyl-1,8-naphthalimide (4DMEAN). *J. Mol. Struct.* 983 (2010): 122-132.

APPENDIX

APPENDIX

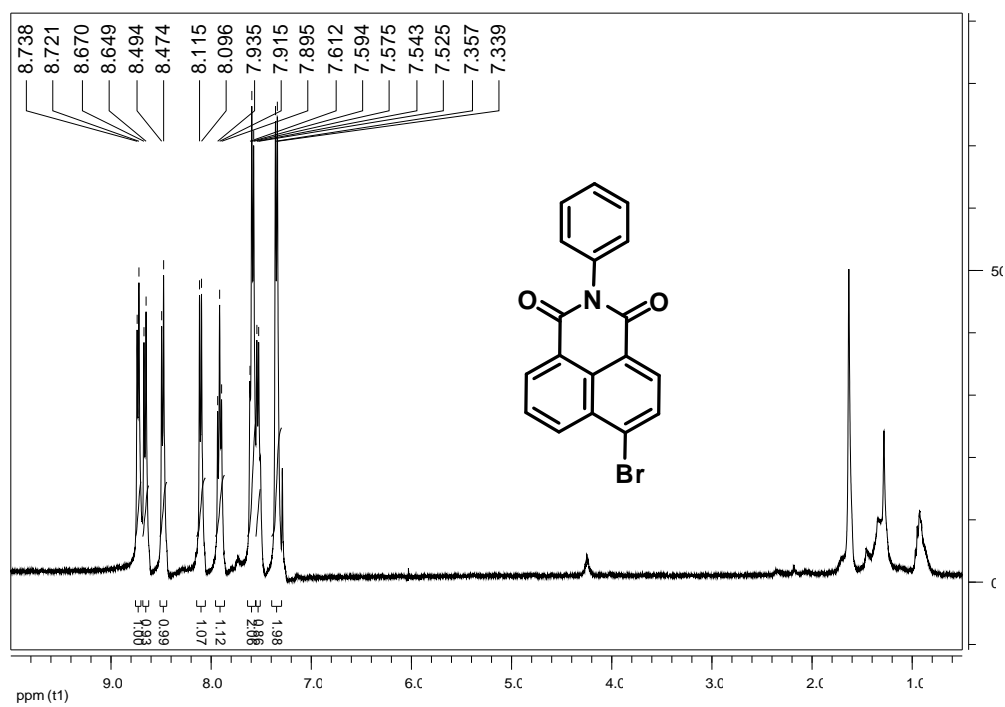


Fig A. 1 ¹H NMR of 4-bromo-N-(phenyl)-1,8-naphthalimide (**2a**) in CDCl₃

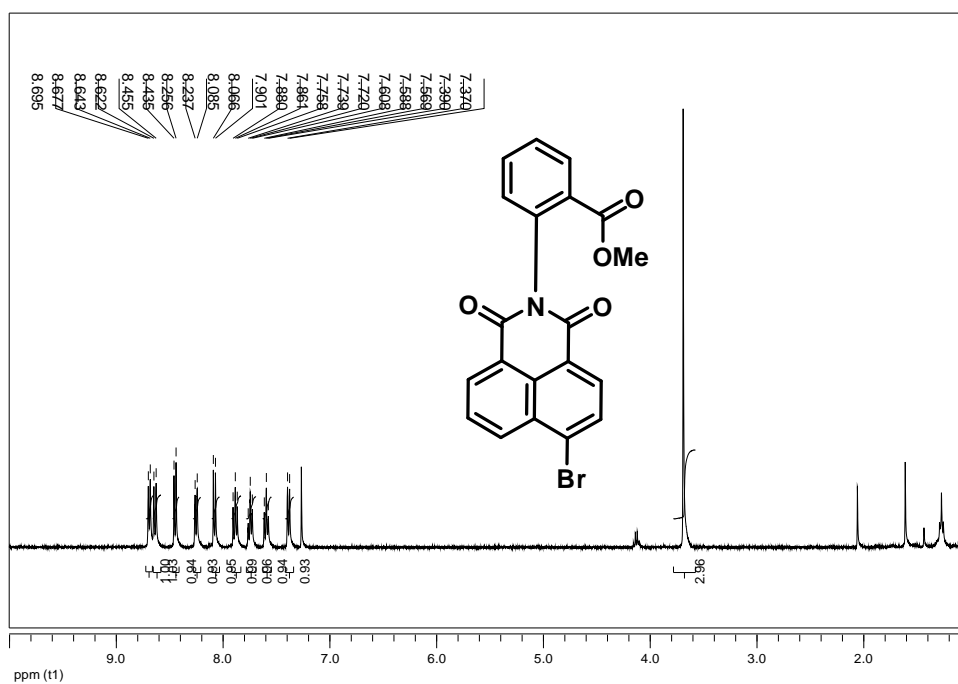


Fig A. 2 ¹H NMR of 4-bromo-N-(2-acethoxy-phenyl)-1,8-naphthalimide (**2b**) in CDCl₃

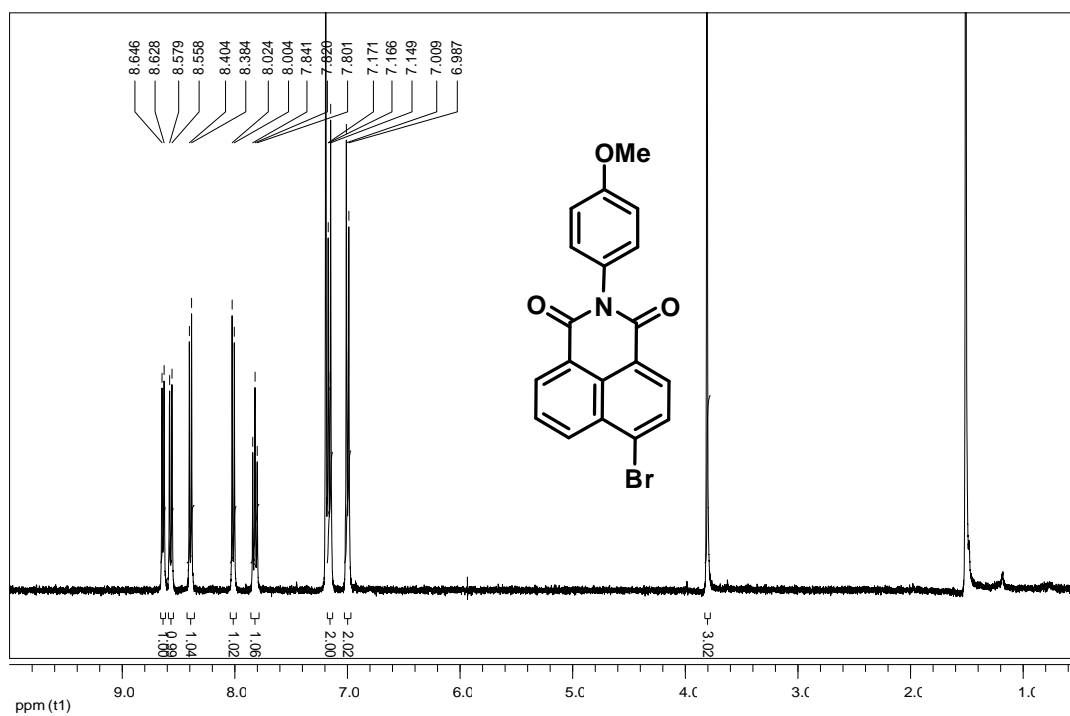


Fig. A. 3 ¹H NMR of 4-bromo-N-(4-methoxyphenyl)-1,8-naphthalimide (**2c**) in CDCl₃

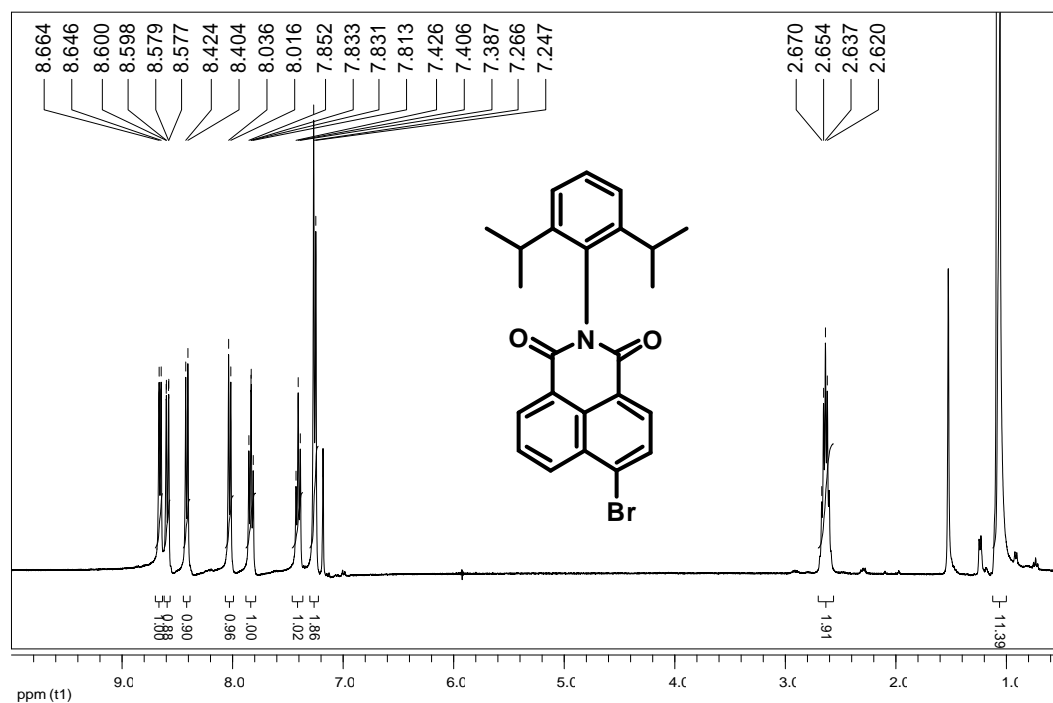


Fig. A. 4 ¹H NMR of 4-bromo-N-(2,6-diisopropylphenyl)-1,8-naphthalimide (**2d**) in CDCl₃

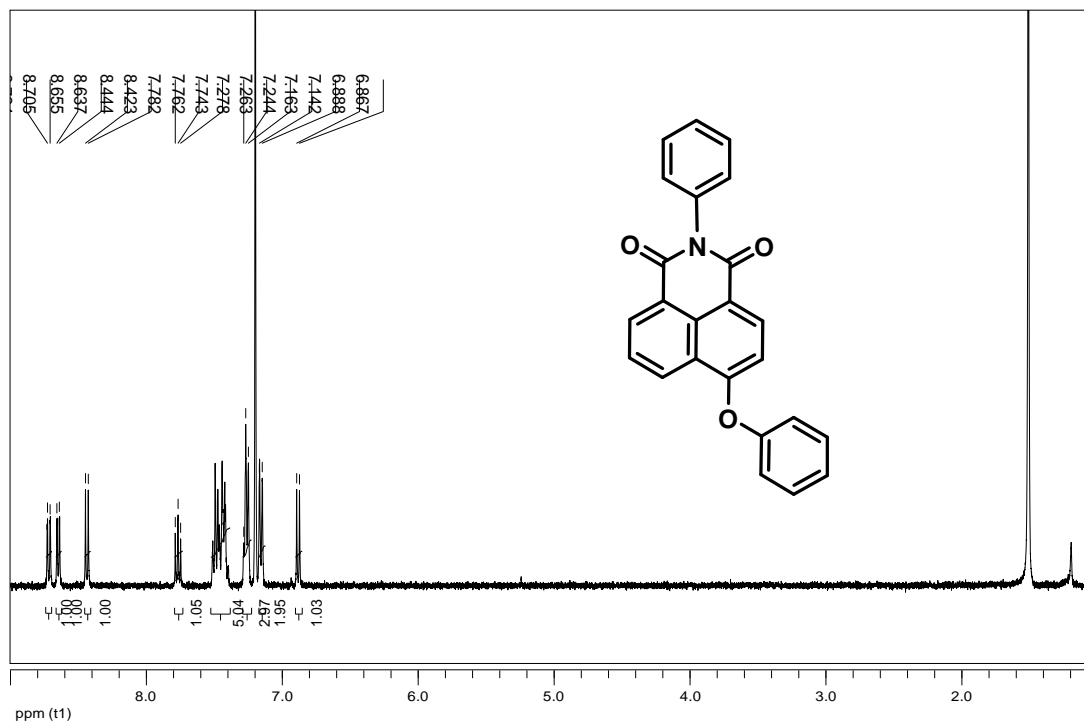


Fig. A. 5 ^1H NMR of 4-phenoxy-*N*-(phenyl)-1,8-naphthalimide (**3a**) in CDCl_3

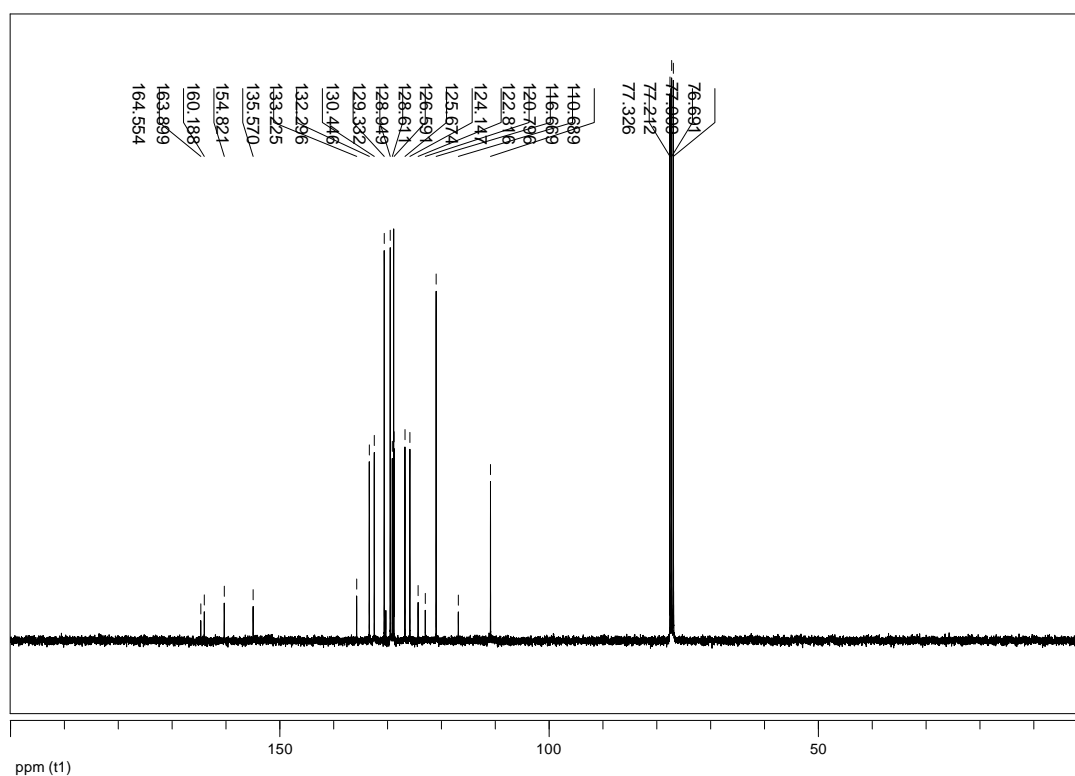


Fig. A. 6 ^{13}C NMR of 4-phenoxy-*N*-(phenyl)-1,8-naphthalimide (**3a**) in CDCl_3

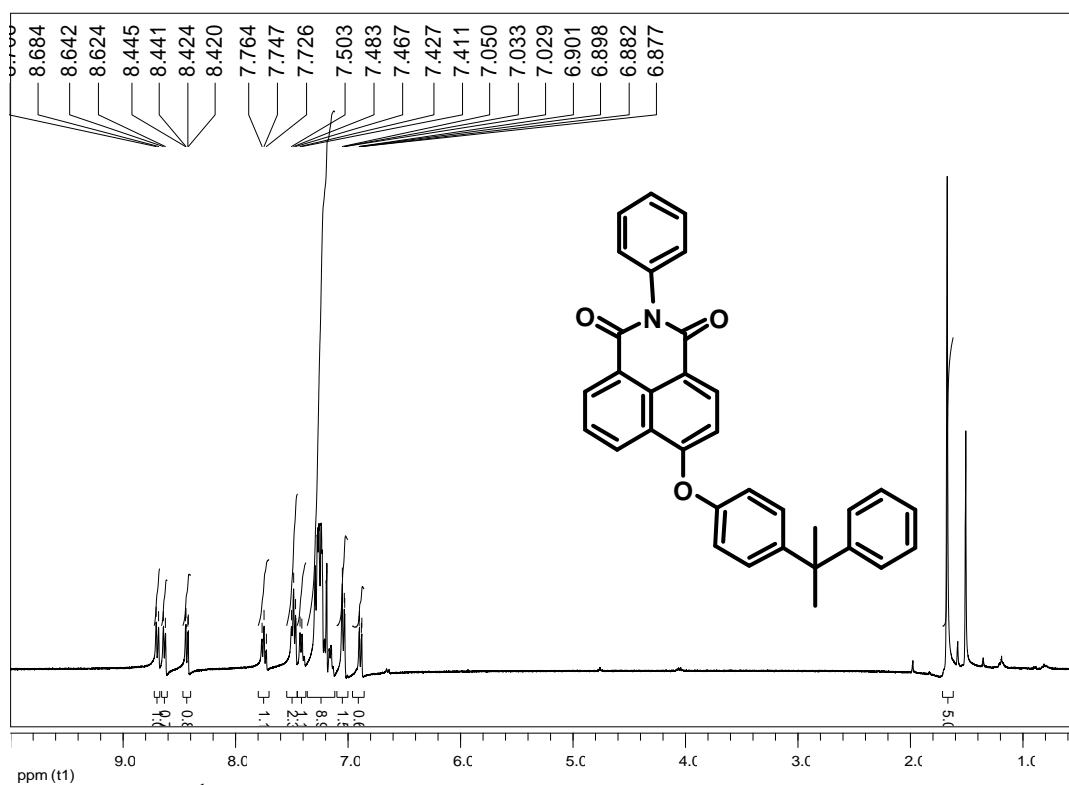


Fig A. 7 ^1H NMR of 4-cumylphenoxy-*N*-(phenyl)-1,8-naphthalimide (**3b**) by KOH in CDCl_3

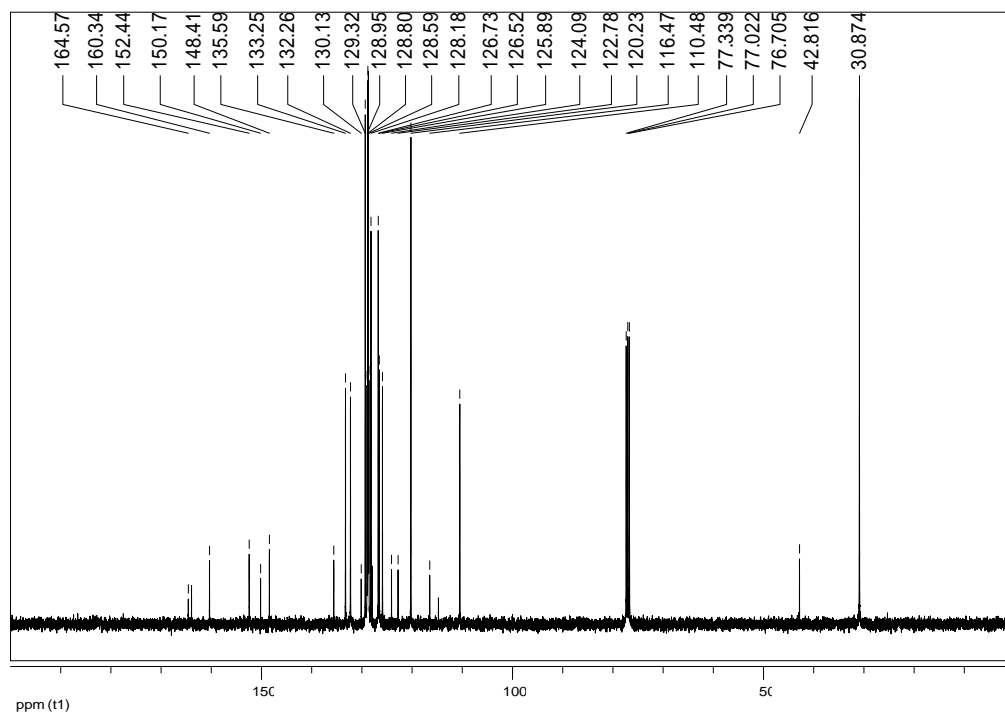


Fig A. 8 ^{13}C NMR of 4-cumylphenoxy-*N*-(phenyl)-1,8-naphthalimide (**3b**) by KOH in CDCl_3

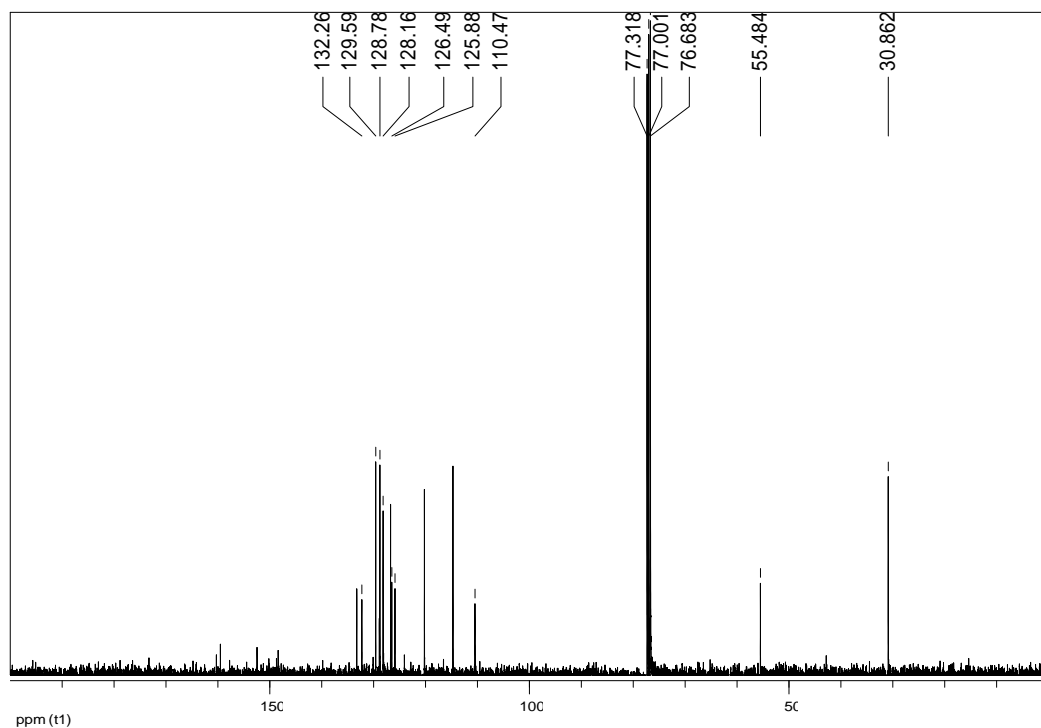


Fig A. 13 ^{13}C NMR of 4-cumylphenoxy-*N*-(4-methoxy-phenyl)-1,8-naphthalimide (**3d**) in CDCl_3

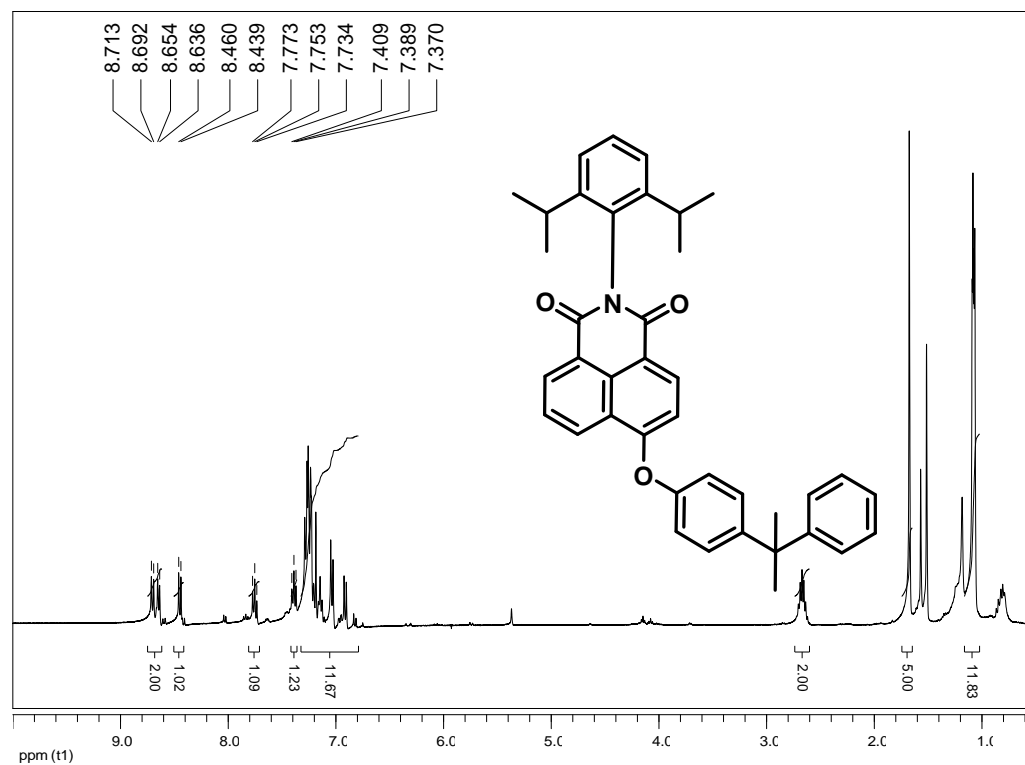


Fig A. 14 ^1H NMR of 4-cumylphenoxy-*N*-(2,6-diisopropyl-phenyl)-1,8-naphthalimide (**3e**) in CDCl_3

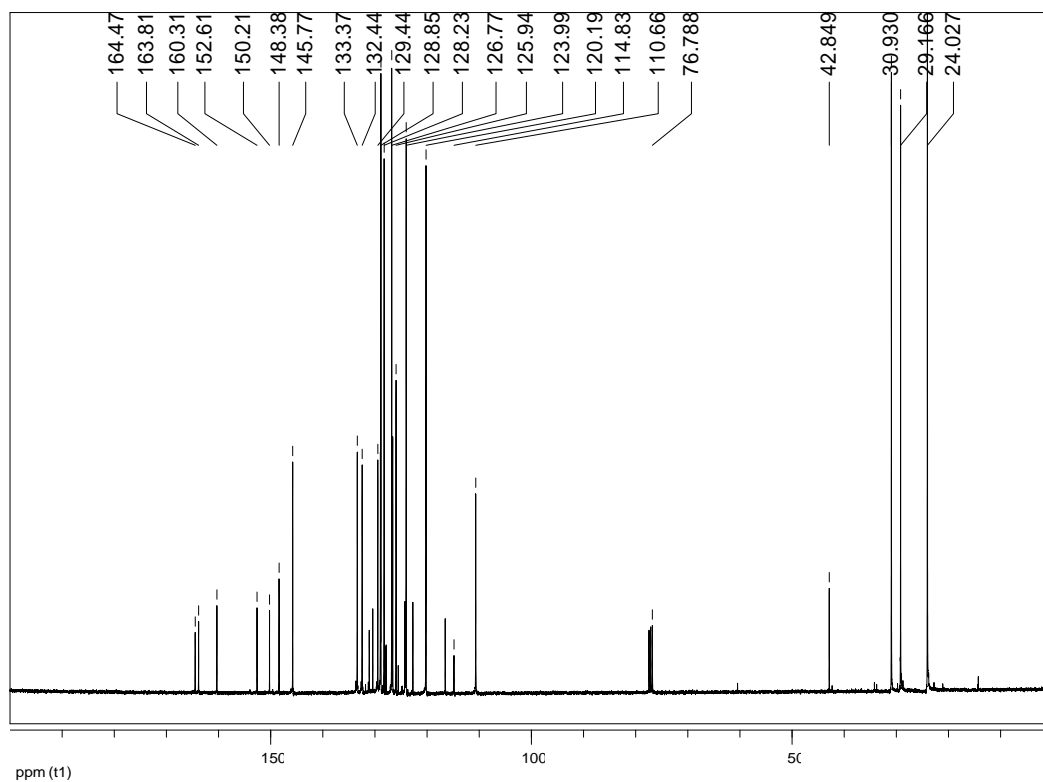


Fig A. 15 ^{13}C NMR of 4-cumylphenoxy-*N*-(2,6-diisopropyl-phenyl)-1,8-naphthalimide (**3e**) in CDCl_3

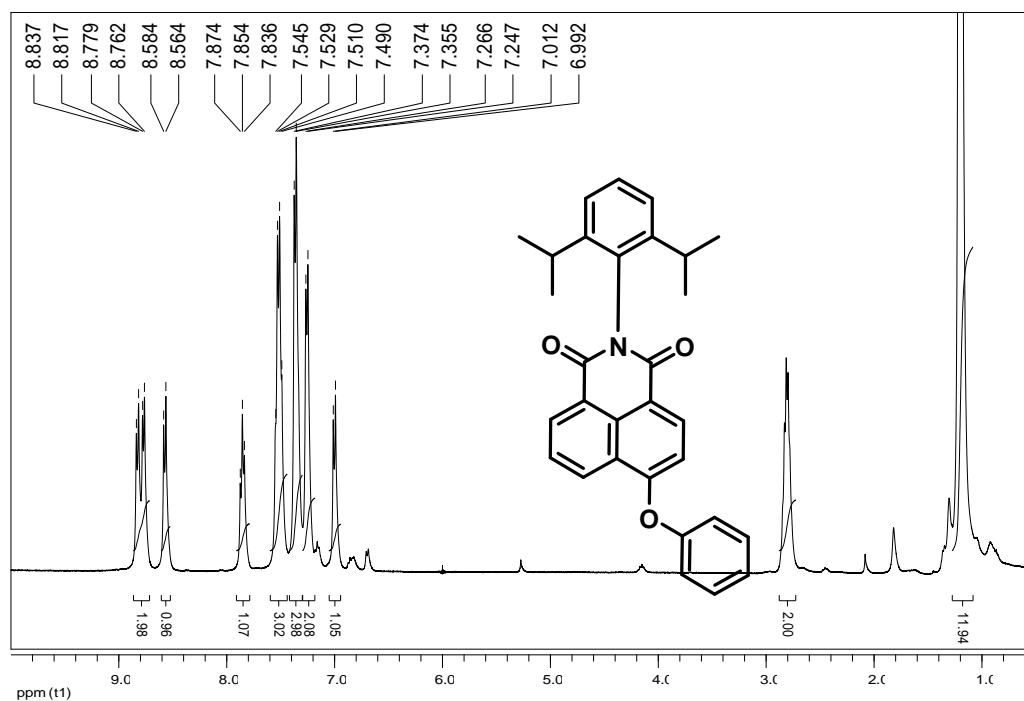


Fig A. 16 ^1H NMR of 4-phenoxy-*N*-(2,6-diisopropyl-phenyl)-1,8-naphthalimide (**3f**) in CDCl_3

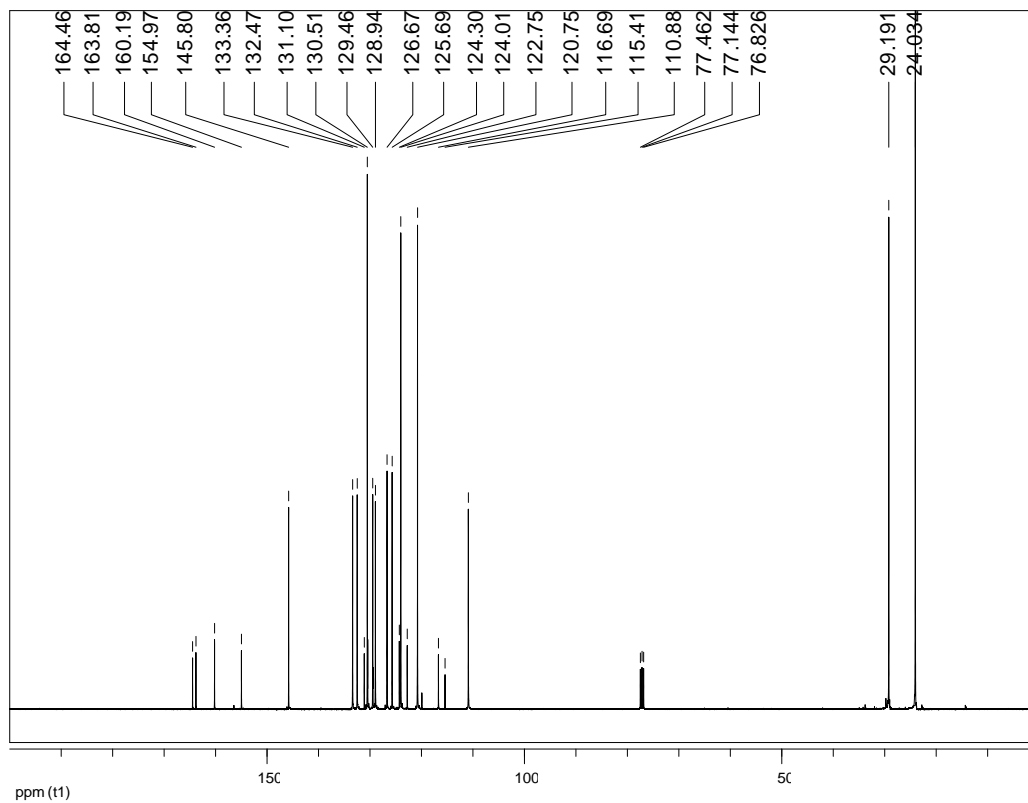


Fig A. 17 ^{13}C NMR of 4-phenoxy-*N*-(2,6-diisopropyl-phenyl)-1,8-naphthalimide (**3f**) in CDCl_3

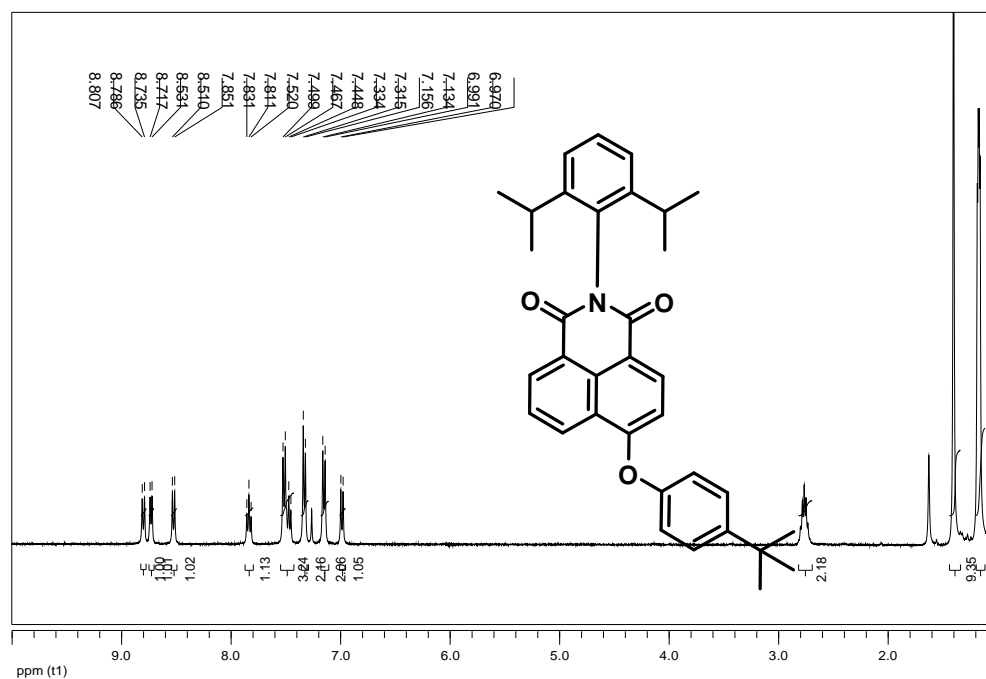


Fig A. 18 ^1H NMR of 4-(4-*tert*-butyl-phenoxy)-*N*-(2,6-diisopropyl-phenyl)-1,8-naphthalimide (**3g**) in CDCl_3

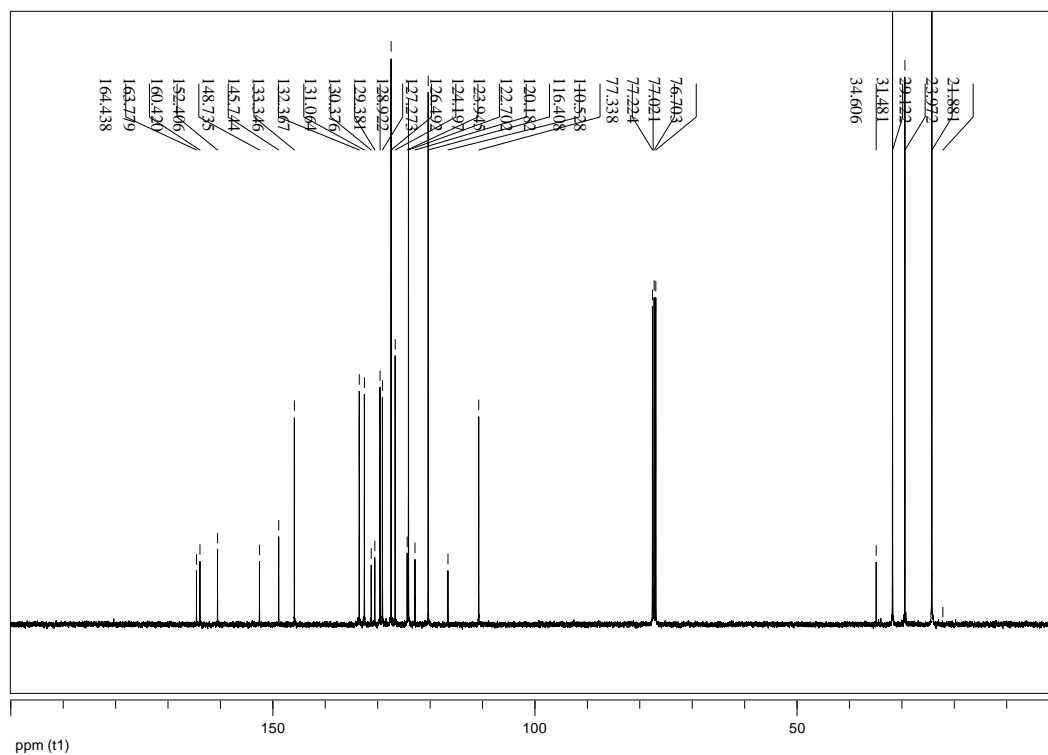


Fig A. 19 ^{13}C NMR of 4-(4-*tert*-butyl-phenoxy)-*N*-(2,6-diisopropyl-phenyl)-1,8-naphthalimide (**3g**) in CDCl_3

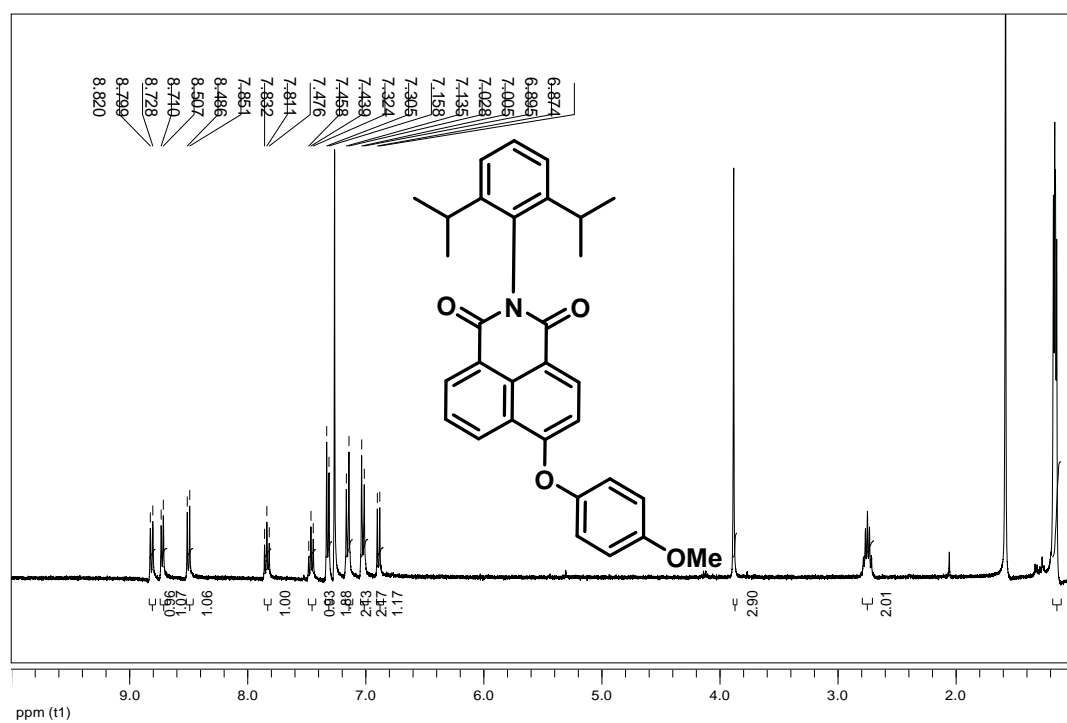


Fig A. 20 ^1H NMR of 4-(4-methoxy-phenoxy)-*N*-(2,6-diisopropyl-phenyl)-1,8-naphthalimide (**3h**) in CDCl_3

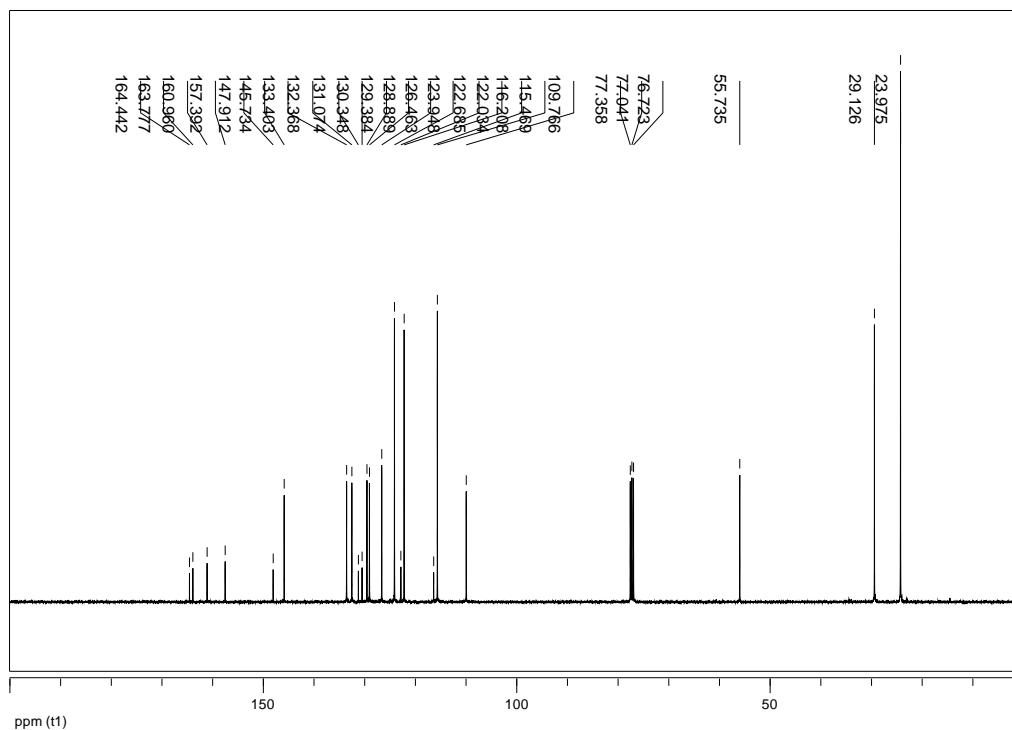


Fig A. 21 ¹³C NMR of 4-(4-methoxy-phenoxy)-*N*-(2,6-diisopropyl-phenyl)-1,8-naphthalimide (**3h**) in CDCl₃

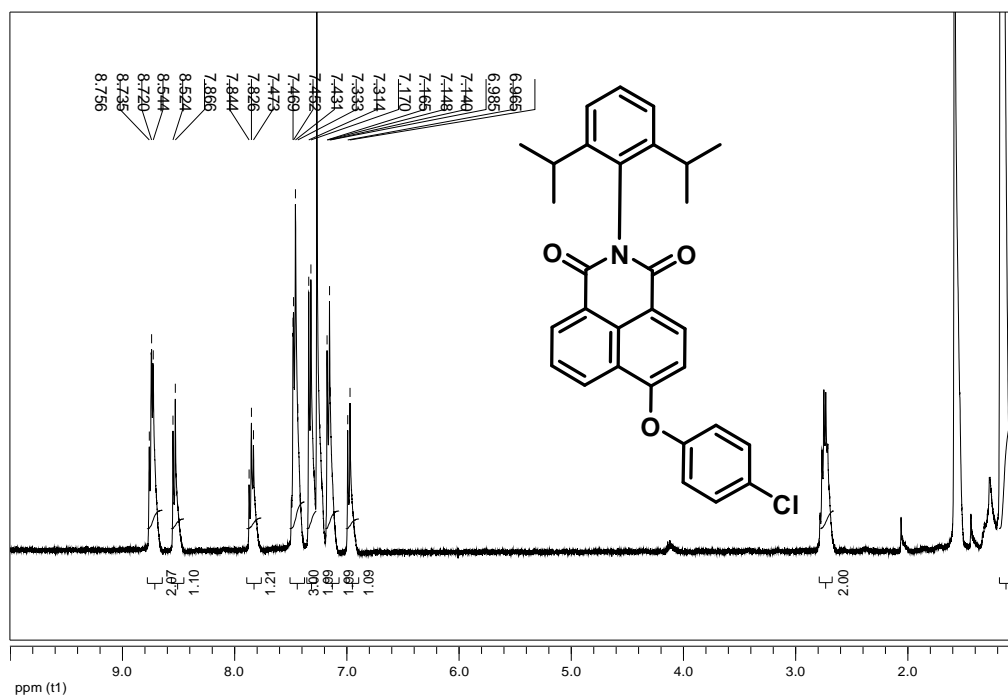


Fig A. 22 ¹H NMR of 4-(4-chloro-phenoxy)-*N*-(2,6-diisopropyl-phenyl)-1,8-naphthalimide (**3i**) in CDCl₃

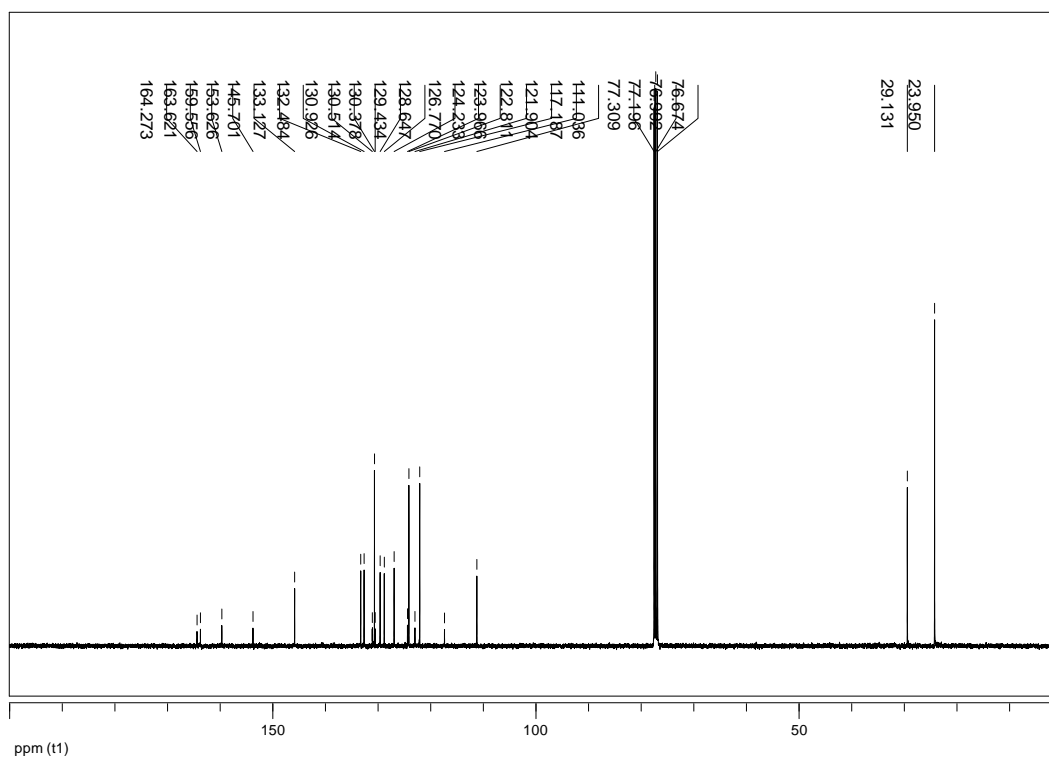


Fig A. 23 ¹³C NMR of 4-(4-chloro-phenoxy)-*N*-(2,6-diisopropyl-phenyl)-1,8-naphthalimide (**3i**) in CDCl₃

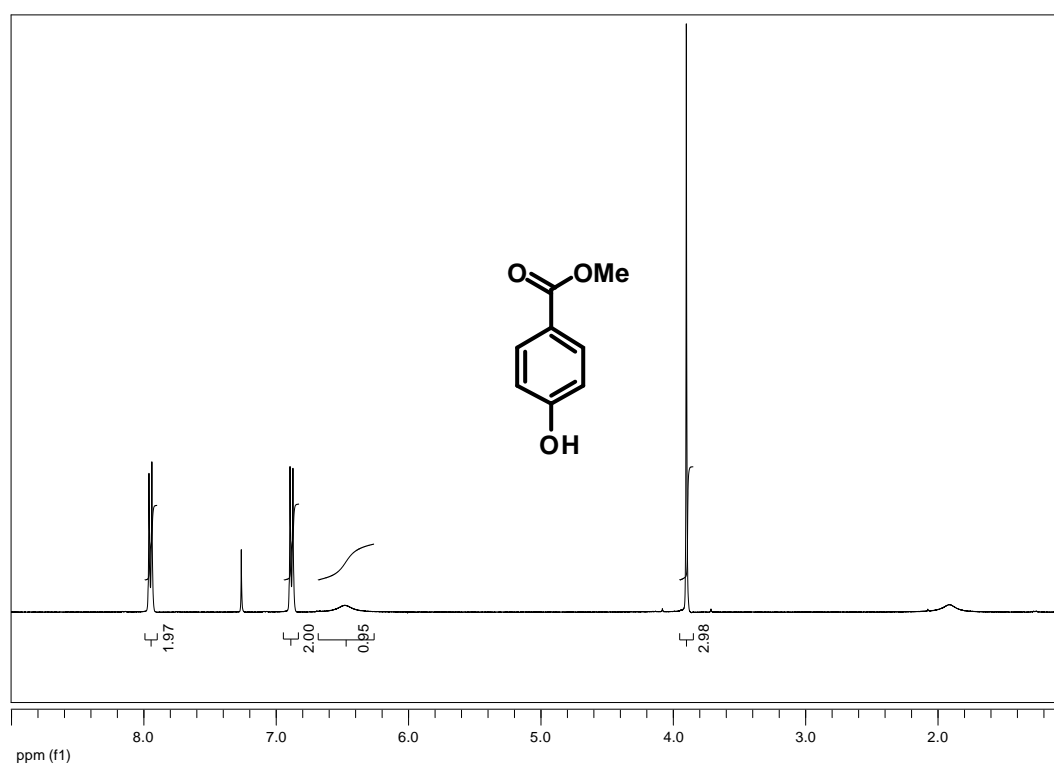


Fig A. 24 ¹H NMR of methyl 4-hydroxybenzoate (**4**) in CDCl₃

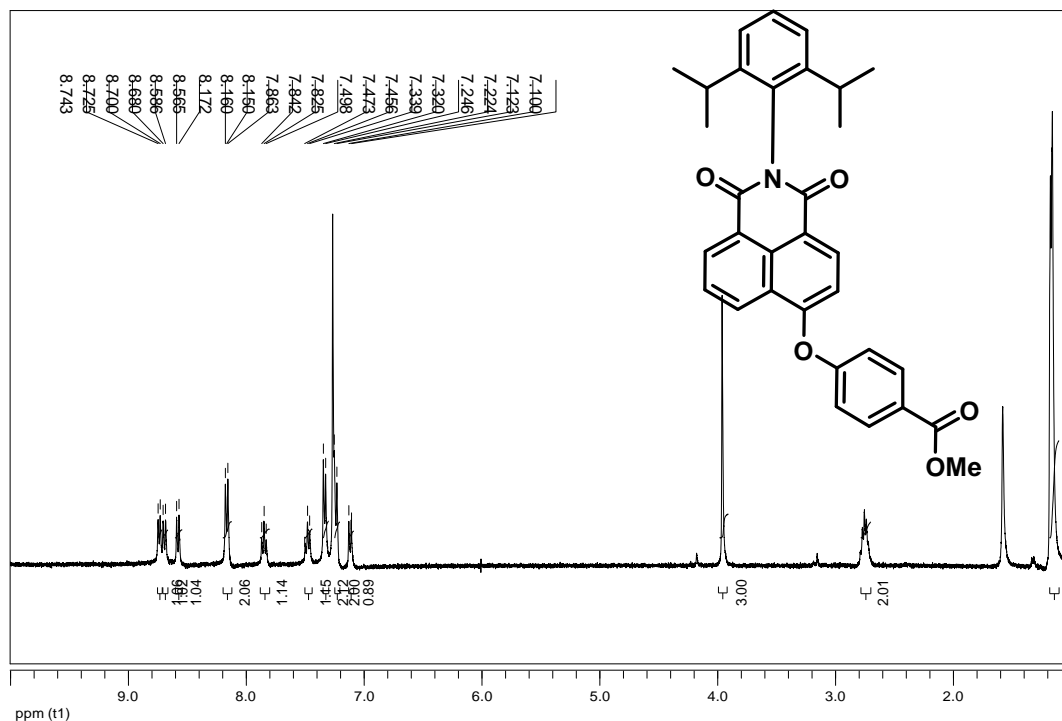


Fig A. 25 ¹H NMR of 4-(4-acethoxy-phenoxy)-*N*-(2,6-diisopropyl-phenyl)-1,8-naphthalimide (**3j**) in CDCl₃

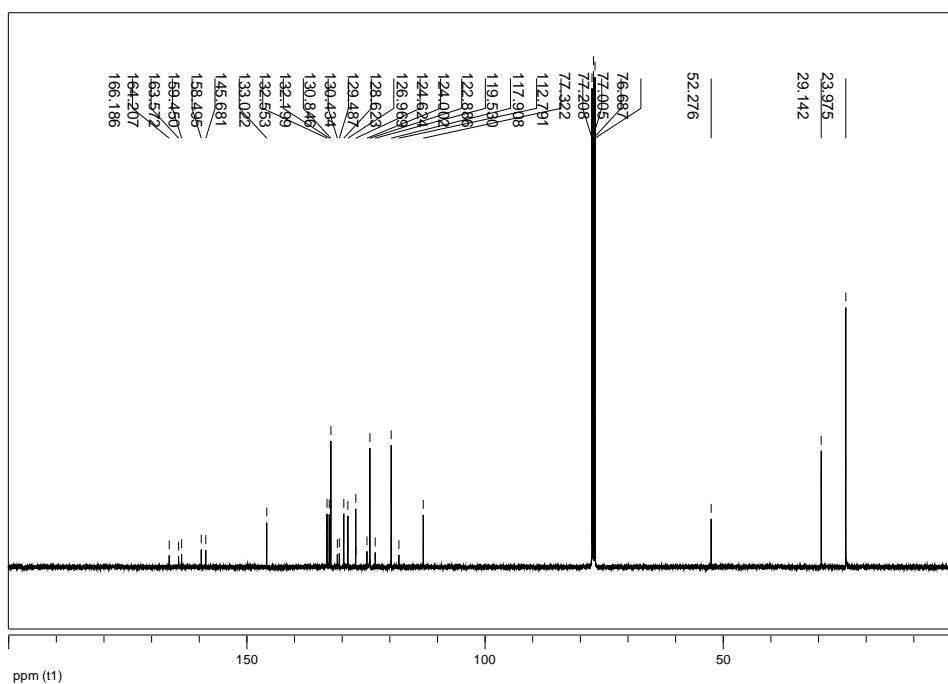


Fig A. 26 ¹³C NMR of 4-(4-acethoxy-phenoxy)-*N*-(2,6-diisopropyl-phenyl)-1,8-naphthalimide (**3j**) in CDCl₃

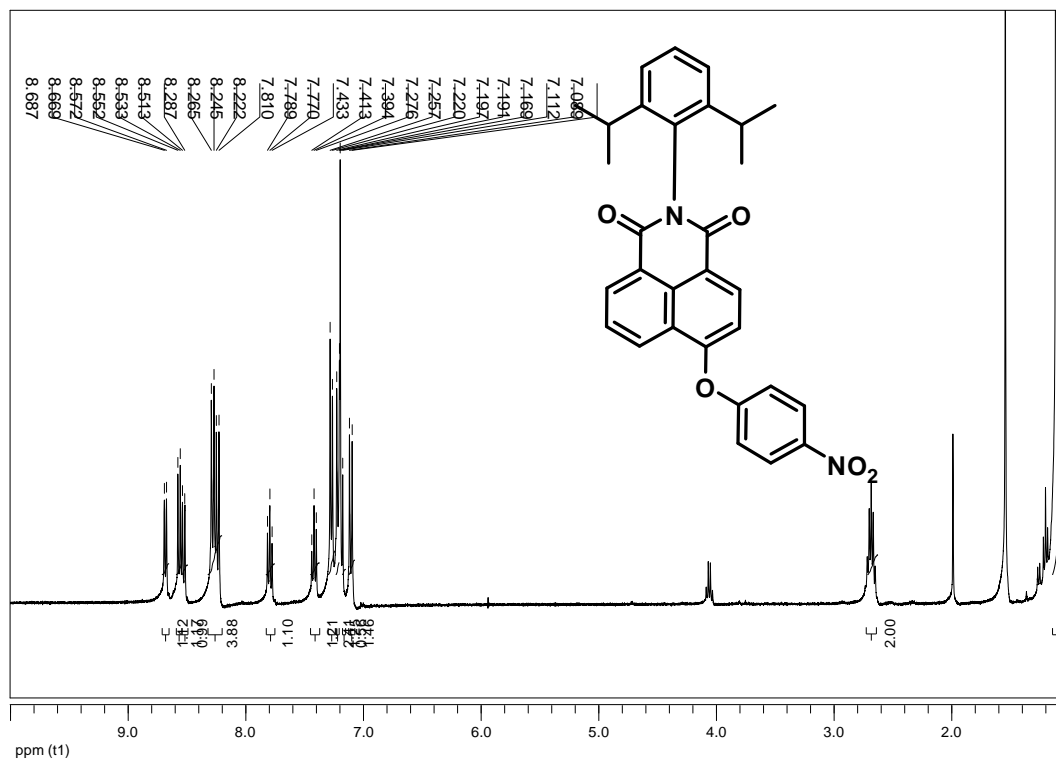


Fig A. 27 ¹H NMR of 4-(4-nitro-phenoxy)-*N*-(2,6-diisopropyl-phenyl)-1,8-naphthalimide (**3k**) in CDCl₃

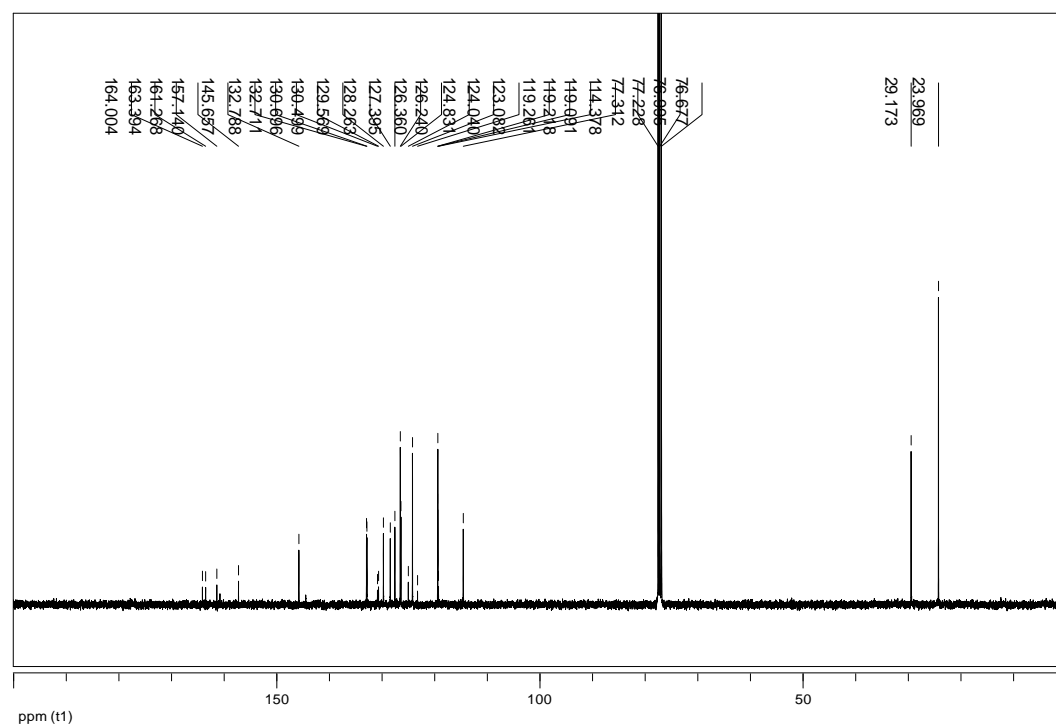


Fig A. 28 ¹³C NMR of 4-(4-nitro-phenoxy)-*N*-(2,6-diisopropyl-phenyl)-1,8-naphthalimide (**3k**) in CDCl₃

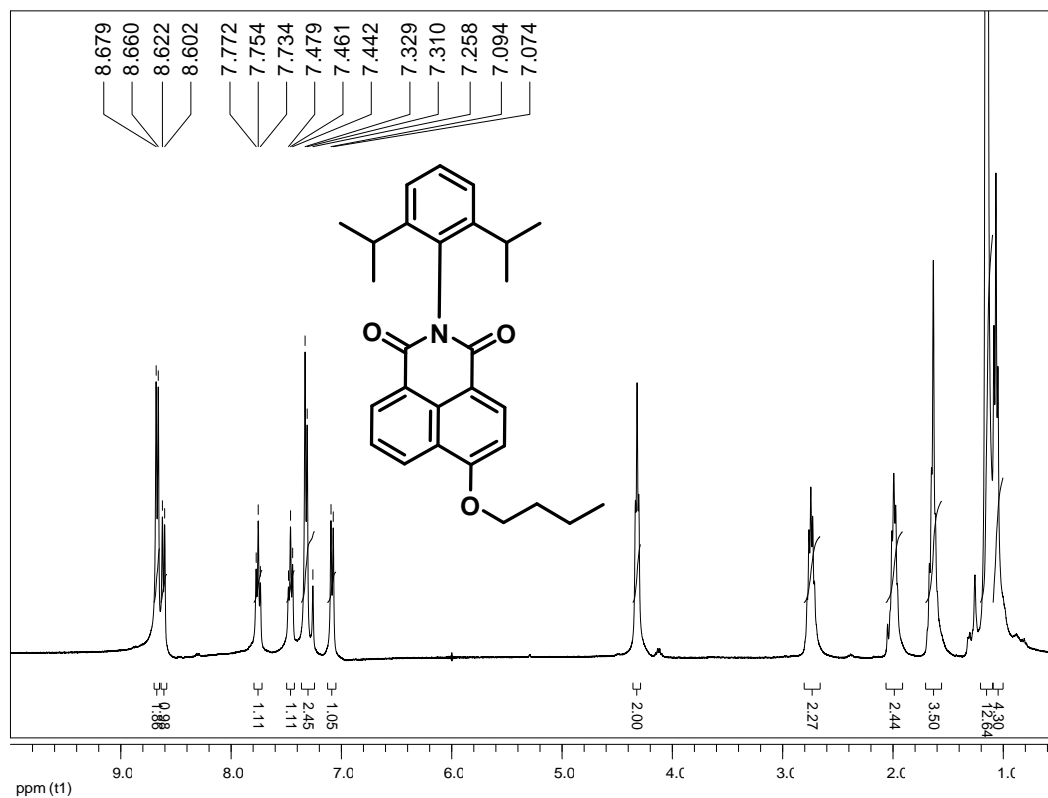


Fig A. 29 ¹H NMR of 4-butoxy-*N*-(2,6-diisopropyl-phenyl)-1,8-naphthalimide (**31**) in CDCl₃

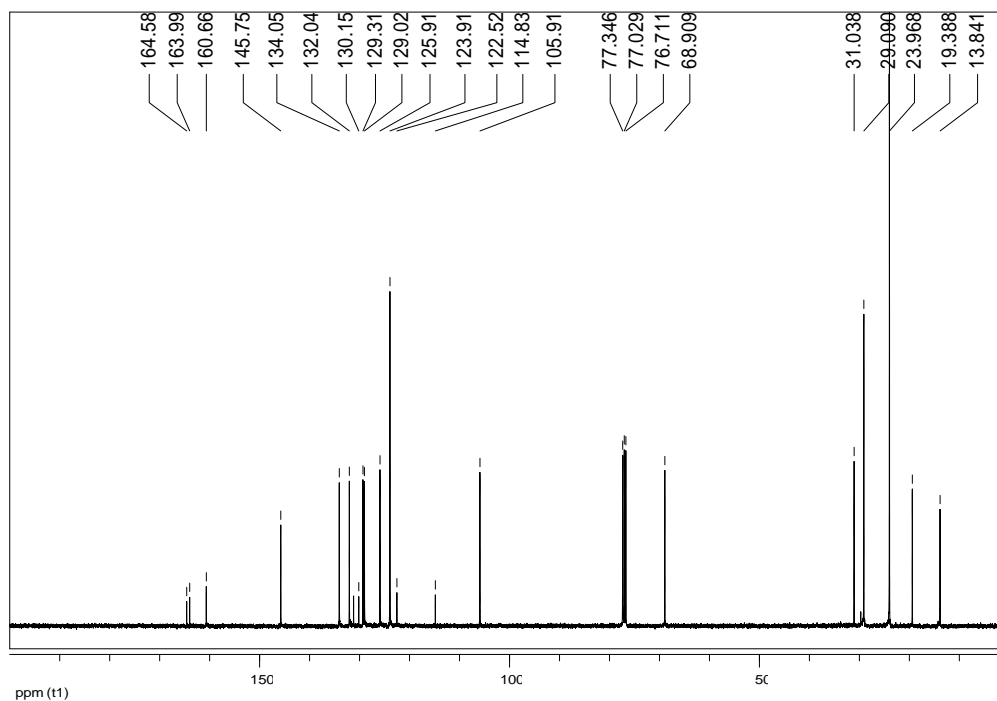


Fig A. 30 ¹³C NMR of 4-butoxy-*N*-(2,6-diisopropyl-phenyl)-1,8-naphthalimide (**31**) in CDCl₃

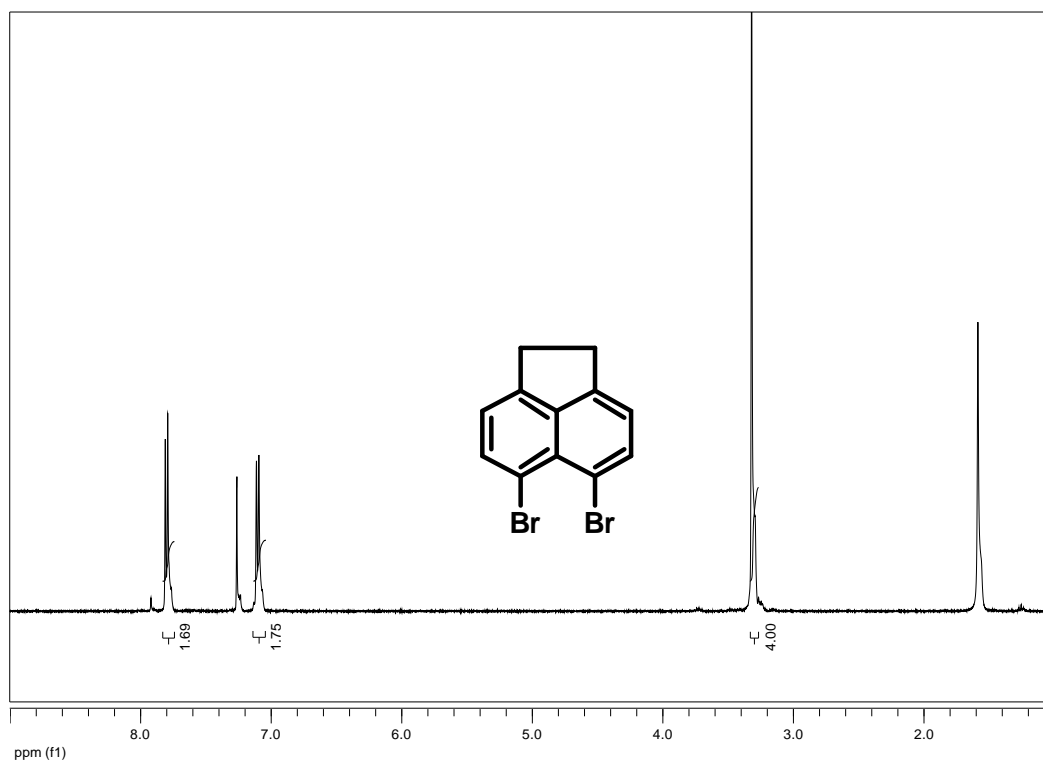


Fig A. 31 ^1H NMR of 5,6-dibromoacenaphthene (5) in CDCl_3

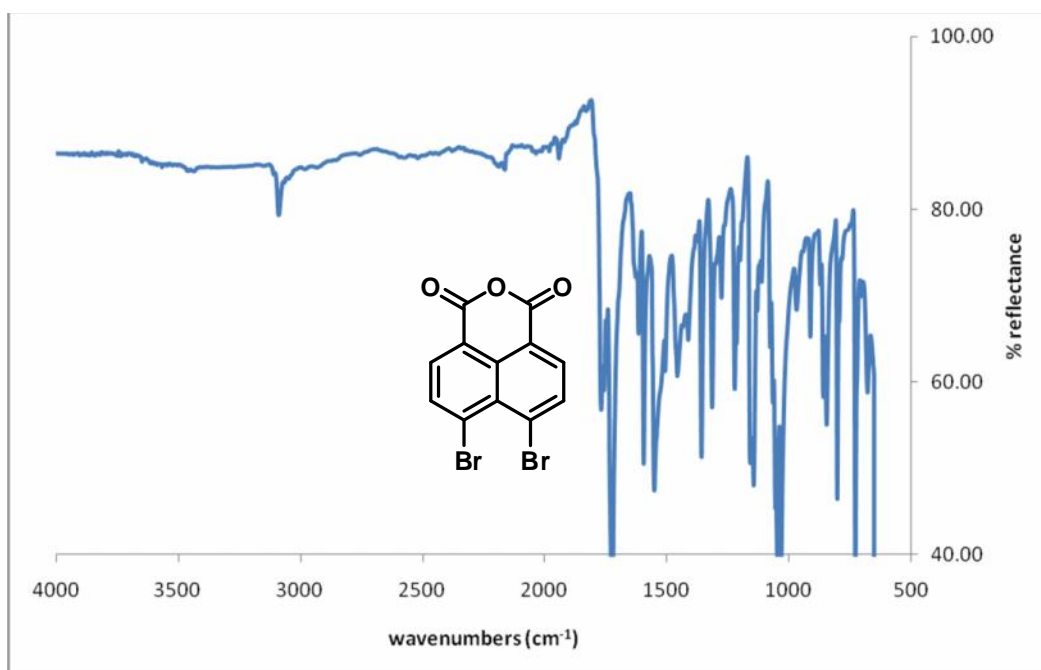


Fig A. 32 FT-IR spectrum of 4,5-dibromo-1,8-naphthalic anhydride (6)

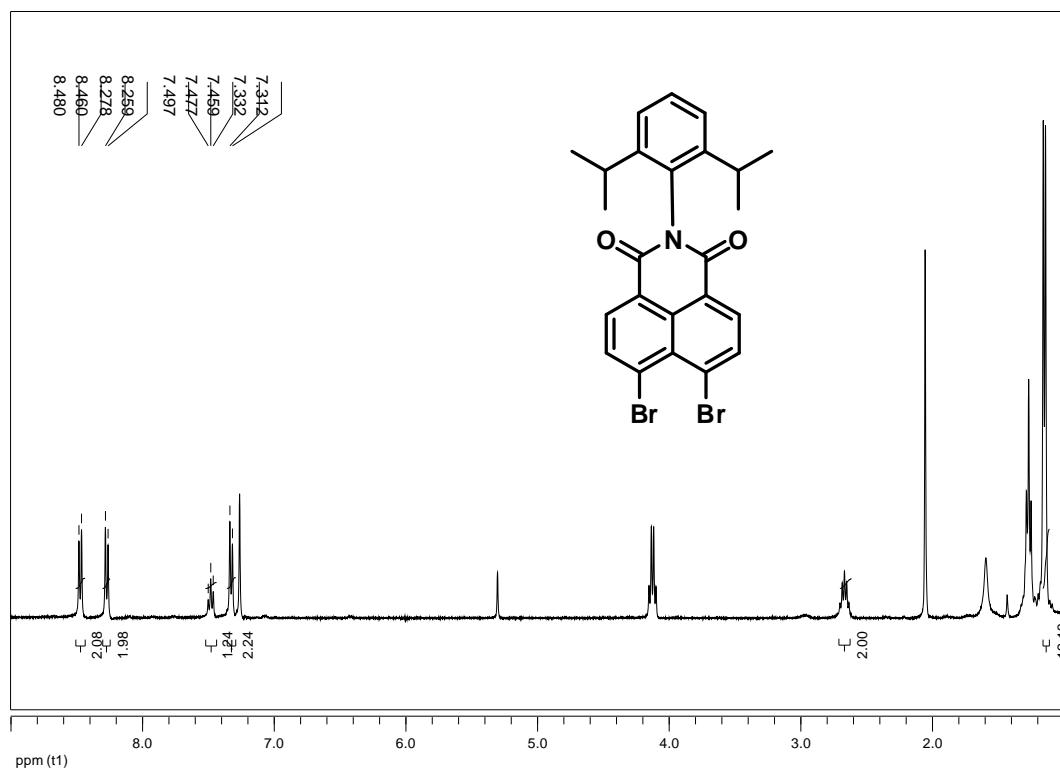


Fig A. 33 ^1H NMR of 4,5-dibromo-*N*-(2,6-diisopropyl-phenyl)-1,8-naphthalimide (**2e**) in CDCl_3

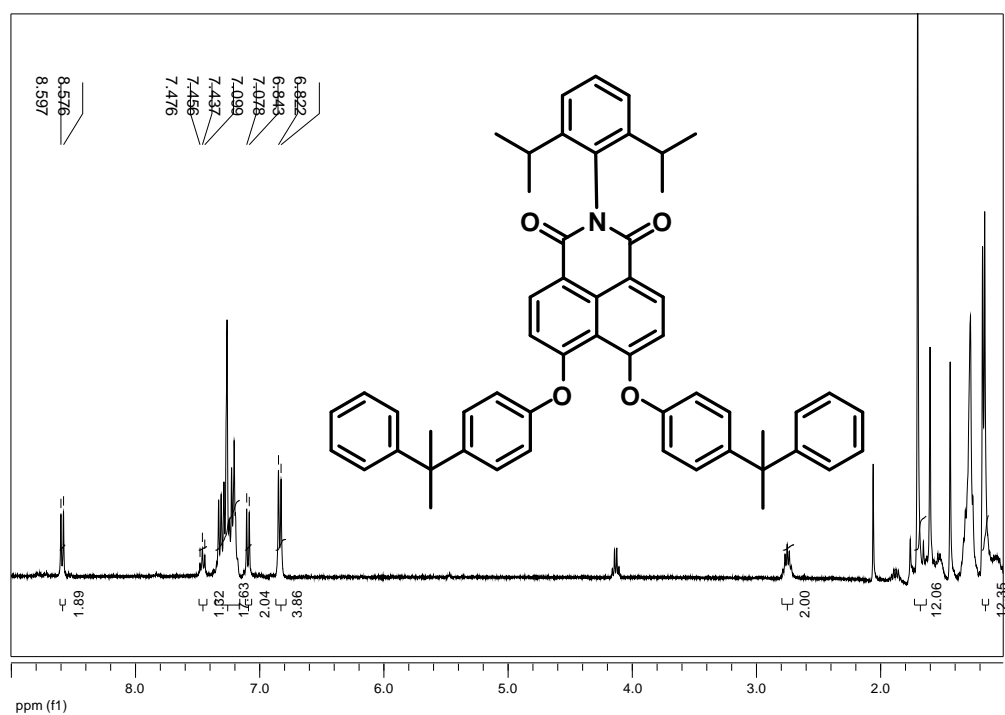


Fig A. 34 ^1H NMR of 4,5-dicumylphenoxy-*N*-(2,6-diisopropyl-phenyl)-1,8-naphthalimide (**3m**) in CDCl_3

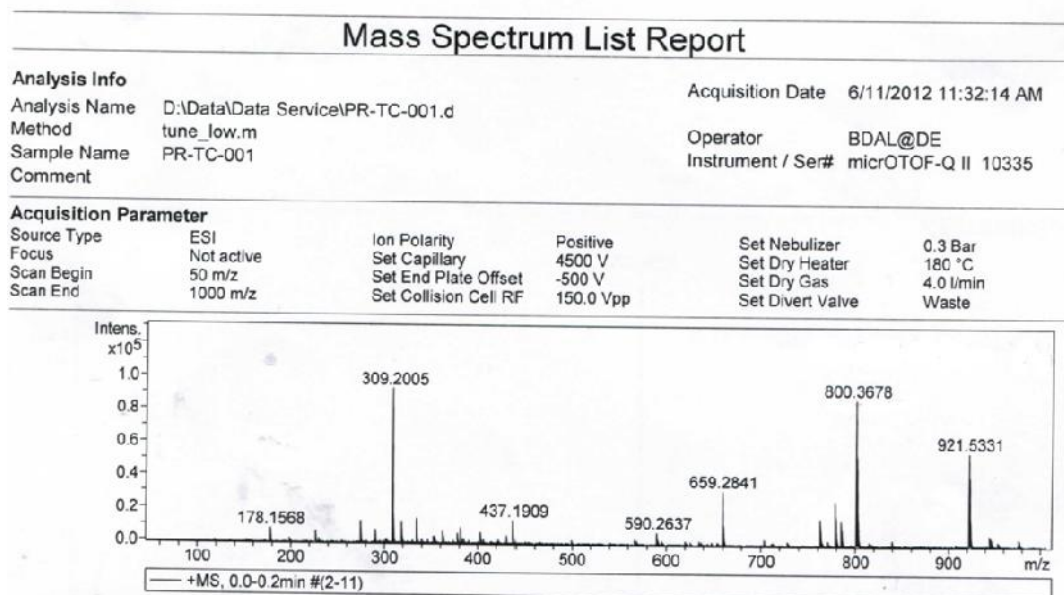


Fig A. 35 Mass spectrum of 4,5-dicumylphenoxy-*N*-(2,6-diisopropyl-phenyl)-1,8-naphthalimide (**3m**) in EtOAc

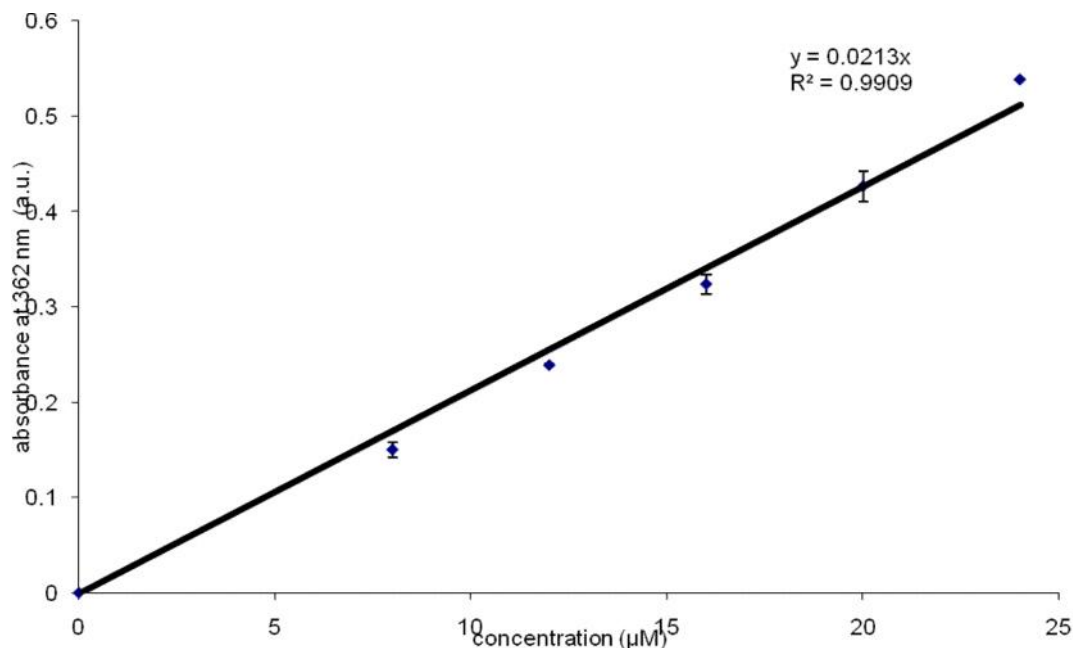


Fig A. 36 Molar absorption coefficient plot of 4-phenoxy-*N*-(phenyl)-1,8-naphthalimide (**3a**) in CH₂Cl₂

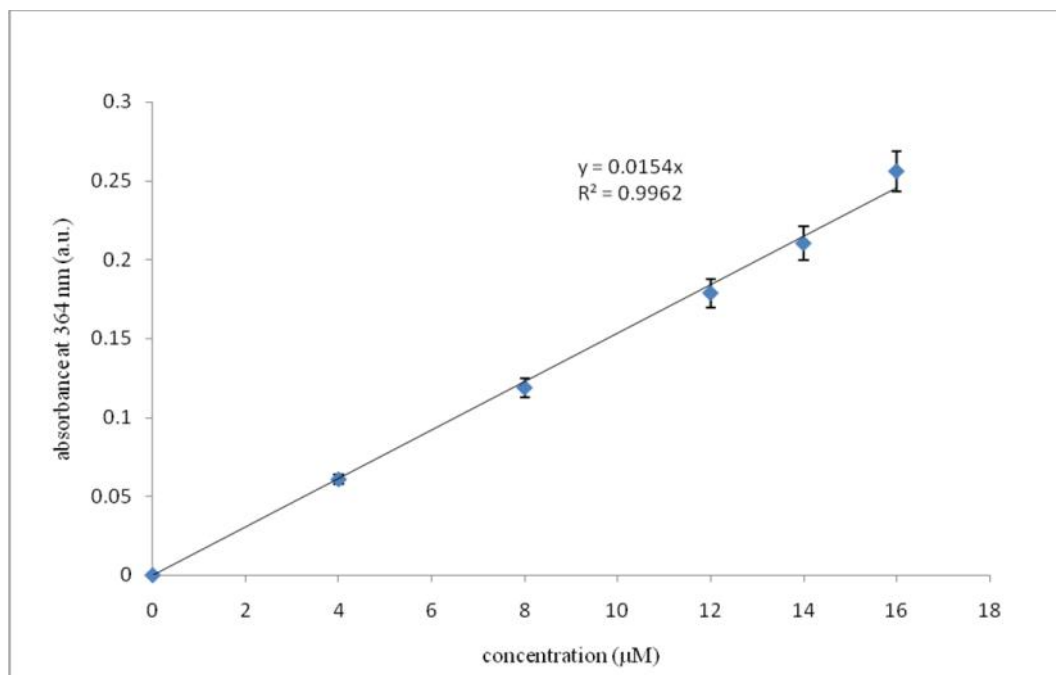


Fig A. 37 Molar absorption coefficient plot of 4-cumylphenoxy-*N*-(phenyl)-1,8-naphthalimide (**3b**) in CH_2Cl_2

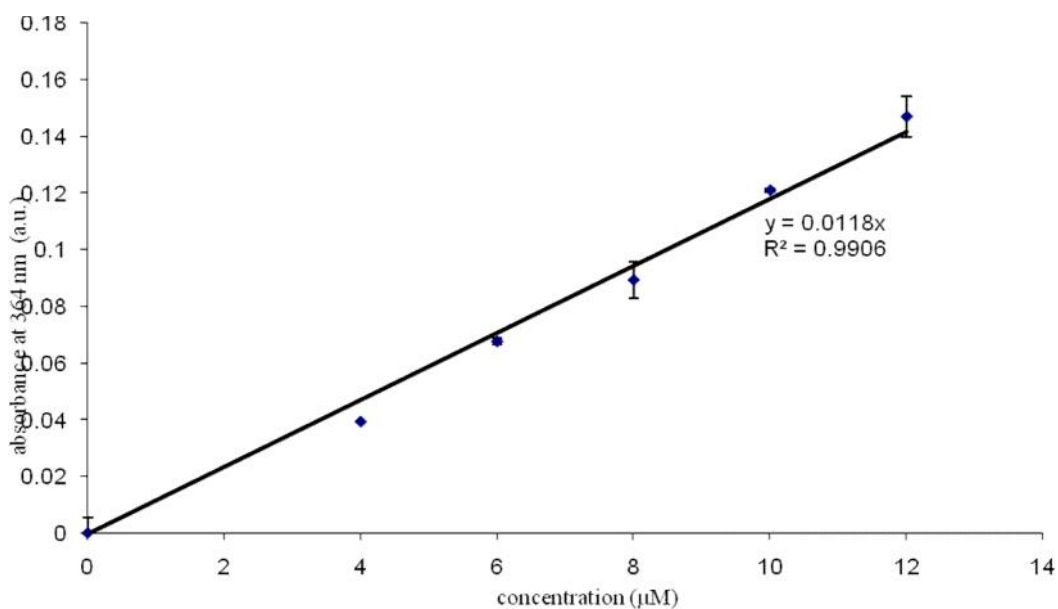


Fig A. 38 Molar absorption coefficient plot of 4-cumylphenoxy-*N*-(2-acethoxyphenyl)-1,8-naphthalimide (**3c**) in CH_2Cl_2

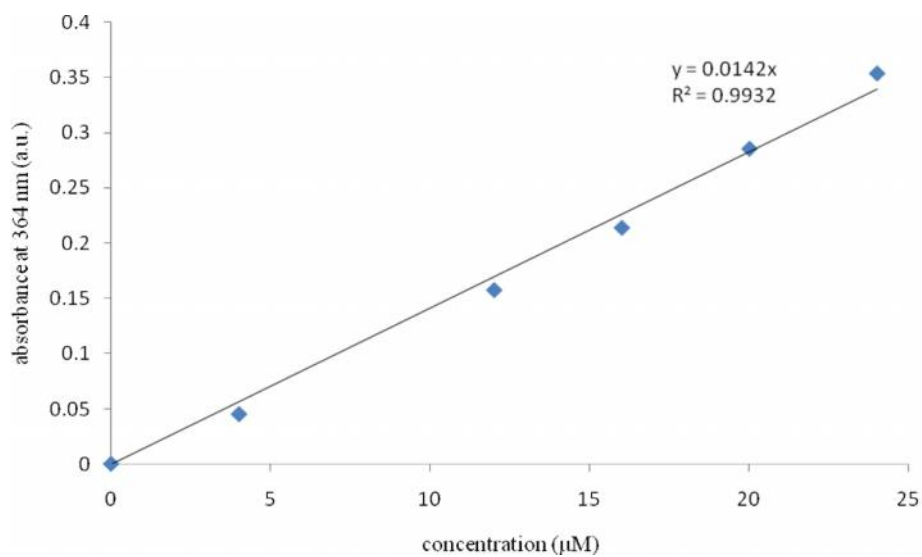


Fig A. 39 Molar absorption coefficient plot of 4-cumylphenoxy-*N*-(4-methoxyphenyl)-1,8-naphthalimide (**3d**) in CH_2Cl_2

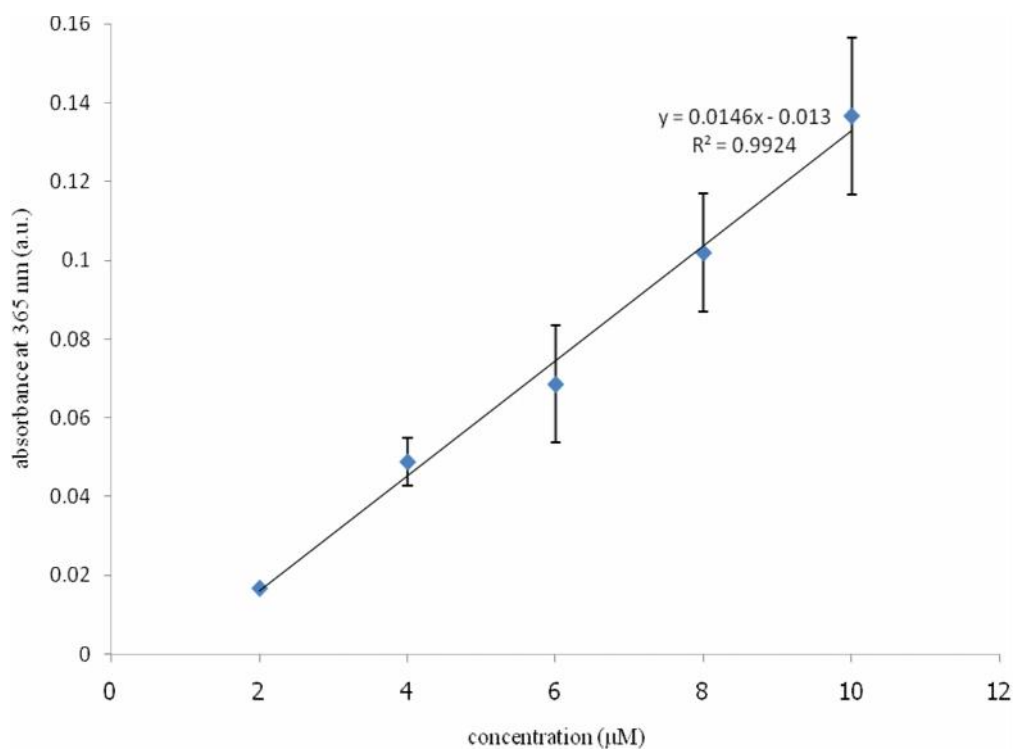


Fig A. 40 Molar absorption coefficient plot of 4-cumylphenoxy-*N*-(2,6-diisopropyl-phenyl)-1,8-naphthalimide (**3e**) in CH_2Cl_2

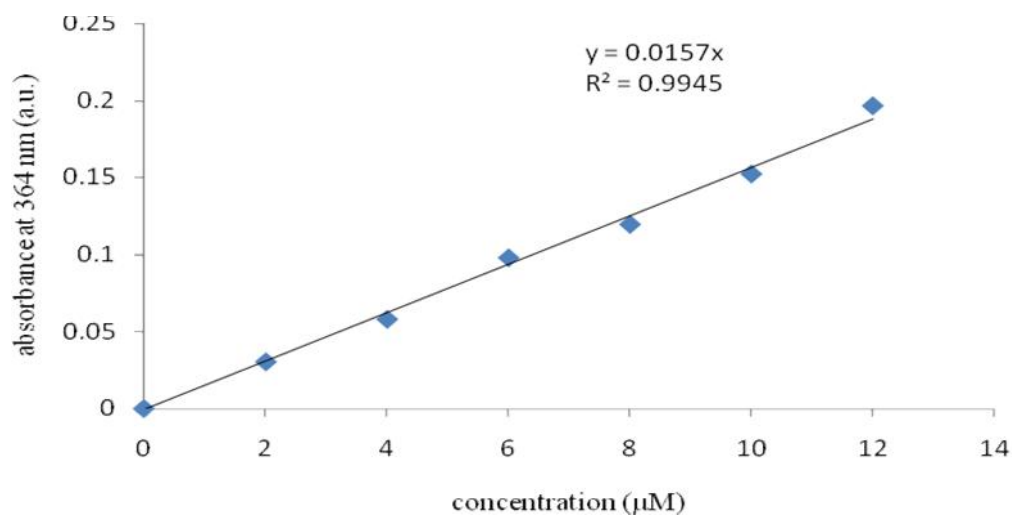


Fig A. 41 Molar absorption coefficient plot of 4-phenoxy-*N*-(2,6-diisopropyl-phenyl)-1,8-naphthalimide (**3f**) in CH₂Cl₂

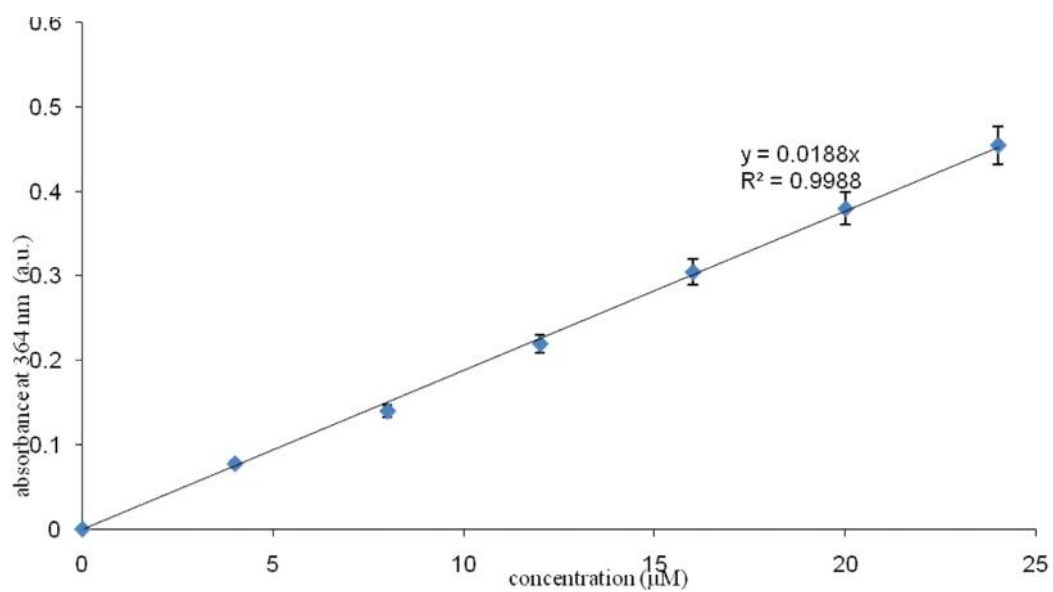


Fig A. 42 Molar absorption coefficient plot of 4-(4-*tert*-butyl-phenoxy)-*N*-(2,6-diisopropyl-phenyl)-1,8-naphthalimide (**3g**) in CH₂Cl₂

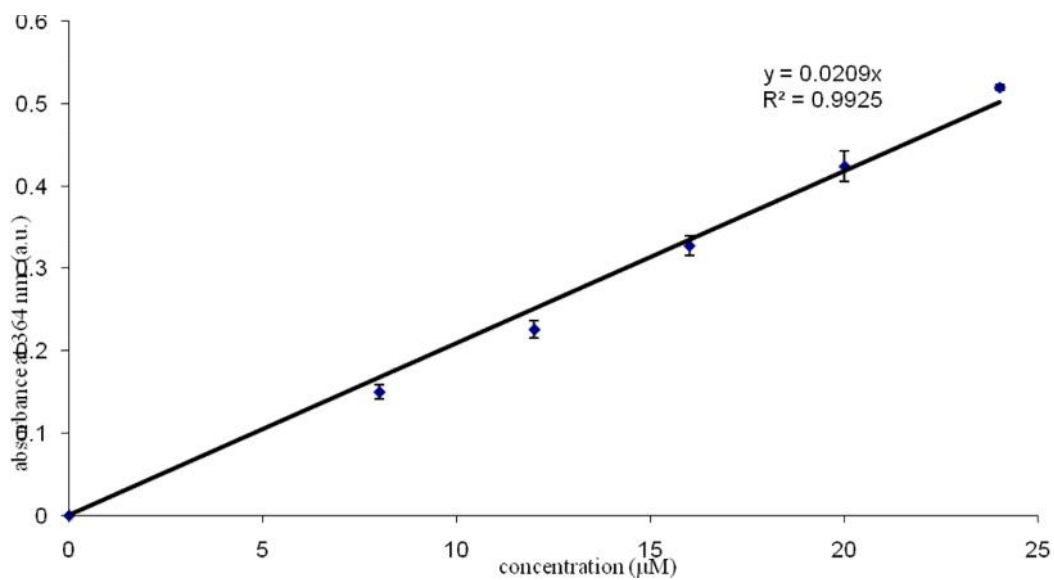


Fig A. 43 Molar absorption coefficient plot of 4-(4-methoxy-phenoxy)-*N*-(2,6-diisopropyl-phenyl)-1,8-naphthalimide (**3h**) in CH_2Cl_2

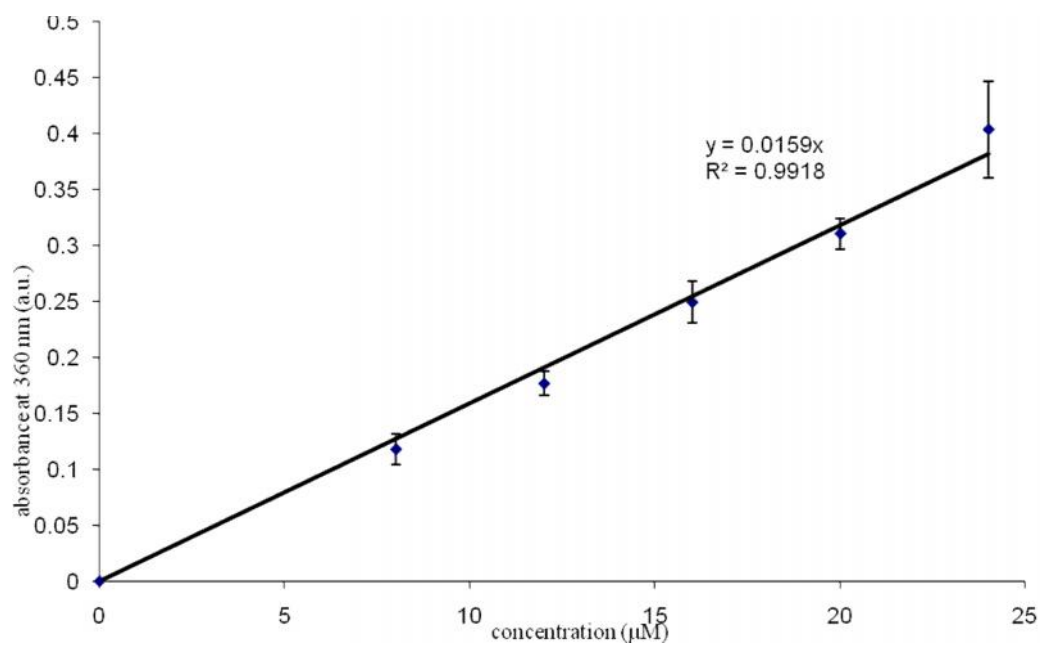


Fig A. 44 Molar absorption coefficient plot of 4-(4-chloro-phenoxy)-*N*-(2,6-diisopropyl-phenyl)-1,8-naphthalimide (**3i**) in CH_2Cl_2

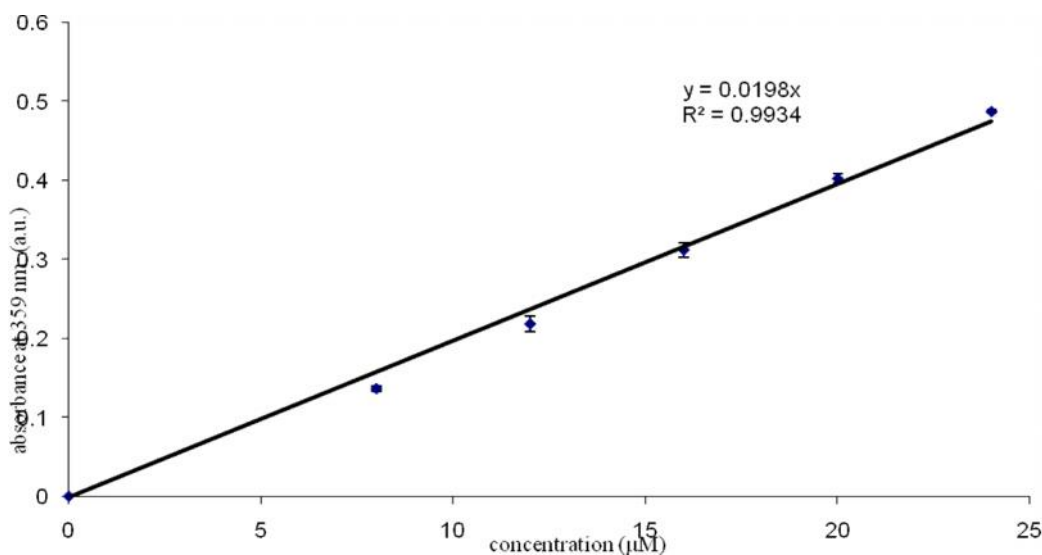


Fig A. 45 Molar absorption coefficient plot of 4-(4-acethoxy-phenoxy)-*N*-(2,6-diisopropyl-phenyl)-1,8-naphthalimide (**3j**) in CH_2Cl_2

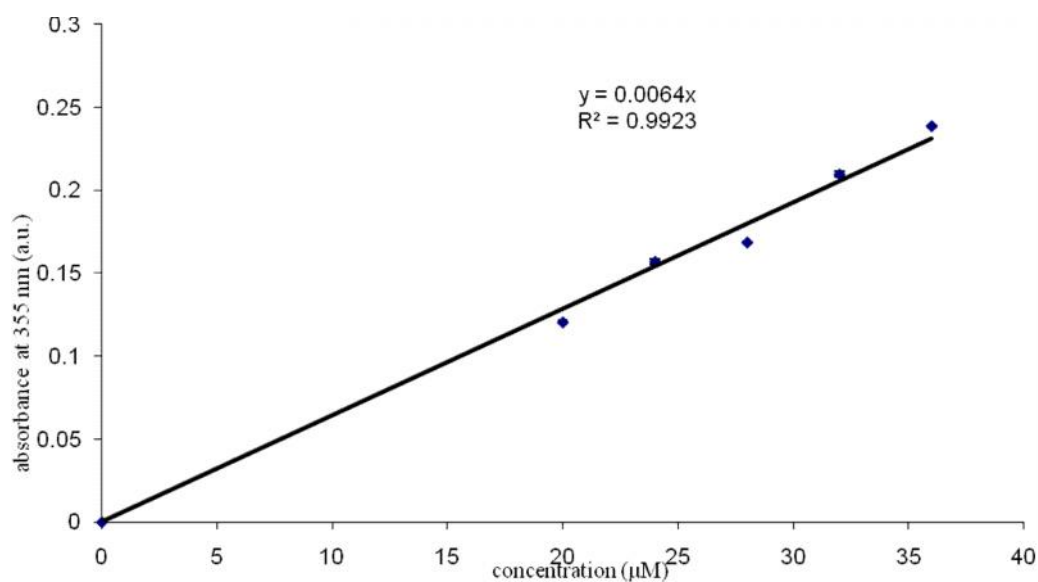


Fig A. 46 Molar absorption coefficient plot of 4-(4-nitro-phenoxy)-*N*-(2,6-diisopropyl-phenyl)-1,8-naphthalimide (**3k**) in CH_2Cl_2

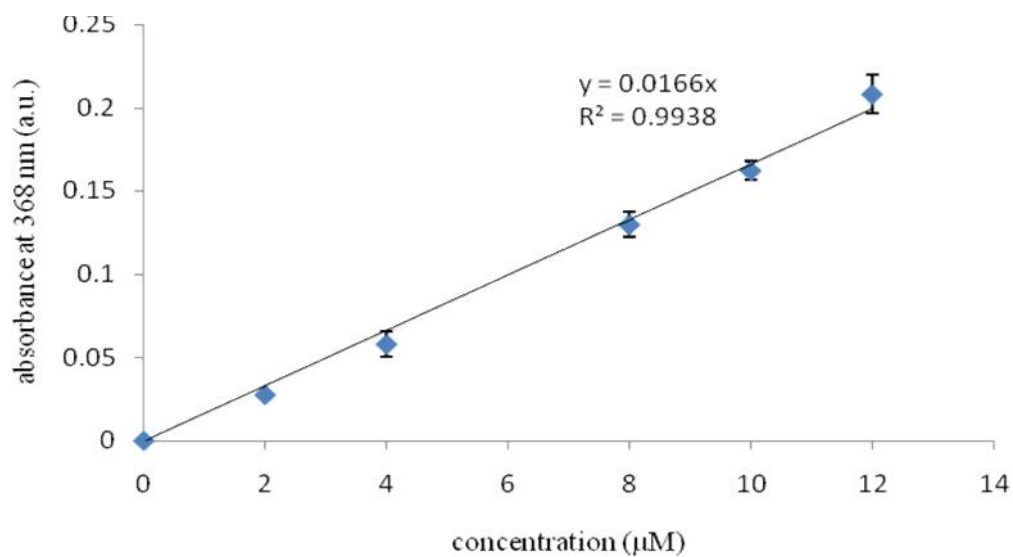


Fig A. 47 Molar absorption coefficient plot of 4-butoxy-*N*-(2,6-diisopropylphenyl)-1,8-naphthalimide (**3l**) in CH₂Cl₂

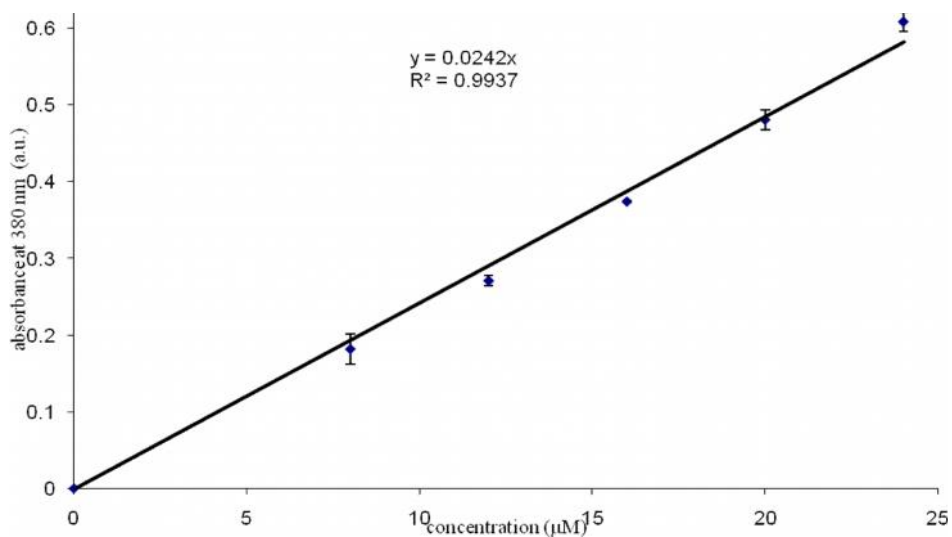


Fig A. 48 Molar absorption coefficient plot of 4,5-dicumylphenoxy-*N*-(2,6-diisopropylphenyl)-1,8-naphthalimide (**3m**) in CH₂Cl₂

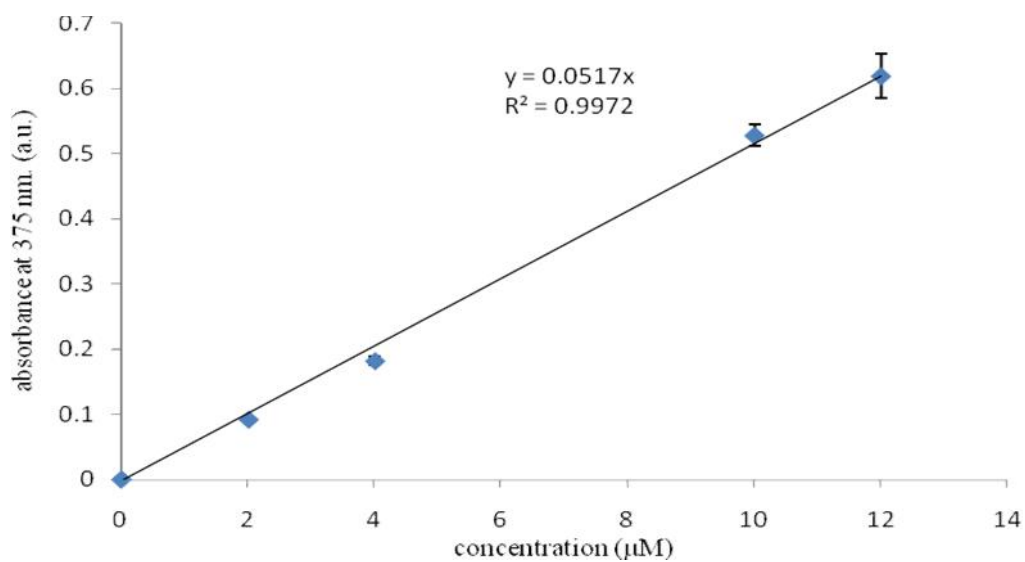


Fig A. 49 Molar absorption coefficient plot of Tinopal OB (**7**) in CH_2Cl_2

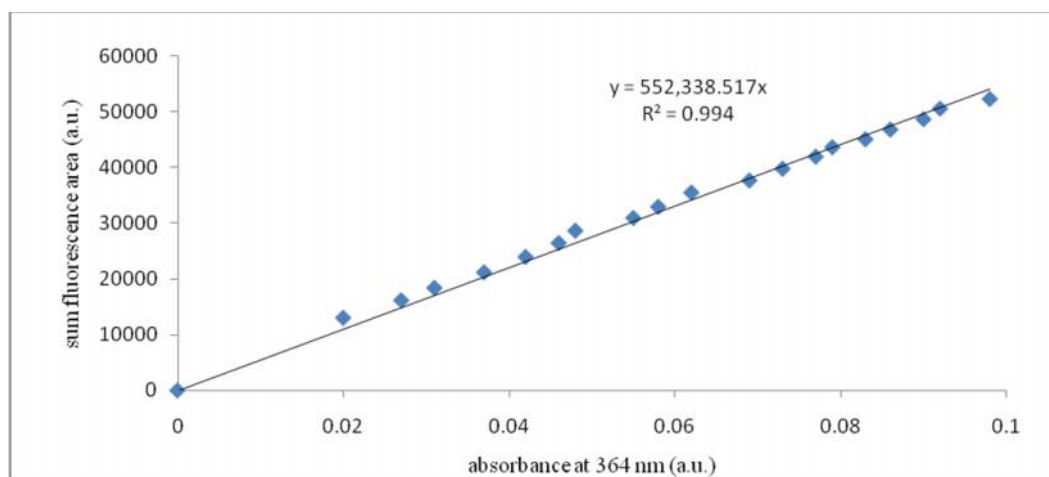


Fig A. 50 Quantum yield plot of 4-phenoxy-*N*-(phenyl)-1,8-naphthalimide (**3a**) in CH_2Cl_2 at PMT 540

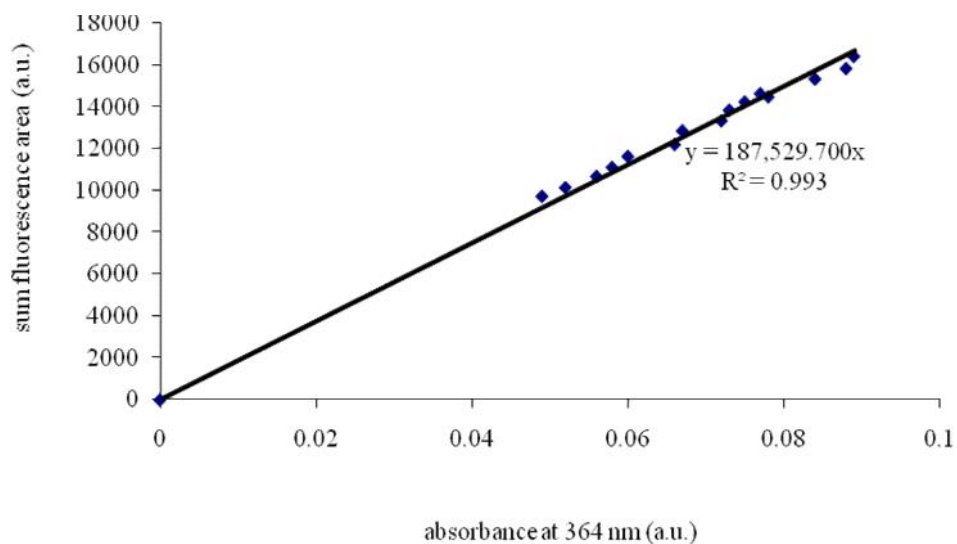


Fig A. 51 Quantum yield plot of 4-cumylphenoxy-*N*-(phenyl)-1,8-naphthalimide (**3b**) in CH_2Cl_2 at PMT 595

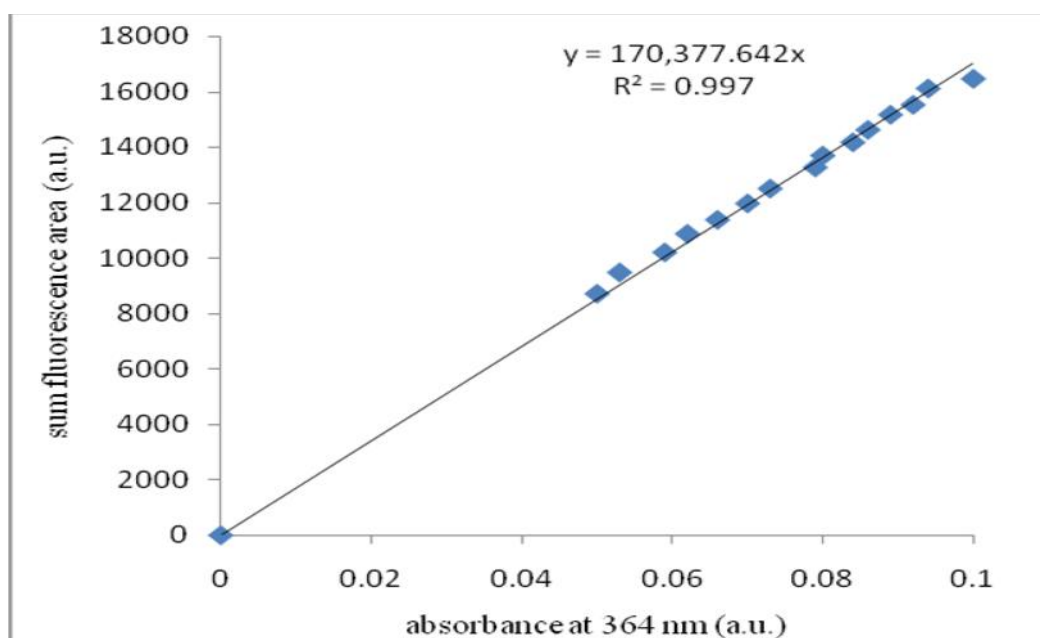


Fig A. 52 Quantum yield plot of 4-cumylphenoxy-*N*-(2-acethoxy-phenyl)-1,8-naphthalimide (**3c**) in CH_2Cl_2 at PMT 595

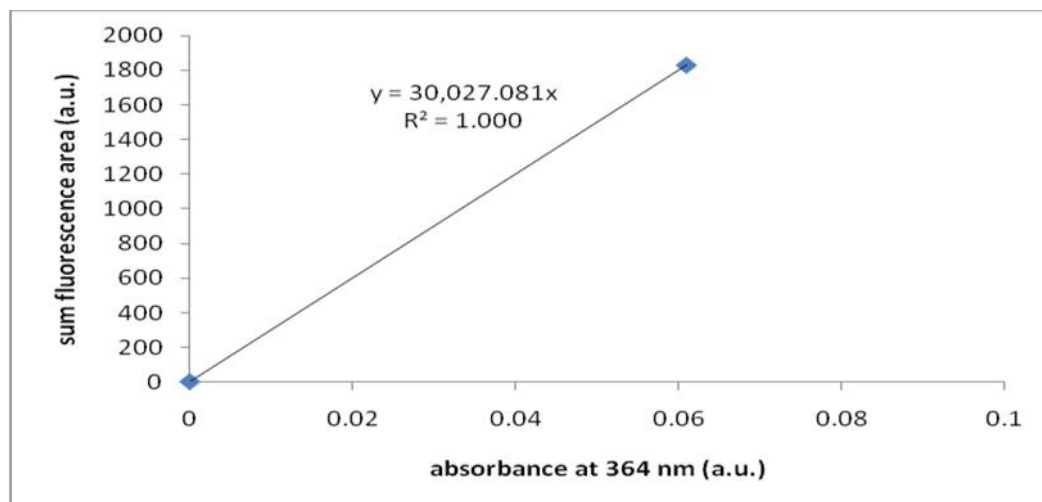


Fig A. 53 Quantum yield plot of 4-cumylphenoxy-*N*-(4-methoxy-phenyl)-1,8-naphthalimide (**3d**) in CH_2Cl_2 at PMT 595

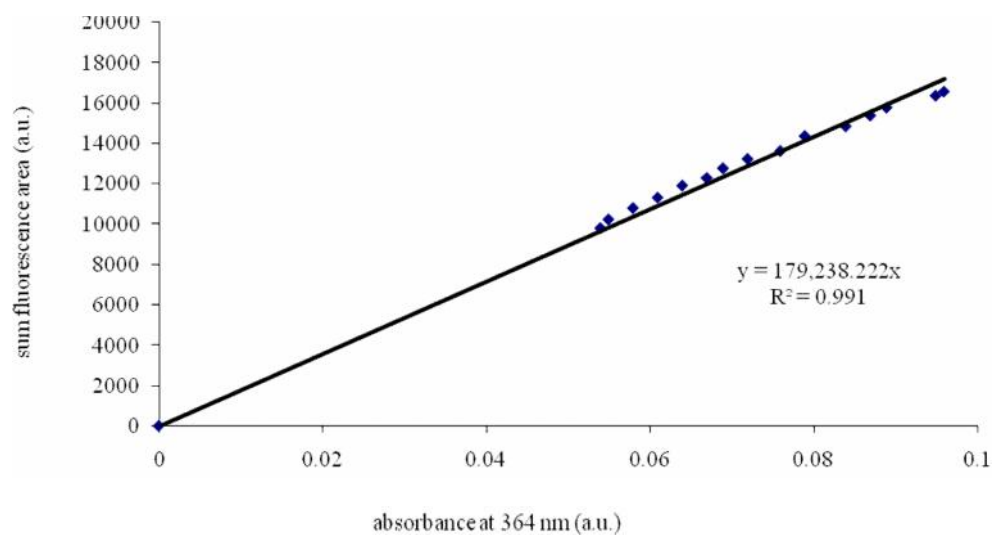


Fig A. 54 Quantum yield plot of 4-cumylphenoxy-*N*-(2,6-diisopropyl-phenyl)-1,8-naphthalimide (**3e**) in CH_2Cl_2 at PMT 595

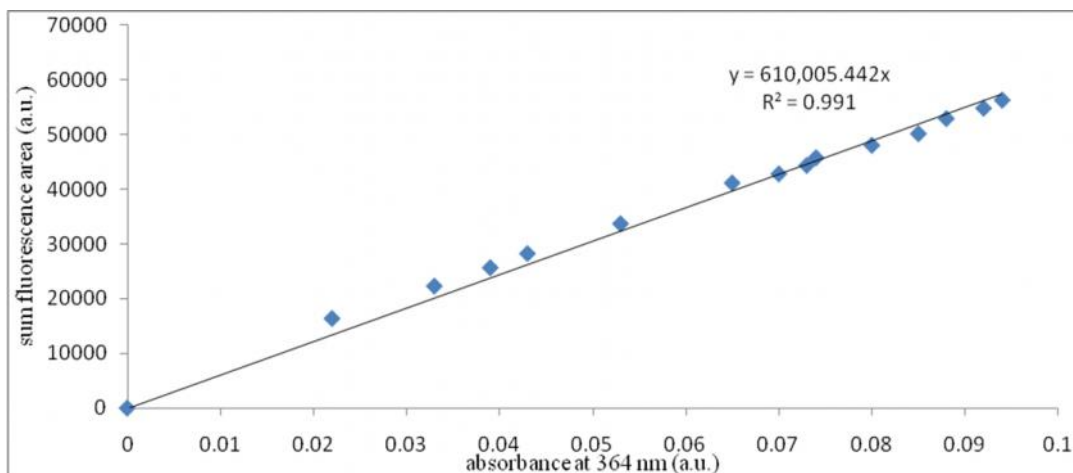


Fig A. 55 Quantum yield plot of 4-phenoxy-*N*-(2,6-diisopropyl-phenyl)-1,8-naphthalimide (**3f**) in CH₂Cl₂ at PMT 540

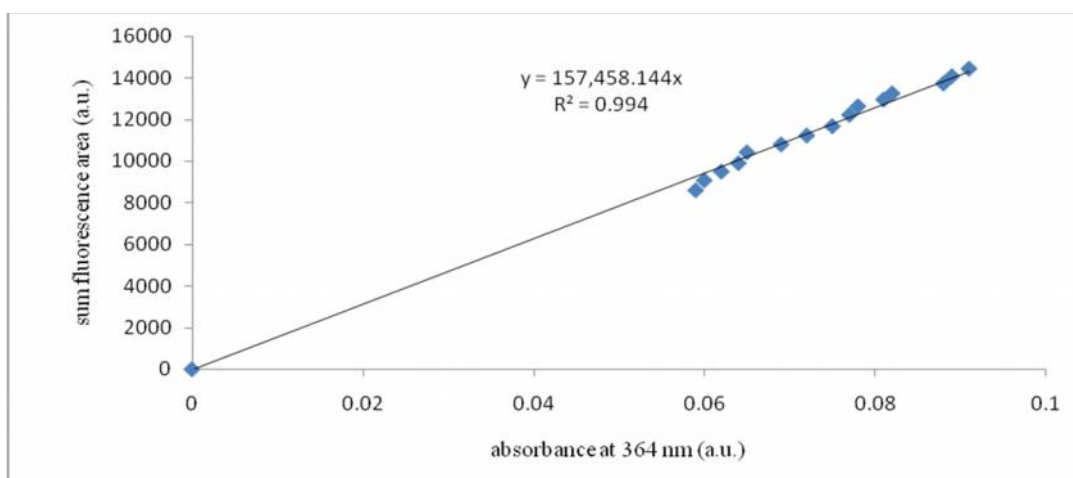


Fig A. 56 Quantum yield plot of 4-(4-*tert*-butyl-phenoxy)-*N*-(2,6-diisopropyl-phenyl)-1,8-naphthalimide (**3g**) in CH₂Cl₂ at PMT 595

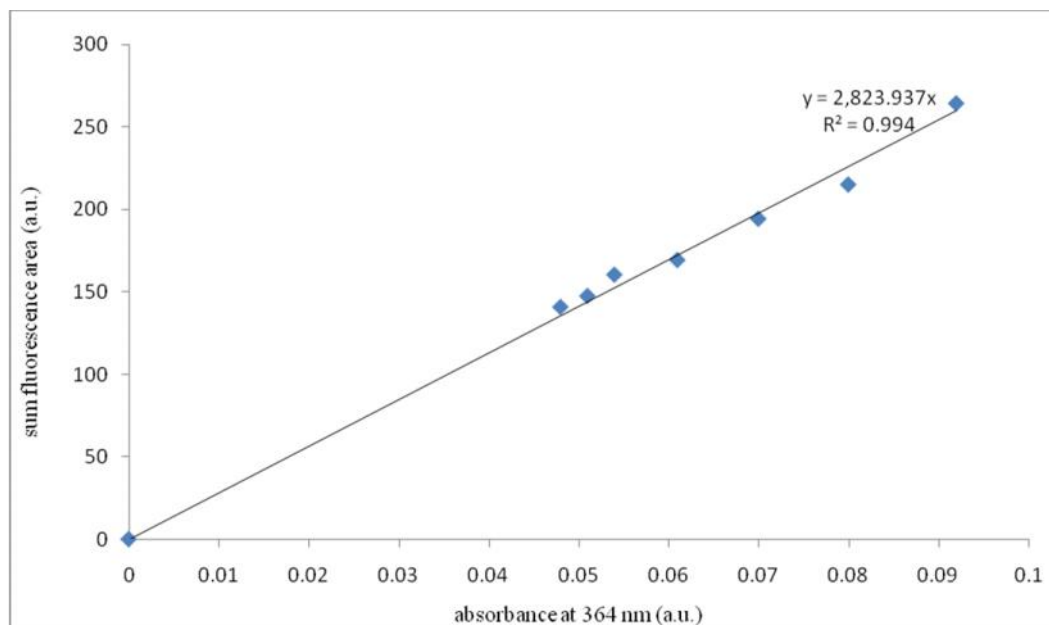


Fig A. 57 Quantum yield plot of 4-(4-methoxy-phenoxy)-*N*-(2,6-diisopropyl-phenyl)-1,8-naphthalimide (**3h**) in CH_2Cl_2 at PMT 595

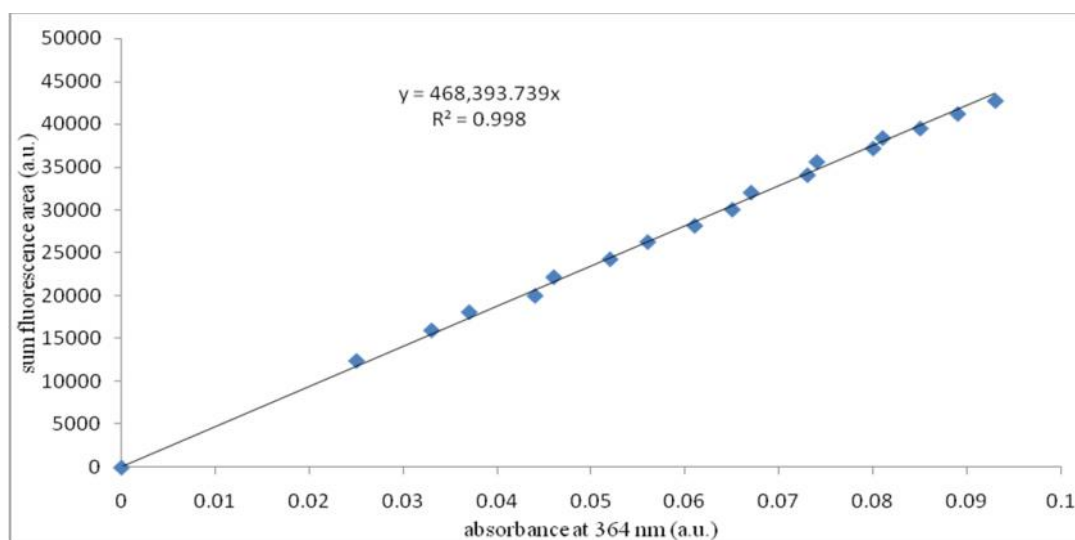


Fig A. 58 Quantum yield plot of 4-(4-chloro-phenoxy)-*N*-(2,6-diisopropyl-phenyl)-1,8-naphthalimide (**3i**) in CH_2Cl_2 at PMT 540

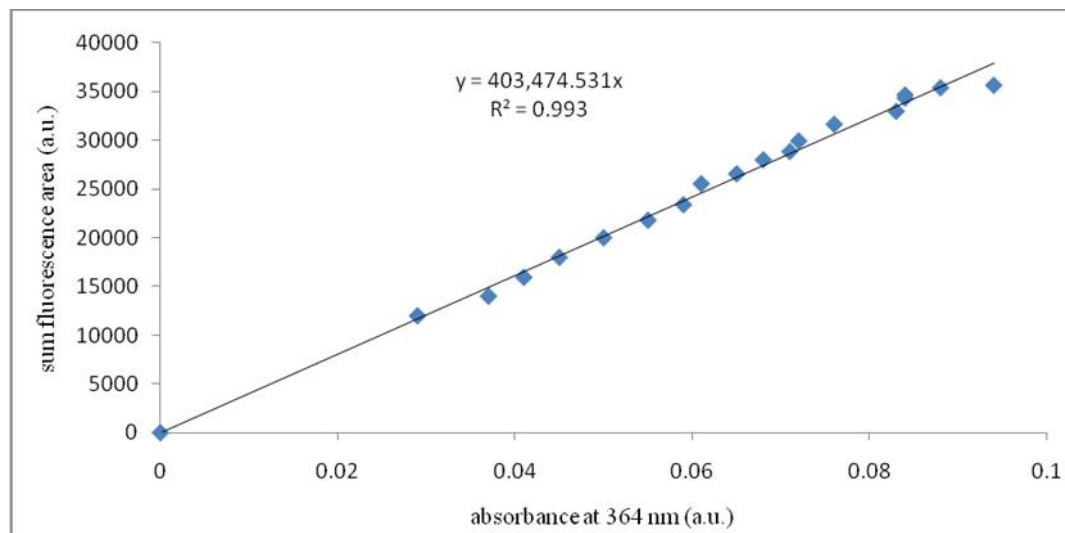


Fig A. 59 Quantum yield plot of 4-(4-acethoxy-phenoxy)-*N*-(2,6-diisopropyl-phenyl)-1,8-naphthalimide (**3j**) in CH_2Cl_2 at PMT 540

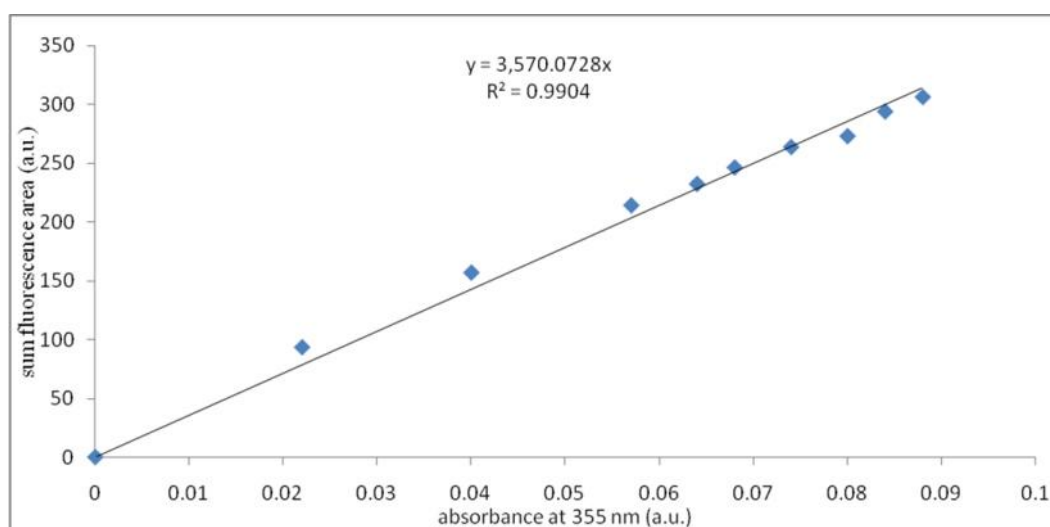


Fig A. 60 Quantum yield plot of 4-(4-nitro-phenoxy)-*N*-(2,6-diisopropyl-phenyl)-1,8-naphthalimide (**3k**) in CH_2Cl_2 at PMT 595

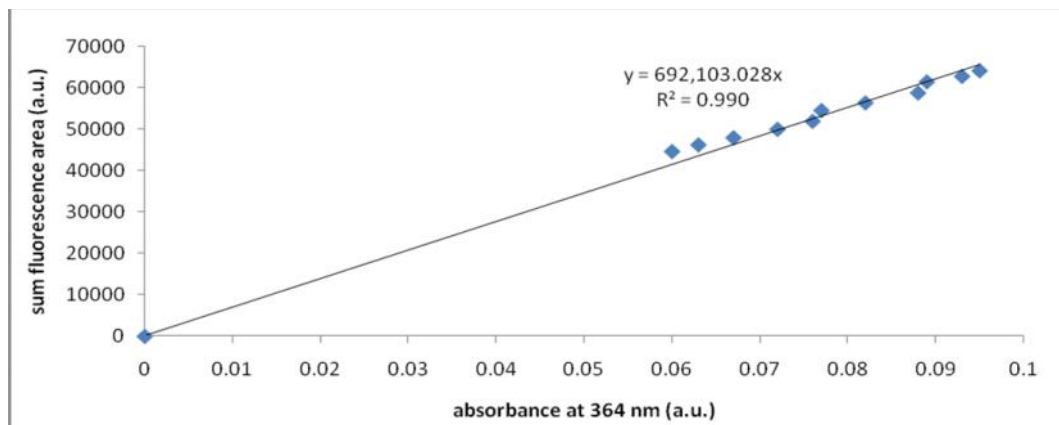


Fig A. 61 Quantum yield plot of 4-butoxy-*N*-(2,6-diisopropylphenyl)-1,8-naphthalimide (**3l**) in CH₂Cl₂ at PMT 540

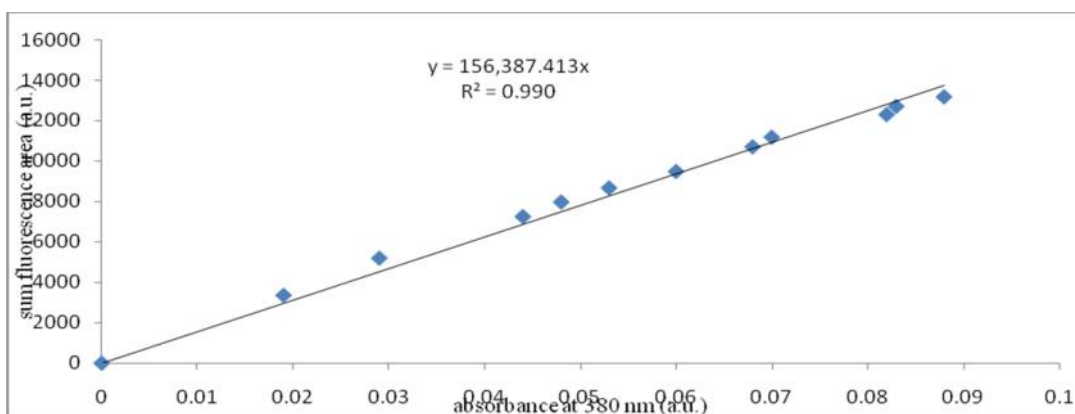


Fig A. 62 Quantum yield plot of 4,5-dicumylphenoxy-*N*-(2,6-diisopropylphenyl)-1,8-naphthalimide (**3m**) in CH₂Cl₂ at PMT 595

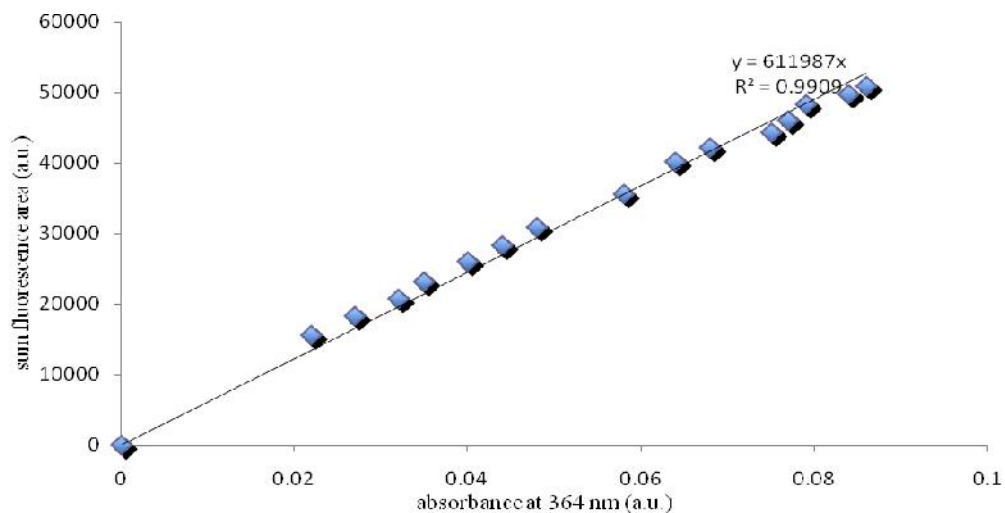


Fig A. 63 Quantum yield plot of Tinopal OB (7) in CH_2Cl_2 at PMT 540

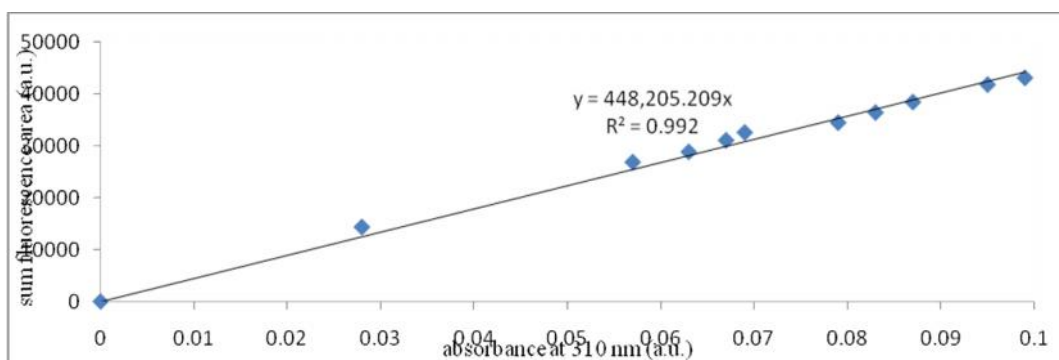


Fig A. 64 Quantum yield plot of Quinine sulfate in 0.1 M H_2SO_4 at PMT 540

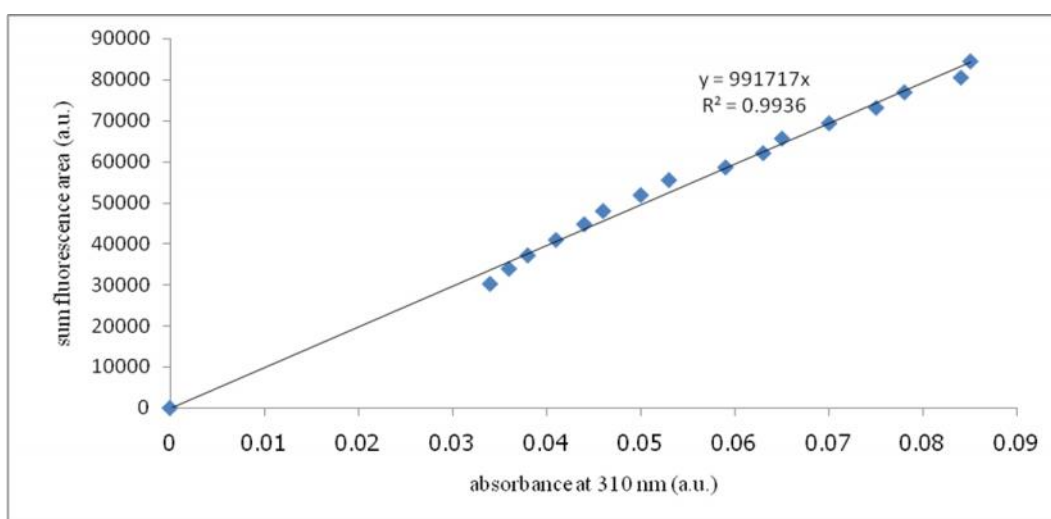


Fig A. 65 Quantum yield plot of Quinine sulfate in 0.1 M H_2SO_4 at PMT 595

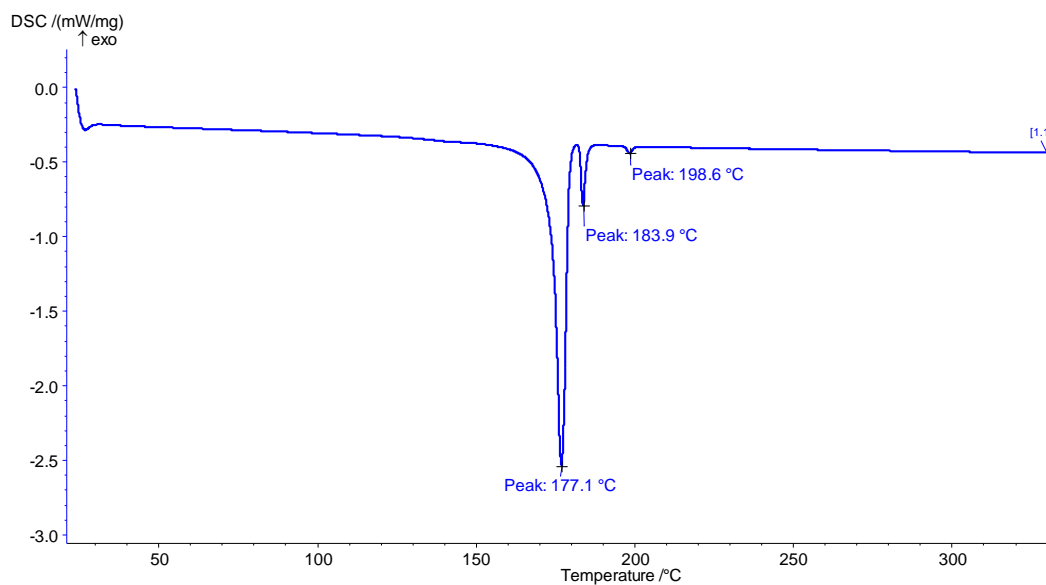


Fig A. 66 DSC measurement of 4-cumylphenoxy-*N*-(phenyl)-1,8-naphthalimide (**3b**) on the first heating cycle with a heating rate of 10 °C per minute under N₂

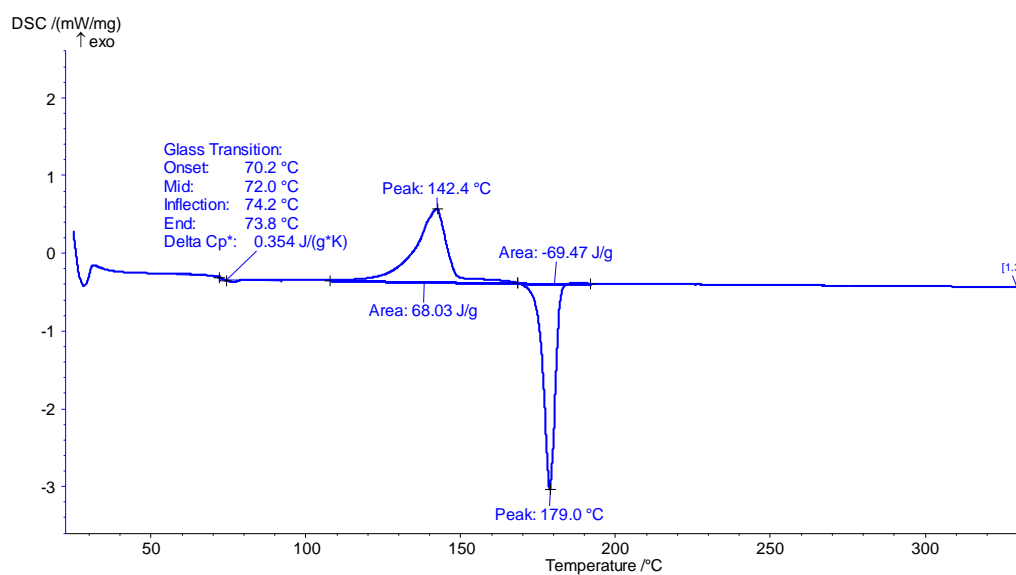


Fig A. 67 DSC measurement of 4-cumylphenoxy-*N*-(phenyl)-1,8-naphthalimide (**3b**) on the second heating cycle with a heating rate of 10 °C per minute under N₂

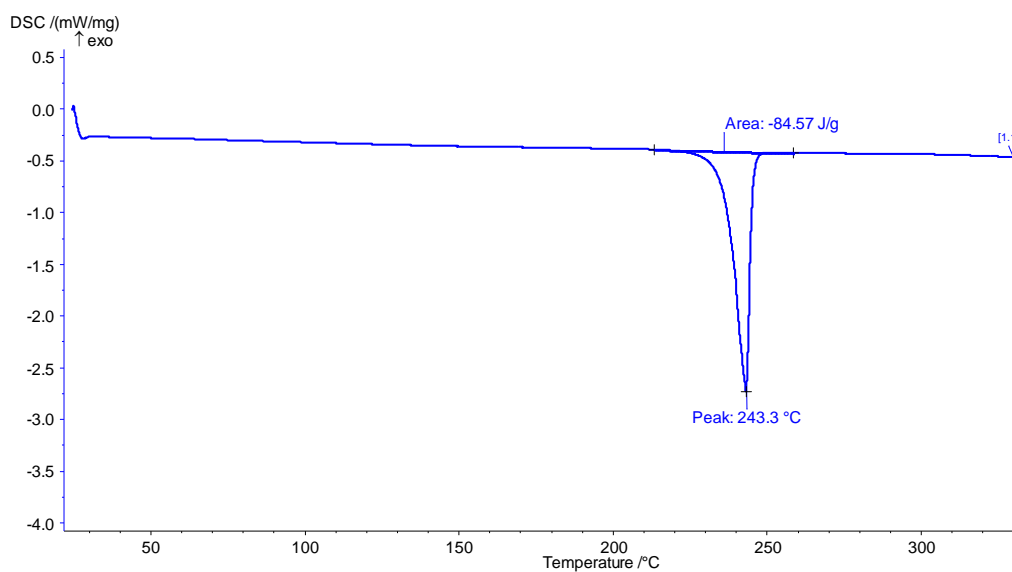


Fig A. 68 DSC measurement of 4-cumylphenoxy-*N*-(4-methoxy-phenyl)-1,8-naphthalimide (**3d**) on the first heating cycle with a heating rate of 10 °C per minute under N₂

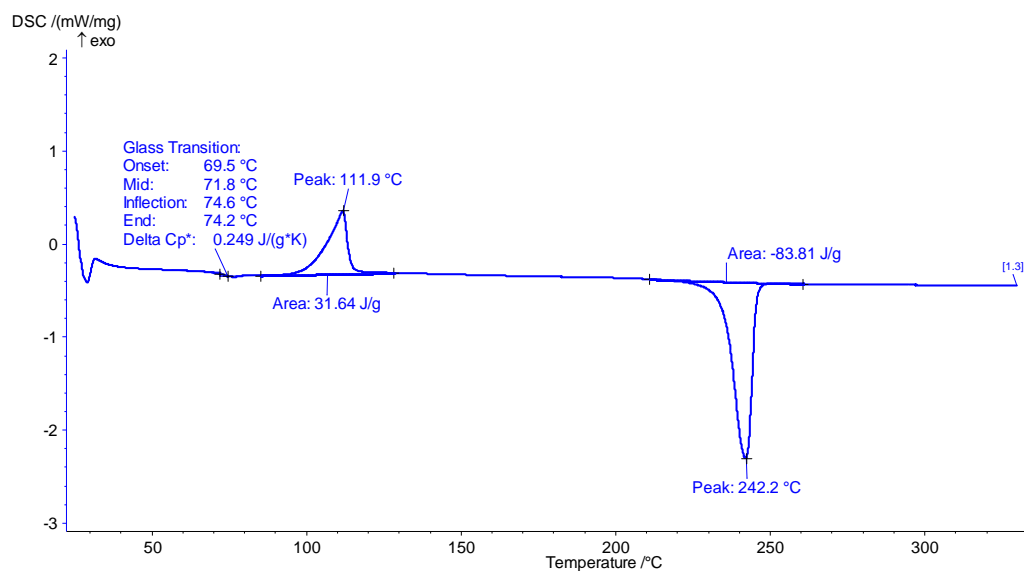


Fig A. 69 DSC measurement of 4-cumylphenoxy-*N*-(4-methoxy-phenyl)-1,8-naphthalimide (**3d**) on the second heating cycle with a heating rate of 10 °C per minute under N₂

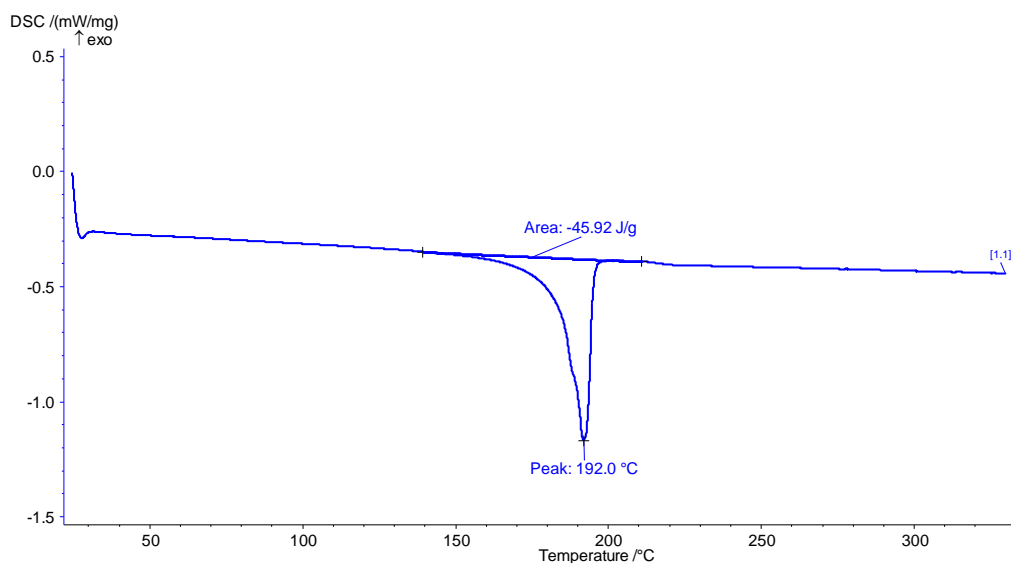


Fig A. 70 DSC measurement of 4-cumylphenoxy-*N*-(2,6-diisopropyl-phenyl)-1,8-naphthalimide (**3e**) on the first heating cycle with a heating rate of 10 °C per minute under N₂

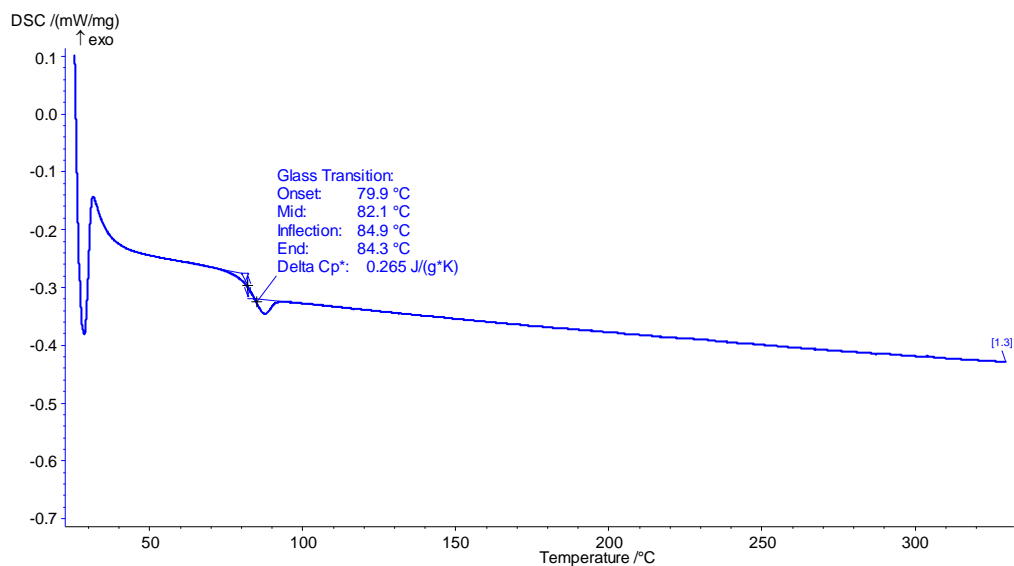


Fig A. 71 DSC measurement of 4-cumylphenoxy-*N*-(2,6-diisopropyl-phenyl)-1,8-naphthalimide (**3e**) on the second heating cycle with a heating rate of 10 °C per minute under N₂

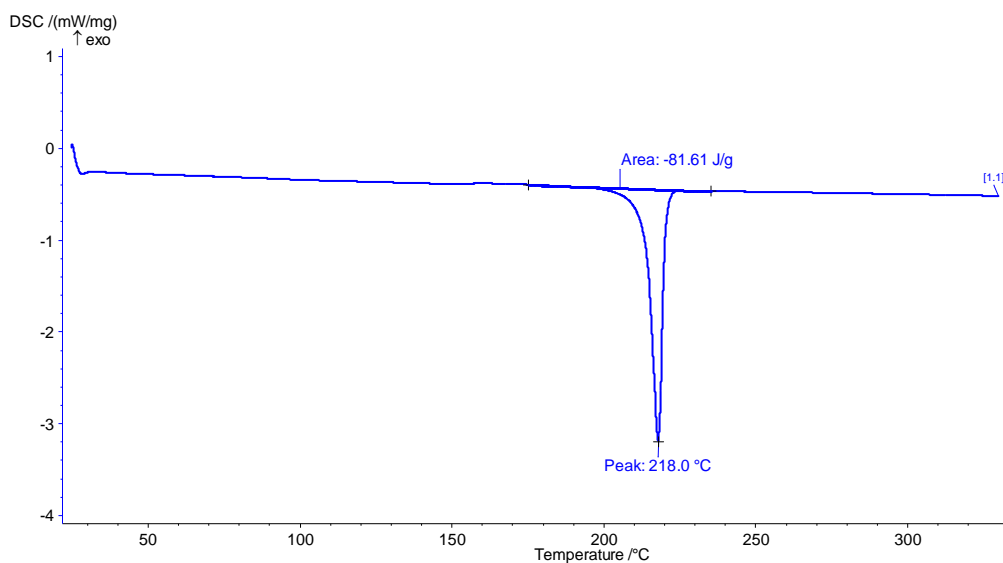


Fig A. 72 DSC measurement of 4-phenoxy-*N*-(2,6-diisopropyl-phenyl)-1,8-naphthalimide (**3f**) on the first heating cycle with a heating rate of 10 °C per minute under N₂

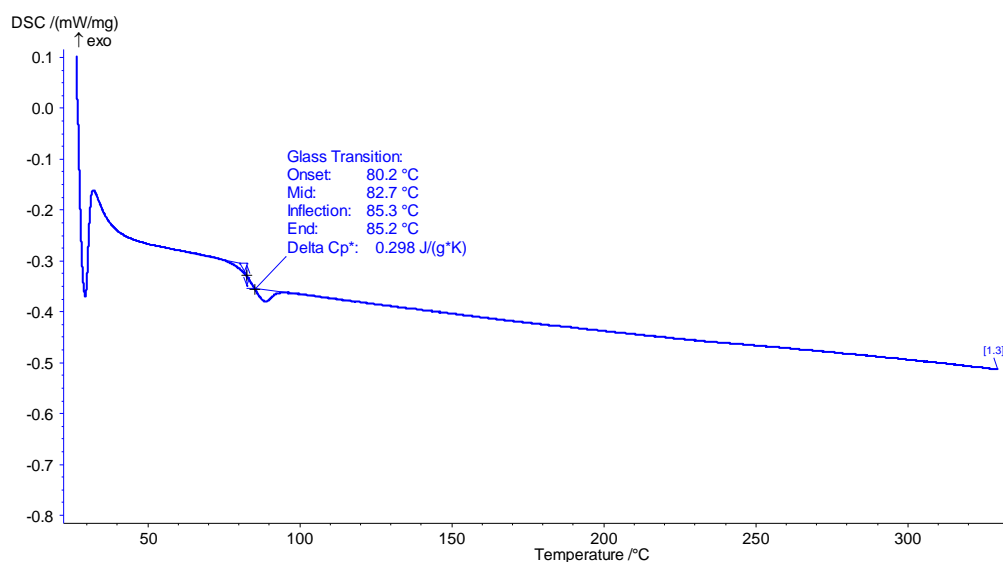


Fig A. 73 DSC measurement of 4-phenoxy-*N*-(2,6-diisopropyl-phenyl)-1,8-naphthalimide (**3f**) on the second heating cycle with a heating rate of 10 °C per minute under N₂

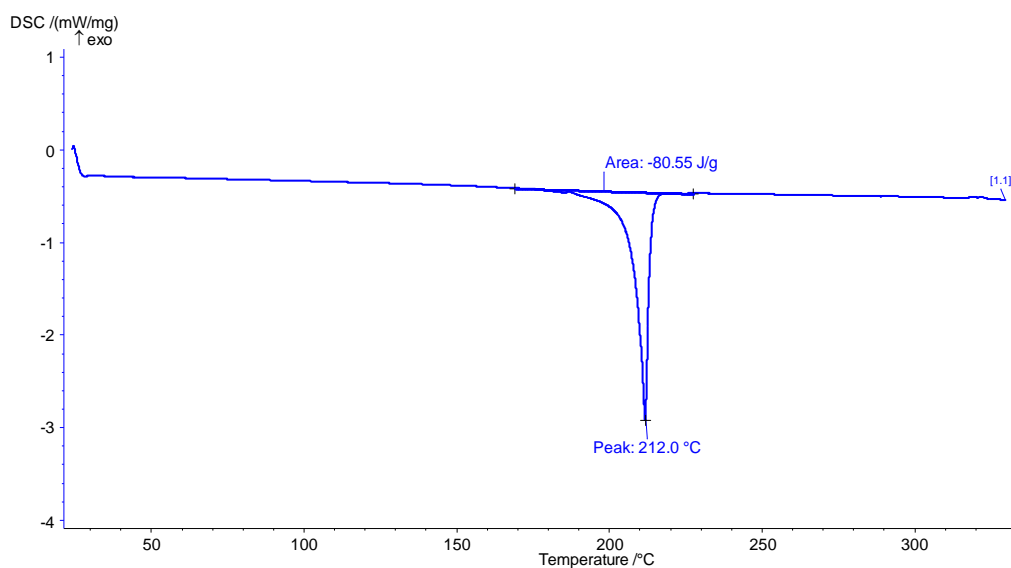


Fig A. 74 DSC measurement of 4-butoxy-*N*-(2,6-diisopropyl-phenyl)-1,8-naphthalimide (**31**) on the first heating cycle with a heating rate of 10 °C per minute under N₂

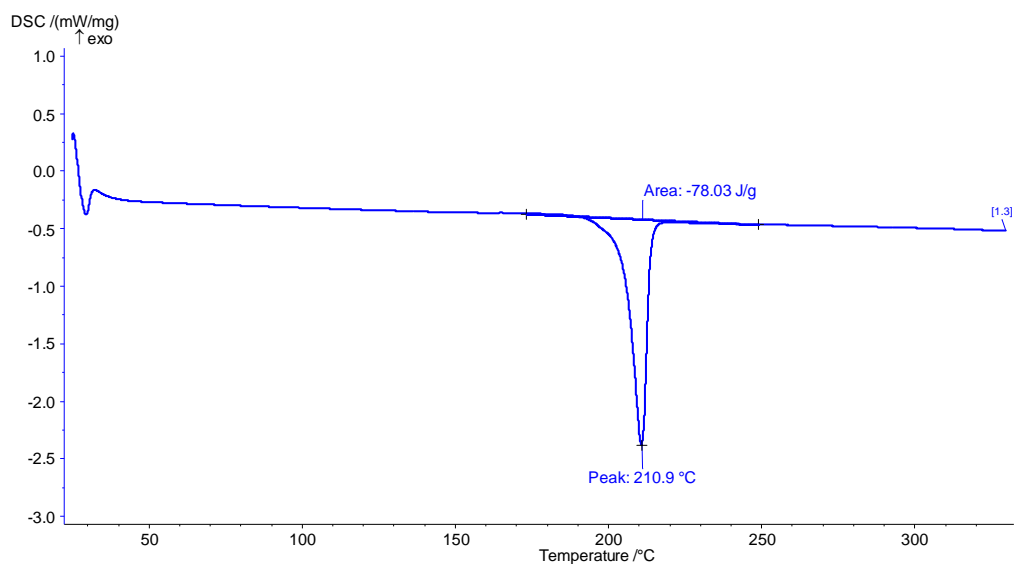


Fig A. 75 DSC measurement of 4-butoxy-*N*-(2,6-diisopropyl-phenyl)-1,8-naphthalimide (**31**) on the second heating cycle with a heating rate of 10 °C per minute under N₂

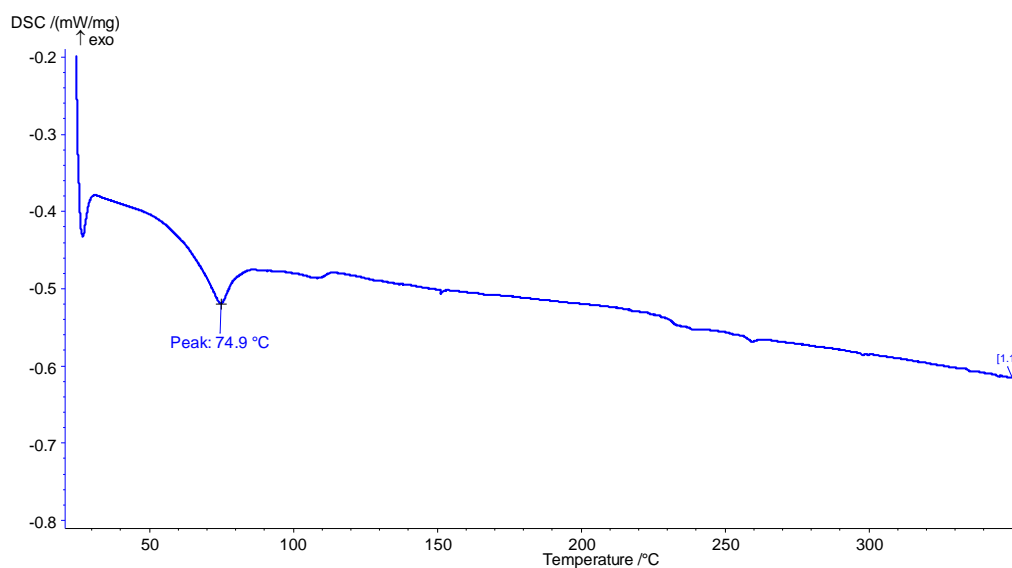


Fig A. 76 DSC measurement of 4,5-dicumylphenoxy-*N*-(2,6-diisopropylphenyl)-1,8-naphthalimide (**3m**) on the first heating cycle with a heating rate of 10 °C per minute under N₂

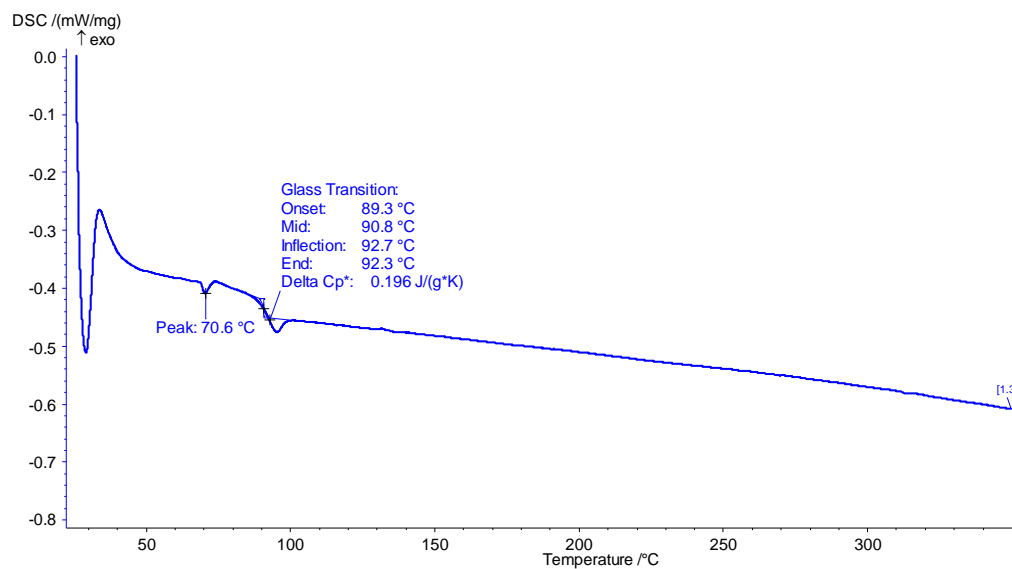


Fig A. 77 DSC measurement of 4,5-dicumylphenoxy-*N*-(2,6-diisopropylphenyl)-1,8-naphthalimide (**3m**) on the second heating cycle with a heating rate of 10 °C per minute under N₂

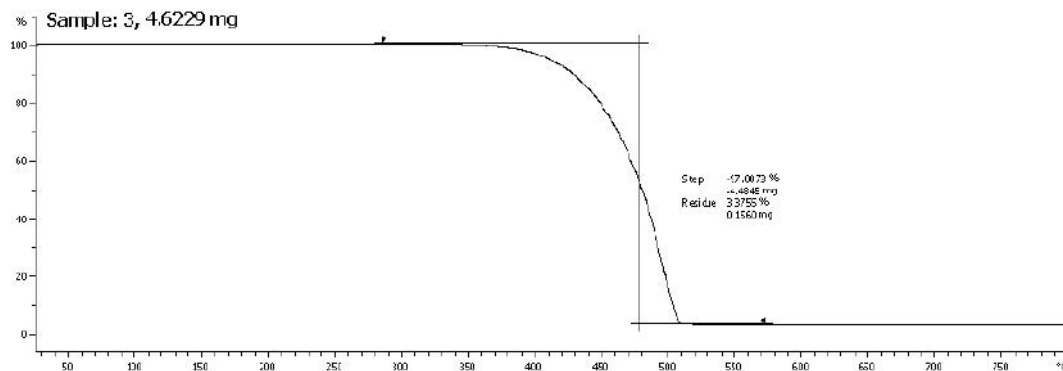


Fig A. 78 TGA measurement of 4-cumylphenoxy-*N*-(phenyl)-1,8-naphthalimide (**3b**) with a heating rate of 10 °C per minute under N₂

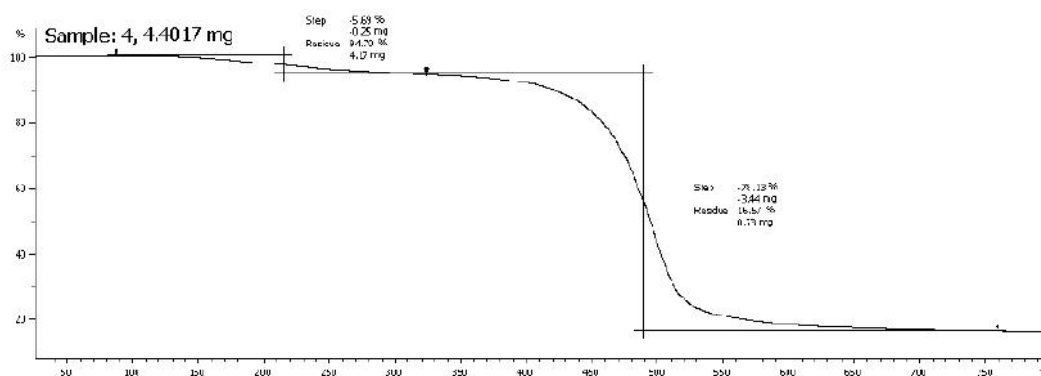


Fig A. 79 TGA measurement of 4-cumylphenoxy-*N*-(4-methoxy-phenyl)-1,8-naphthalimide (**3d**) with a heating rate of 10 °C per minute under N₂

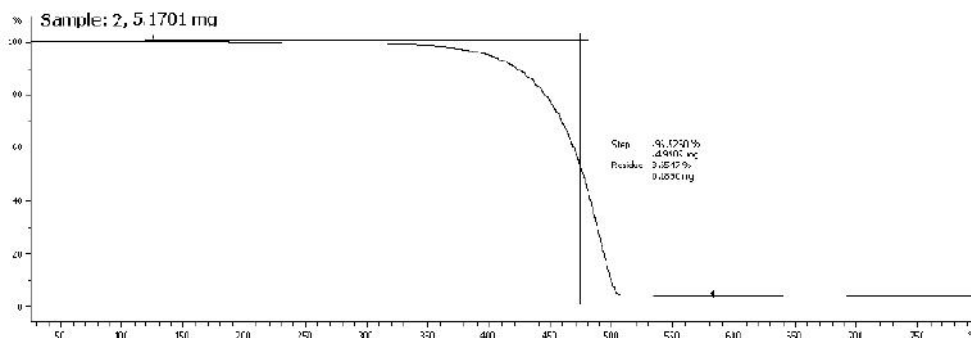


Fig A. 80 TGA measurement of 4-cumylphenoxy-*N*-(2,6-diisopropyl-phenyl)-1,8-naphthalimide (**3e**) with a heating rate of 10 °C per minute under N₂

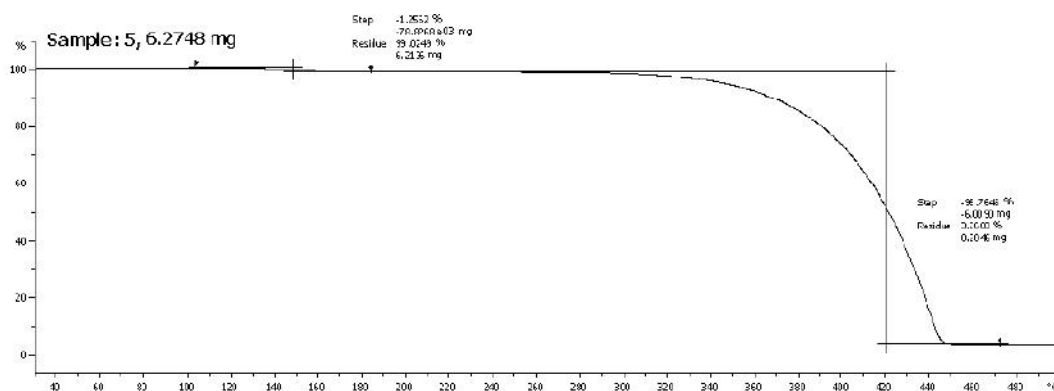


Fig A. 81 TGA measurement of 4-phenoxy-*N*-(2,6-diisopropyl-phenyl)-1,8-naphthalimide (**3f**) with a heating rate of 10 °C per minute under N₂

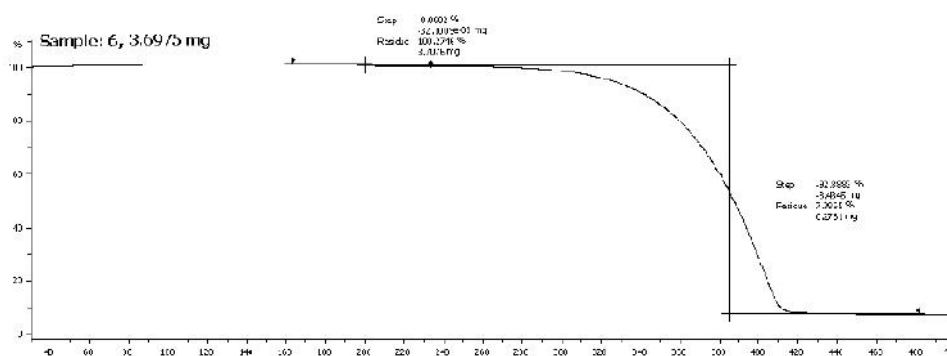


Fig A. 82 TGA measurement of 4-butoxy-*N*-(2,6-diisopropyl-phenyl)-1,8-naphthalimide (**3l**) with a heating rate of 10 °C per minute under N₂

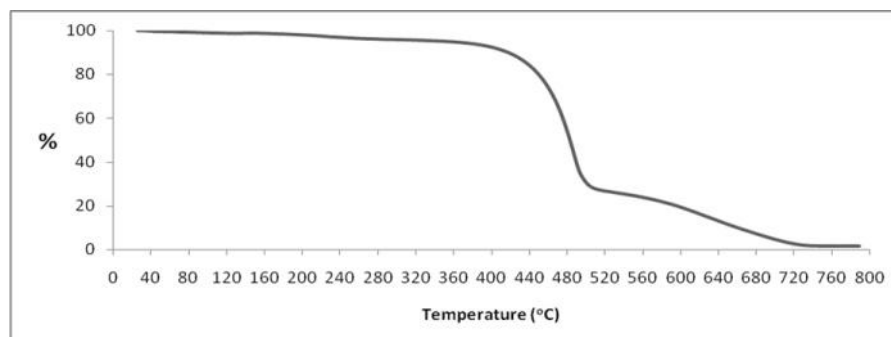


Fig A. 83 TGA measurement of 4,5-dicumylphenoxy-*N*-(2,6-diisopropyl-phenyl)-1,8-naphthalimide (**3m**) with a heating rate of 10 °C per minute under N₂

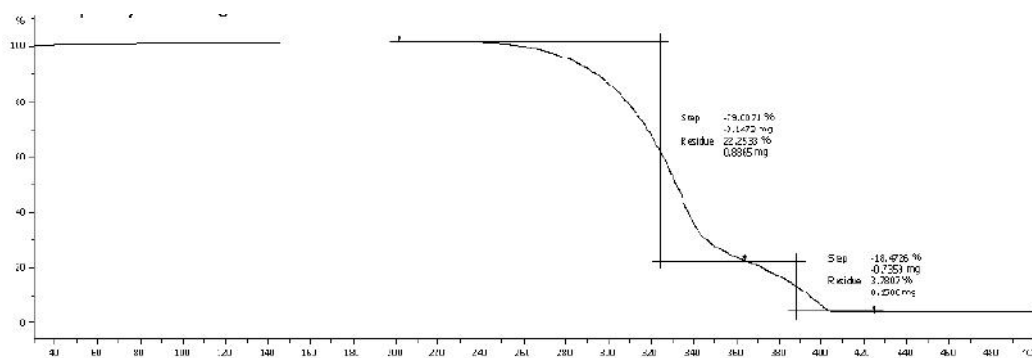


Fig A. 84 TGA measurement of Tinopal OB (7) with a heating rate of 10 °C per minute under N₂

Photostability calculation

All compounds were exposed 200 W per sq. m. by UVA lamp in DMSO.

$$\% \text{ remained} = \frac{\text{abs}_{t \text{ hr}}}{\text{abs}_{0 \text{ hr}}} * 100$$

4-cumylphenoxy-*N*-(phenyl)-1,8-naphthalimide (**3b**) (λ_{max} 364 nm)

	abs 1	% 1	abs 2	% 2	abs 3	% 3	% AVE	SD
0 hr	0.626	100	0.623	100	0.608	100	100	0
4 hr	0.577	92.17252	0.579	92.9374	0.572	94.07895	93.06296	0.959394
12 hr	0.543	86.74121	0.534	85.71429	0.531	87.33553	86.59701	0.820184
24 hr	0.495	79.07348	0.502	80.57785	0.504	82.89474	80.84869	1.924971
48 hr	0.464	74.12141	0.453	72.71268	0.463	76.15132	74.32847	1.728644

4-cumylphenoxy-*N*-(4-methoxy-phenyl)-1,8-naphthalimide (**3d**) (λ_{max} 364 nm)

	abs 1	% 1	abs 2	% 2	abs 3	% 3	% AVE	SD
0 hr	0.466	100	0.517	100	0.502	100	100	0
4 hr	0.412	88.41202	0.469	90.71567	0.46	91.63347	90.25372	1.659663
12 hr	0.377	80.90129	0.409	79.11025	0.419	83.46614	81.15922	2.189368
24 hr	0.352	75.53648	0.385	74.46809	0.395	78.68526	76.22994	2.192443
48 hr	0.324	69.5279	0.345	66.73114	0.348	69.32271	68.52725	1.558855

4-cumylphenoxy-*N*-(2,6-diisopropyl-phenyl)-1,8-naphthalimide (**3e**) (λ_{max} 365 nm)

	abs 1	% 1	abs 2	% 2	abs 3	% 3	% AVE	SD
0 hr	0.72	100	0.724	100	0.706	100	100	0
4 hr	0.612	85	0.649	89.64088	0.643	91.07649	88.57246	3.176016
12 hr	0.592	82.22222	0.589	81.35359	0.605	85.69405	83.08995	2.296654
24 hr	0.55	76.38889	0.542	74.86188	0.567	80.31161	77.18746	2.811262
48 hr	0.491	68.19444	0.476	65.74586	0.519	73.51275	69.15102	3.970821

4-phenoxy-*N*-(2,6-diisopropyl-phenyl)-1,8-naphthalimide (**3f**) (λ_{\max} 364 nm)

	abs 1	% 1	abs 2	% 2	abs 3	% 3	% AVE	SD
o hr	0.733	100	0.742	100	0.715	100	100	0
4 hr	0.645	87.99454	0.656	88.4097	0.646	90.34965	88.91797	1.257132
12 hr	0.596	81.30969	0.598	80.59299	0.589	82.37762	81.42677	0.898058
24 hr	0.535	72.98772	0.547	73.71968	0.534	74.68531	73.79757	0.851473
48 hr	0.451	61.52797	0.462	62.26415	0.457	63.91608	62.5694	1.222971

4-butoxy-*N*-(2,6-diisopropyl--phenyl)-1,8-naphthalimide (**3l**) (λ_{\max} 368 nm)

	abs 1	% 1	abs 2	% 2	abs 3	% 3	% AVE	SD
o hr	0.688	100	0.741	100	0.699	100	100	0
4 hr	0.655	95.20349	0.723	97.57085	0.694	99.28469	97.35301	2.049304
12 hr	0.65	94.47674	0.704	95.00675	0.689	98.56938	96.01763	2.225721
24 hr	0.636	92.44186	0.692	93.38731	0.682	97.56795	94.46571	2.727895
48 hr	0.635	92.29651	0.684	92.30769	0.666	95.27897	93.29439	1.718705

Tinopal OB (**7**) (λ_{\max} 375 nm)

	abs 1	% 1	abs 2	% 2	abs 3	% 3	% AVE	SD
o hr	1.117	100	1.088	100	1.194	100	100	0
4 hr	1.02	91.31603	0.999	91.81985	1.116	93.46734	92.20107	1.12518
12 hr	0.97	86.83975	0.923	84.83456	1.064	89.11223	86.92885	2.140226
24 hr	0.913	81.73679	0.867	79.6875	1.003	84.00335	81.80922	2.158836
48 hr	0.865	77.43957	0.79	72.61029	0.942	78.89447	76.31478	3.289619

VITAE

Mr. Tianchai Chooppawa was born on December 5, 1987 in Bangkok, Thailand. His address is 337/2 Rama 1 Road, Rong Muang, Phatumwan, Bangkok, 10330. To contact him, please call 0840117923 or send e-mail to tianchaic@windowslive.com. In 2009, he finished in Bachelor's Degree of Science in Chemistry from Chulalongkorn University. In next year, he began his Master's Degree of Science in Chemistry (Organic Chemistry) at Chulalongkorn University. In the middle of program, he started his thesis in "Synthesis of *p*-cumylphenoxy-1,8-naphthalimide brighteners". After that, he had presented "Synthesis of *p*-cumylphenoxy-1,8-naphthalimide brighteners" in Pure and Applied Chemistry International Conference (PACCON 2013) by poster presentation.